International Scientific-Theoretical and Production Journal

ADVANCES IN ELECTROMETALLURGY

1, 2005

Quarterly

English translation of the quarterly «Sovremennaya Elektrometallurgiya» journal published in Russian since January 1985

Founders: *E.O. Paton Electric Welding Institute of the NASU*
International Association «Welding»

Publisher: *International Association «Welding»*

Editorial and advertising offices are located at PWI:
International Association «Welding»,
E.O. Paton Electric
Welding Institute of the NASU,
11, Bozhenko str., 03680,
Kiev, Ukraine
Tel.: (38044) 287 67 57,
529 26 23,
Fax: (38044) 528 04 86
E-mail: journal@paton.kiev.ua
http://www.nas.gov.ua/pwj

Subscriptions:
4 issue per year;
184$** — regular, **150$ — for subscription agencies, **100$** — for students;
postage and packaging included.
Back issues available.

CONTENTS

ELECTROSLAG REMELTING OF HIGH-NITROGEN STEELS

A. MITCHELL[1] and **H. FREDERIKSSON**[2]
[1]Advanced Materials Laboratories, University of British Columbia, Vancouver, Canada
[2]Royal Technical University, Stockholm, Sweden

Steels containing nitrogen at levels which are at or above the 1 bar saturation solubility limit in the liquid at the liquidus temperature offer considerable metallurgical property advantages in many respects. For example, when nitrogen is used as a substitute for carbon in stainless grades, the alloys have superior corrosion properties especially in biomedical applications: nitrogen as a strengthening element in tool steels offers advantages in freedom from carbide particles which affect the polishability. Most of the steels grade of interest require electroslag remelting to control segregation without loss of nitrogen and the behaviour of nitrogen during this process is the subject of this work. It is concluded that the required process pressures are closely related to the alloy composition and that to prevent porosity in the product the ESR step must be carried out at an appropriate overpressure of either nitrogen or argon. The addition of nitrogen during ESR is also discussed and it is shown that this is possible only through solid additives.

Keywords: electroslag remelting, high-nitrogen steels, nitrogen, chromium, carbon, austenite, ferrite, liquidus temperature, crystallization

The thermochemistry of nitrogen solutions in steels is very well established through laboratory experimentation, principally using the direct method developed by Sieverts [1–3]. Generally, the saturation solubility of nitrogen closely follows Sieverts' law as a function of pressure and is a positive function of temperature. The most pertinent features of these properties are that there is a very substantial difference in the solubility around the liquidus temperature depending on whether or not the alloy solidifies as the ferrite or austenite phase. Nitrogen is not very soluble in ferrite but is quite soluble in austenite, to the extent that if the alloy solidifies as the austenite phase, the solubility below the liquidus temperature is an inverse function of temperature, in contrast to the direct function above that temperature. This behaviour is illustrated in Figures 1–3, where we contrast the two different aspects of the solubility function.

The solubility is enhanced by additions of elements which form stable nitrides relative to Fe_3N, such as Ti, V and Cr, but is decreased notably by Si and C. The balance between Cr, C and N is the dominating feature in the formulation of the high-nitrogen stainless grades, where the ultimate aim is to reduce or eliminate the carbide precipitation reactions and at the same time reduce the Ni content without compromising the alloy properties. The reduction in carbide precipitation imparts better corrosion resistance to pitting: the elimination of Ni makes the alloy more suitable for biomedical applications. With respect to the tool steels, primary carbide precipitation is re-

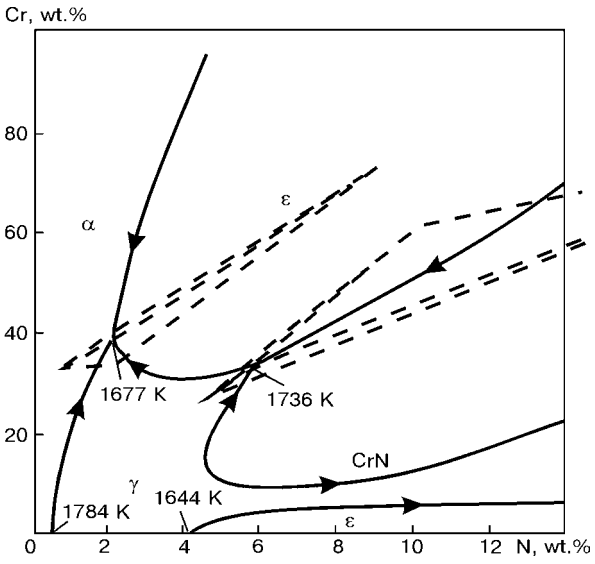

Figure 1. Fe–Cr–N liquidus projection surface

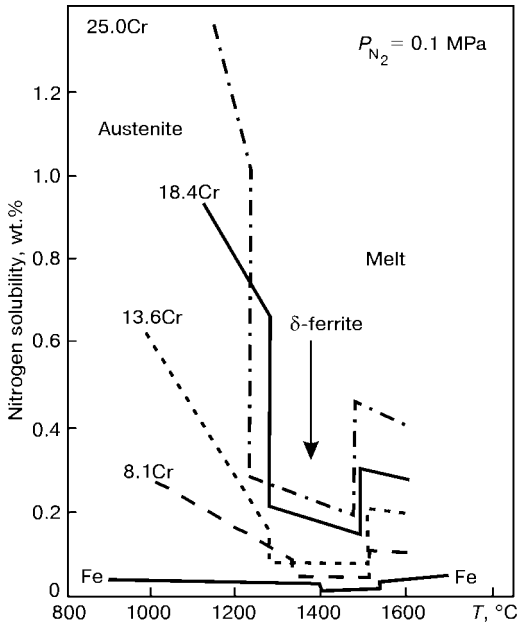

Figure 2. Nitrogen solubility in binary Fe–Cr alloys

duced by substitution of nitrogen to the point where no primary carbides are formed, hence considerable enhancing the alloy polishability which is a key factor in the use of these alloys as die materials.

The ESR process is commonly used for these steel grades since almost all of them are required in ingot diameters which produce significant centre segregation if permitted to freeze in a conventional static cast mode. It is feasible to carry out the ESR process under elevated pressure (although the mechanical complications are significant) which introduces the possibility of making alloys which have nitrogen contents exceeding the 1 bar solubility limits. Pressure melting also provides a means of controlling the development of porosity due to ex-solution of nitrogen during phase change or cooling. Equipment for pressure ESR has demonstrated the practicality of melting at pressures up to 16 bar [4] in ingot diameters up to 800 mm. The ESR technique itself is not sensitive to pressure and the principal complicating factors are mechanical rather than metallurgical. The main difficulty in the process sequence lies in the decision of how to add the alloying amounts of nitrogen. The most straightforward addition method is by blowing nitrogen into the bath of an electric furnace, or adding a high-nitrogen master alloy such as ferrochromium or ferromanganese or an addition of silicon nitride. If the furnace is operating under atmospheric pressure the maximum nitrogen addition will be the solubility limit at the liquid temperature. The nitrogen will be rejected during cooling and solidification and the usual result is a cast electrode structure which contains a large amount of porosity. Upon subsequent electroslag remelting the porosity will be released as nitrogen gas, some of which will go into solution in the alloy at the electrode tip to an extent which depends on the temperature in that region. Since the liquid metal on the electrode tip is not substantially superheated above the liquidus temperature, the nitrogen content of the liquid falling from the electrode is lower than the maximum content in the liquid in the original electric-arc melt, which causes the content of the final ingot to be lower than the addition amount in the electrode. If the ESR melt is carried out under an elevated pressure (of either argon or nitrogen), the nitrogen content of the electrode can be carried into the ingot so producing an ingot which has the same nitrogen content as the electrode. Nitrogen pick-up from the gas phase is negligible since the solubility of nitrogen in a conventional ESR slag is very small. (The small nitrogen loss frequently experienced during ESR of similar steels is probably due to the release of nitrogen gas from electrode porosity.)

The above technique will serve as a method for producing alloys in a conventional ESR furnace when the requirement for nitrogen content is significantly below the saturation solubility. It is regularly used in industrial practice for alloys such as tool steels and some ferritic stainless grades where only a small addition of nitrogen is called for in the specifications.

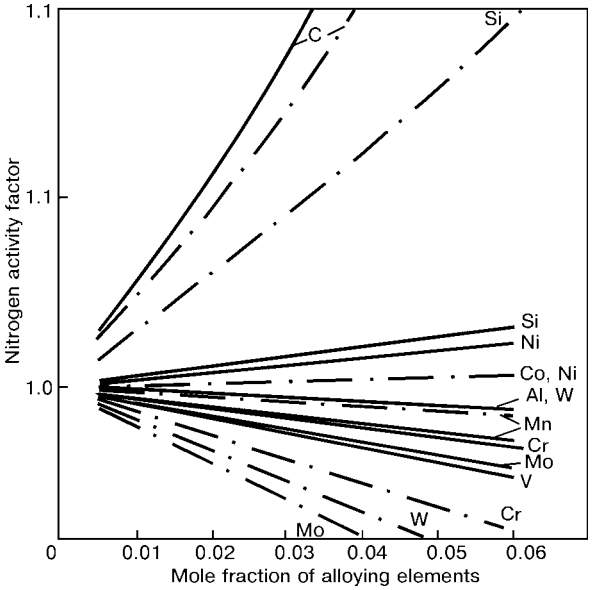

Figure 3. Effect of alloy elements on the solubility of nitrogen in iron: solid line — α-phase; chain — γ-phase

Using a pressure ESR larger amounts can be retained, but the limit remains that of the cast electrode. High-strength ferritic steels have been proposed, for example, for LBGT applications, in which the nitrogen content is very close to the saturation solubility at the liquidus. In these steels, although the nominal nitrogen content can be retained, unless elevated pressures are used the ingot will contain porosity which cannot be removed by forging. One of the questions to be addressed in this study is that of determining what over-pressure must be applied to prevent the formation of such porosity.

It has been proposed that additions of nitrogen directly to the ESR furnace would circumvent some of the above limitations. In order to add a sufficient quantity of nitrogen without seriously changing the alloy composition with respect to other elements there are few potential additives. Compounds such as calcium nitride which would provide only nitrogen to the alloy are not sufficiently stable to permit handling in an industrial system. High-nitrogen ferroalloys do not contain sufficient nitrogen and iron nitride itself has an unacceptable content of oxygen as normally prepared in bulk. The compound most widely used at present is silicon nitride, available in bulk in a good level of purity at an acceptable cost. However, this addition introduces a significant content of silicon into the alloy and can only be used in small amounts in low silicon alloys such as tool steel grades in the H13 class. The problem of a suitable additive for this type of steel remains at present unsolved.

Studies are reported [5] on pressure induction melting in which nitrogen is introduced into the alloy by prolonged exposure of the liquid to a high pressure of nitrogen gas, up to 50 bar. The equipment is complex and at present limited to small volumes of liquid. However, if the casting is also made under a slightly higher pressure, the porosity formed by ex-solution of nitrogen during solidification can be avoided and

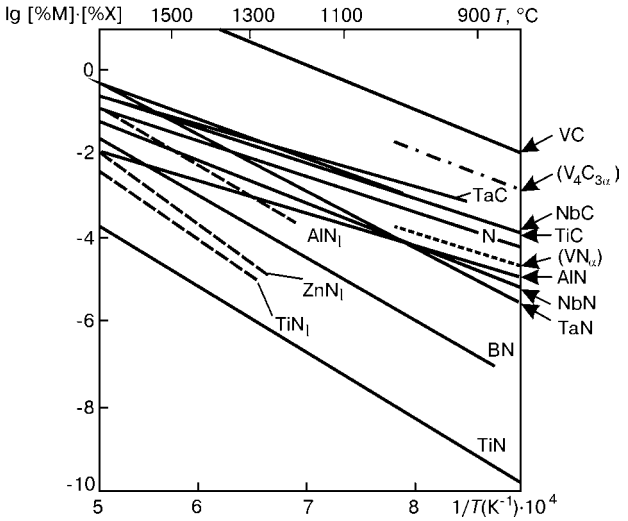

Figure 4. Stability of various nitrides

in this way samples of high-nitrogen steels for experimental work have been prepared.

An alternative technique, proposed by Medovar et al. [6], is to use the ionising property of either a plasma or an arc. The exchange rate of nitrogen across a liquid steel surface has been extensively studied with the conclusion that the rate is controlled by the surface combination or dissociation of nitrogen molecules. Since nitrogen is not surface active in liquid steels the rate is strongly reduced by the presence of surfactants such as oxygen and sulphur in amounts down to the ppm level [7]. In conventional melting techniques such as ESR the oxygen activity in steels is sufficiently high that the nitrogen exchange rate is very slow, leading to the need for additions of nitrides directly into the solution rather than additions from gas-phase nitrogen. The presence of a an atomic nitrogen plasma (either from a nitrogen plasma torch or from the plasma region of an arc through nitrogen gas) greatly accelerates the pick-up of nitrogen by eliminating the need for the dissociation step on the surface since atomic nitrogen is absorbed directly into atomic solution in the metal. This situation also leads to equilibrium contents which are higher than those predicted from Sieverts law. The simplest mechanism for this process is the use of nitrogen blowing in an arc furnace, but plasma torches [8] and the «arc-slag»

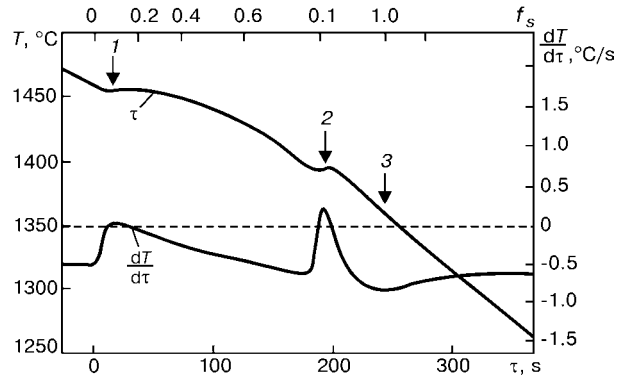

Figure 5. Solidification of H13 steel at a rate of 0.5 °C / s: *1* — onset of ferrite solidification; *2* — austenite initiation; *3* — final eutectic

process [6] have been extensively used for the same purpose. Unfortunately, none of these processes offers the precise solidification control of ESR and although they are potentially useful for the manufacture of steels which are not segregation sensitive, their usefulness in many of the required steel grades appears to be limited. They are, however, processes which could be used for the manufacture of electrodes to be subsequently remelted by ESR. A general review of the melting of high nitrogen steels by various processes is given by Feichtinger [9].

Solidification of high nitrogen steels. *Definition of the problem*. The example steel class studied in this work is that of the hot-work die steel, (Dievar), which is similar to the general grade H13. Dievar composition, wt.%: 0.36C; 0.18Si; 0.5Mn; 0.006P; <0.0001S; 5.3Cr; 0.05Ni; 2.3Mo; 0.002W; 0.54V; 0.001Al; 0.03N.

The purpose of nitrogen substitution for carbon in this composition is to reduce the presence of large carbides and also to increase the secondary hardening capability of the alloy. The mechanical property advantages are summarised in «high nitrogen steels» [10]. This alloy solidifies initially as ferrite and when the composition of the remaining liquid has been sufficiently changed by segregation austenite precipitates leading to a final solidification of a very small amount of carbide eutectic. Nitrogen is relatively insoluble in the ferrite phase, but is much more soluble in the austenitic phase than it is in the liquid at the liquidus temperature. It follows, therefore, that if we were able to convert the solidification mechanism to one in which a suitably large fraction of the solidification were to austenite, there would be no rejection of nitrogen and no formation of porosity in the solid. The definition of this situation is the objective of this study.

Precipitation reactions. Within the general composition of the tool steels there are two possible precipitation reactions:

$$[V] + [N] = VN_{(s)};$$
$$[V] + [C] = VC_{(s)}.$$

Data on these reactions as they relate to solubility products is available in the literature [11] and is shown in Figure 4. It can be seen from this data that the composition of this steel should not precipitate any primary carbide even allowing for the level of microsegregation normally found in large ESR ingots. However, since both V and N segregate strongly in the solidification reaction, it is possible that primary VN could precipitate in compositions with a high level of nitrogen, leading to the presence of undesirable large, hard particles in the final structure.

Solidification structure. A steel with a composition close to that of the present alloy has been studied previously [12] with the results shown in Figure 5. We can observe the formation of a very small amount of eutectic carbide (due principally to the segregation reaction of carbon) but no formation of primary car-

bide. The initial solidification is to ferrite at a liquidus temperature of 1470 °C, followed by the peritectic reaction to austenite at 1412 °C. The austenite primary solidification accounts for approximately 10 % of the solidification process. Since the segregation coefficients of V and N are less than unity (ferrite precipitation is k_V = 0.65, k_N = 0.2; austenite precipitation is k_V = 0.4, k_N = 0.5) it is to be expected that substantial rejection of nitrogen will take place during the formation of the ferrite phase and so either porosity or VN precipitation could arise during this temperature interval. Solidification in the ESR system is quite slow, with solidification times of the order of 1000–4000 s. We would therefore expect that the solidification structures and segregation reactions in an ESR ingot would be close to those predicted by the equilibrium phase diagram. Although the phase diagram for this base composition has not been determined relative to additions of nitrogen, it is possible to obtain a good estimate of the structure and composition changes by using the THERMOCALC programme. When this is done, we find the results shown in Figure 6, when it is seen that since nitrogen is a strong austenite stabiliser, the precipitation reaction can be converted completely to austenite by a sufficiently large nitrogen addition. As a result such a modified alloy would not develop porosity during solidification under ESR conditions.

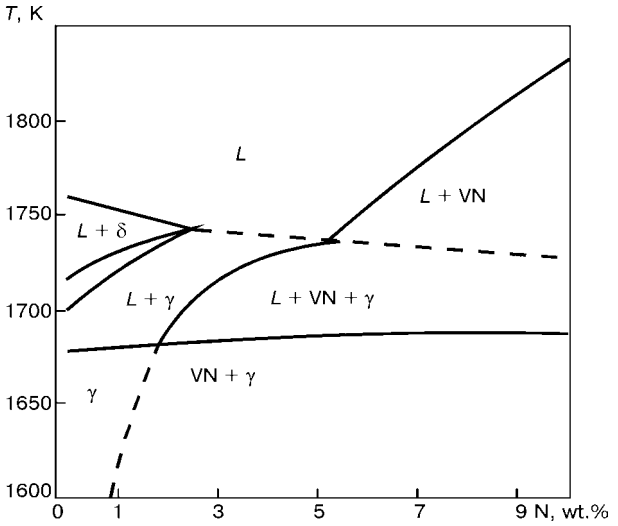

Figure 6. THERMOCALC equilibrium diagram for the Dievar base composition

Experimental programme. *Directional solidification*. ESR ingots in the diameter range appropriate to this study (d < 1000 mm) solidify in a temperature gradient which is a function of radius. However, when combined with the appropriate ingot growth rate, this temperature gradient produces solidification times which are small enough to give columnar-dendritic structures which can readily be reproduced by the laboratory technique of directional solidification. A typical spectrum of secondary dendrite arm spacings in such and ingot would range from 100 μm at the ingot periphery to 400 μm (a cooling rate of approximately 0.05 °C / s in the ingot centre). Typical ingot structures are shown in the literature.

Samples of the steel were processed by the method of directional solidification + quenching (DSQ) in an apparatus shown in Figure 7 under a gradient of 10 °C / mm and a solidification speed of 60 μm / s, giving a cooling rate of 0.6 °C / s.

The sample was quenched when it was partially solid, giving the structure shown in Figure 8 where the dendrite tips can be seen penetrating into the cooling liquid at the liquidus line.

Since the temperature gradient was previously calibrated, the quenched structure could be correlated with temperature in the axial direction. Several features of the structure are of note. First, the initial solidification produces a dendrite network which is relatively open and it is reasonable to expect (as has been assumed in many models of the ESR process) that there will be a significant mixing between the bulk liquid and the interdendritic liquid, thus reducing the level of segregated elements in the latter in this initial stage. The structure rapidly becomes more dense, as previously found and any mixing must be greatly reduced within 10–20 °C below the liquidus temperature. The primary dendrite spacing was ap-

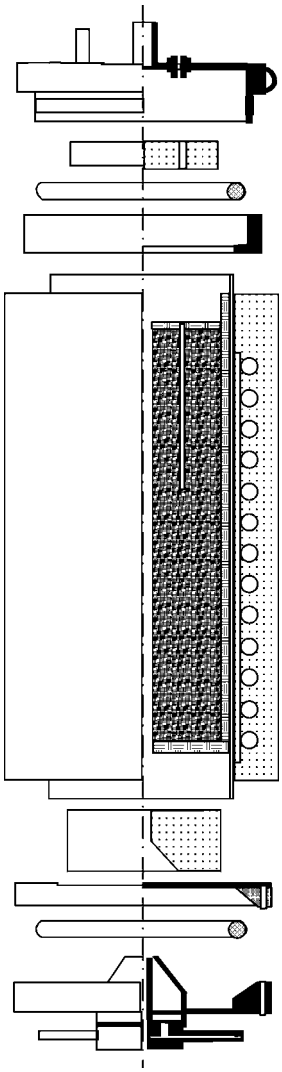

Figure 7. Structure of the directional solidification furnace

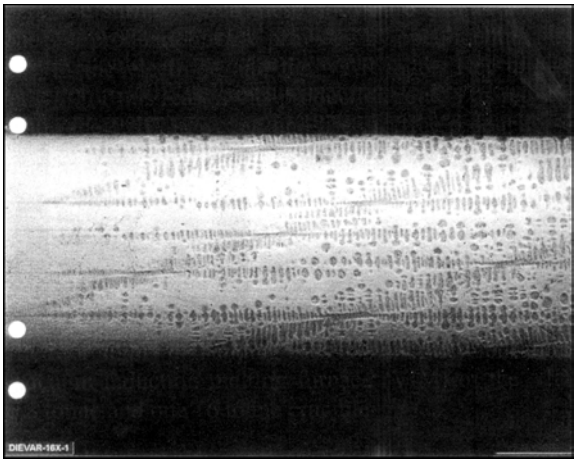

Figure 8. Solidification structure of Dievar

proximately 350 μm, as anticipated from previous work [12].

The structure of the alloy solidified under argon is shown in Figure 9, where it can be seen that almost all of the dendrite structure consists of ferrite, with the final solidification as austenite, followed by a small amount of carbide eutectic.

When the ambient nitrogen pressure is increased to 2 bar, the additional nitrogen content (0.15 wt.%) is not sufficient to produce austenite as the first solid to precipitate, but subsequent segregation converts the precipitation to austenite at a higher liquid fraction than previously observed in argon, but also produces VN precipitates in the final solidification (Figure 10).

Under higher pressures, up to 4 bar, this trend continues until at a nitrogen content of 10 Bar, the initial solidification is to austenite. The nitrogen contents in this alloy composition are at the limits of detection by wavelength dispersive spectrometry (WDS), and so the segregation coefficient of nitrogen could not be determined directly. However, WDS determination of the V segregation could be carried out and confirms the estimates given above for the ferrite phase.

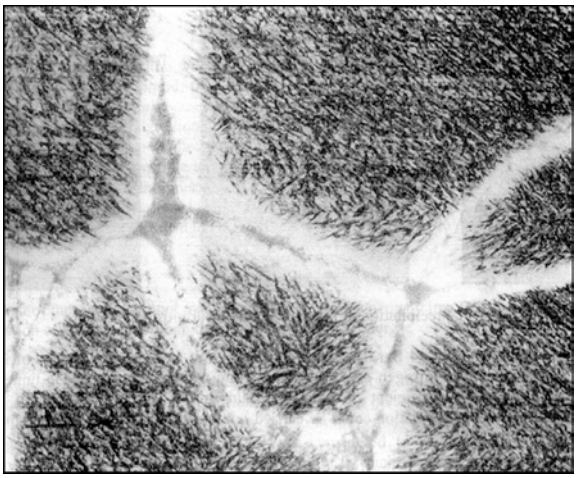

Figure 9. Solidification structure of Dievar showing austenite and final eutectic precipitation (solidification time is 1000 s) (×500)

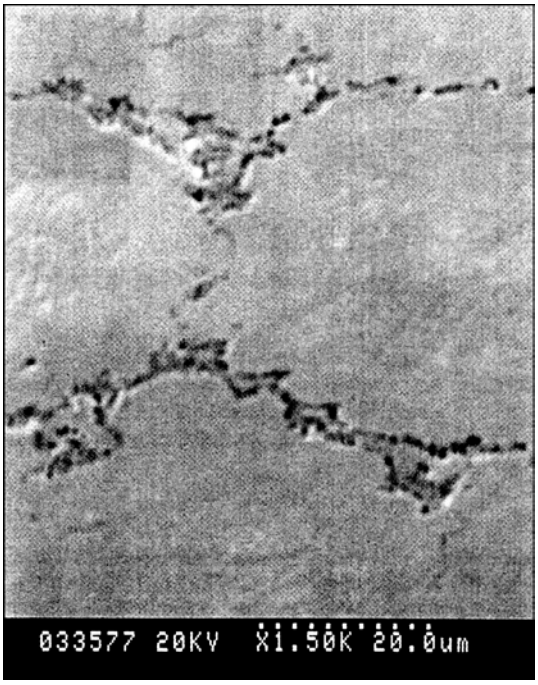

Figure 10. Precipitation of primary VN at the austenite boundary

From the experimental results obtained it can be seen that the addition of nitrogen to the alloy can result in both the primary precipitation of the austenite phase and VN under the solidification rates experienced in ESR.

Discussion. *Relation to the predicted phase equilibria. 1 bar nitrogen contents*. The computed phase equilibria, derived from THERMOCALC as shown above, demonstrate that when the nitrogen content of this alloy is low, as normally manufactured (0.05 wt.% N), the solidification observed is almost entirely to ferrite, with the austenite phase appearing only at the last stage of solidification at a solid fraction of 0.8 (1417 °C), as is reported [12], corresponding to an undercooling of approximately 5 °C. No primary precipitation of VC or VN is seen. When the alloy is deliberately saturated with nitrogen by the addition of CrN at 1 bar pressure of nitrogen, the nitrogen content rises to 0.08 wt.% (as would be predicted from thermochemical considerations of the alloy composition). We observe at this content that although the solidification begins as ferrite, the austenitic phase appears at a much lower solid fraction (approximately 0.4) and we now see small precipitates at the austenite boundaries. The strong rejection of nitrogen from the ferrite phase evidently causes a sufficient concentration increase in the remaining liquid to not only precipitate austenite, but also to cross the boundary of VN precipitation. The primary austenite boundary is reached at 0.2 wt.% N, which is in agreement with the ferrite segregation coefficient indicated above at a solid fraction of 0.4, using the Scheil equation. Further segregation into the liquid by nitrogen rejection from austenite leads to a final liquid composition of 0.5 wt.% N at which point VN is co-precipitated with austenite. If the lever rule is assumed, the final liquid concentration of nitrogen would be 0.38 wt.%,

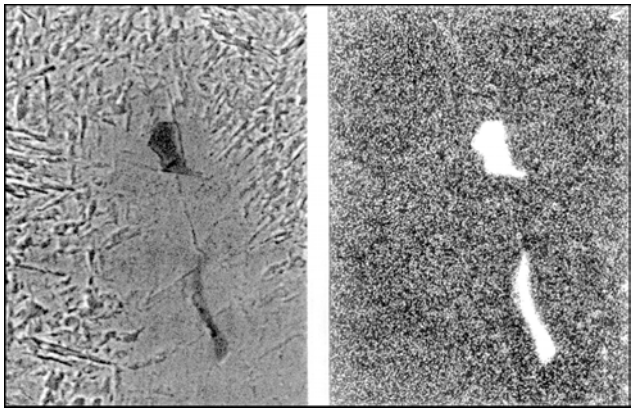

Figure 11. Precipitation of primary VN at 4 bar nitrogen pressure

at which value VN would not be precipitated. It therefore appears from the experimental finding of VN particles that Scheil conditions are appropriate to this case.

Nitrogen contents > 1 bar. When the solidification is carried out under a pressure of 4 bar nitrogen, the liquid composition at the liquidus rises to 0.2 wt.% N. The primary precipitation is ferrite, but the additional amount of nitrogen in solution leads to a much greater precipitation of VN as the austenite phase forms (Figure 11). Additional pressure, to approximately 10 bar would convert the primary solidification to austenite, but at the consequent value of nitrogen content, there would be a rapid onset of VN precipitation with falling temperature, leading to extensive, large primary VN particles in the structure. Previous workers [9] have indicated that with higher pressures the segregation coefficient of nitrogen in the austenite phase rises above unity in which case, therefore, the precipitation of VN should not occur. The work, however, was carried out on 18Mn18Cr steels which may not have the same response to nitrogen pressure as in the present case.

Porosity formation. If a liquid which is in equilibrium with a given nitrogen pressure starts to solidify as ferrite and, therefore, rejects nitrogen into the remaining liquid, the liquid becomes supersaturated with nitrogen with respect to the ambient pressure and should form gaseous nitrogen to be released from the condensed system, i.e. bubbles should be formed in the interdendritic region, leading to porosity in the final solid. The question of how porosity forms in a solidifying alloy has been studied by many workers. The context of the studies varies depending on the form of the casting process and on the alloy concerned. Porosity may form due to solidification shrinkage, gas generation or fluid flow, but in the present case porosity is probably the result of a combination of the first and second of these effects since we do not usually observe extensive macrosegregation defects caused by fluid flow in the solidifying region of the ESR ingot. The pore process consists of a two step reaction: nucleation of the pore and growth of the pore.

Considering the first of these steps, a pore may be nucleated homogeneously in a liquid when the pressure created by ex-solution of gas is greater than the new pore's surface energy:

$$P > 2\sigma / r,$$

where P is the gas pressure; σ is the liquid–gas interfacial energy; and r is the radius of the nucleated pore. Since the interfacial energy of steel–gas interfaces is quite high, the pressure required to nucleate a pore usually exceeds the available gas pressure in «real» systems and so homogenous nucleation is not considered to be the normal way to generate new pores. Instead, pores are considered to nucleate on second-phase particles, principally non-metallic inclusions, which have a size range of r such that the required pressure is within that available from the gas ex-solution reaction. Inserting appropriate values of P and σ in the above equation leads to a value of approximately 10 μm for r when the pressure of gas would be equal to that generated when the solution is supersaturated in nitrogen by a factor of 2×. The implication is that we could prevent gas porosity formation in a typical industrial alloy if the nitrogen content at all stages in the solidification were to be restricted to a level below the 2× supersaturation. Some support for this view is to be found in the literature.

Arola et al. [13] where castings of stainless steels at high nitrogen content were analysed for porosity and the findings related to the presence of alumina inclusions. Castings with many small alumina inclusions formed many micropores, whilst those with low alumina content formed a smaller number of large pores. The porosity was seen to be associated with alumina particles. Since the effect is related to interfacial tension between the particles and the liquid metal, it is also reasonable to assume that features which affect the value of this parameter would also affect the pore nucleation process.

It has been suggested [14, 15] that pore size and incidence could be changed by changing the chemical composition of the inclusions and also by making additions of elements to the alloy which reduce the parameter value, such as S, Se and Te. Most studies on pore formation have assumed, probably correctly, that in the alloys of interest there will always be nucleating particles present, and therefore the item of most interest lies in the growth of the pores, rather than in the nucleation process itself. The pore growth mechanism has been related to dendrite growth during freezing by several workers. Svensson [16] developed a model in which the diffusional transport of the gas to the pore site was balanced against the freezing rate to produce a pore-size distribution which could be tested experimentally. Agreement was found between the predictions and results in the cases of hydrogen and nitrogen porosity formation in steel castings solidified over a range of rates, although in this case the freezing rates were somewhat faster than those found in ESR ingots.

More recently, Rachev [17] has analysed the pore formation process in terms of freezing rate, in nitrogen alloyed tool steels by means of a heat-flow analysis of a conventional casting. The freezing rates were computed from a 2D finite element model of the cast slab and the porosity analysed microscopically. The maximum primary dendrite spacing observed was 220 μm (as opposed to a typical ESR range of 400–800 μm), the solidification speed was 0.35 mm / s and the temperature gradient may be estimated from the published diagrams to be approximately 16 °C / mm. Although these conditions are not the precisely the same as for either DS or a remelted ingot, the data is nonetheless of interest. The pore size under these conditions had an average value of 0.2 mm, i.e. the same as the primary dendrite spacing, and the total porosity was approximately 3 %. The model used is more complex than the diffusional balance considered in [16] since it also takes into account the effect of the pressure reduction due to shrinkage and the modification of this pressure by interdendritic fluid flow. An extension of this general model concept has been presented by Atwood [18]: for the porosity formed by hydrogen evolution during the freezing of aluminium alloys. In this model, the cellular automata technique is used to simulate crystal growth, rather than using the assumptions necessary in a finite element model. The process includes fluid movement, diffusional processes and gas supersaturation and provides a realistic description of the growth process when using a random distribution of nucleating sites of approximately 5 μm in radius, which defines the critical supersaturation necessary to initiate the pore. The model is not directly applicable to the present case since it refers in this form to equiaxial solidification, but illustrates the validity of the concept that a realistic nucleating particle size distribution can accommodate all of the gas evolution likely during solidification.

ESR processing. The relation of the above ideas to the present case of porosity formation in the ESR structure is not direct. In the case of nucleation, although the ESR material is likely to be very clean, there is almost certainly a significant concentration of oxide inclusion particles greater than 10 μm in diameter present in the solidifying region. It is reasonable, therefore, to consider that the nucleation process will be that of gas diffusing to the oxide particle and there forming the pore. Once the pore has been nucleated, depending on its size the nitrogen which it contains may not be re-dissolved on subsequent working and heat-treatment, thereby not only removing it from the alloy's metallurgical properties, but also creating the potential hazard of crack nucleation in the product. If the porosity is dispersed and small, from many nucleation sites, it will be removable by forging in the same way as is the typical shrinkage microporosity present in most as-cast structures. If the alloy is extremely clean and has few nucleation sites, the porosity will be infrequent, but large. It is also possible to conceive of a situation where the growth rate of the solidification front is equal to the growth rate of the pore by gas diffusion and evolution so that the pore will become elongated in the dendrite growth direction. Such elongated, large pores are observed in the case of hydrogen evolution from ESR ingots when the slag used has been unusually wet. They are cylindrical with a diameter comparable with one to four primary dendrite spacings and a length which may be several centimeters in the growth direction. In such cases, growth marks on the pore surface may be observed which correspond to the movement of the bubble of gas creating the pore. Eventually either the pore grows to a diameter which is unstable and the gas bubble detaches from the solidifying surface; or the incoming metal feed becomes lower in gas content and the feeding of the pore is stopped. Pores of this type have also been produced in experimental DS structures [13] at growth rates which approximately twice those of the ESR ingots. They have also been shown to be responsible for some of the «freckle» defect in certain types of high carbon steels [19]. In the present context, the supersaturation of nitrogen is relatively small and the nucleation process must be considered in relation to the progressive rejection of nitrogen into the liquid as the ferrite phase forms and ultimately as VN is precipitated.

It appears that in this range of steel compositions, increasing the nitrogen pressure in order to place more nitrogen in the solid increases the risk of porosity through the accumulation of nitrogen in the residual interdendritic liquid during ferrite precipitation. When the solidification phase changes to austenite, this problem is greatly reduced, but a limit on the nitrogen content is set even in this circumstance by the formation of primary VN. From THERMOCALC considerations it does not appear feasible to convert the solidification entirely to austenite by the application of excess pressure to the ESR furnace since the necessary pressure is unrealistically high. It is therefore desirable to change the steel composition to one in which the onset of primary nitride precipitation is suppressed, but in which the solubility of nitrogen is such that a moderate pressure in ESR can produce the contents required for secondary hardening. The requirements for such a composition change would be that the element substituting for V should not be a strong nitride former and not strongly stabilise the primary ferrite phase. If this change is made, from the above considerations it appears that a pressure of no more than 2–3 bar would be required to maintain the necessary nitrogen content. The pressure could be applied as either Ar or N, since the transfer of nitrogen to or from the gas phase in ESR is small unless a large amount of either Al or Ca is added to the slag during melting. (This type of addition is not normally used in this range of steels due to its tendency to promote the formation of large oxide inclusions.) Nitrogen itself is relatively insoluble in ESR slags. The solubility at 1 bar is in the range of 0.02–0.04 wt.% at the

liquidus temperature depending on the CaF_2, CaO and Al_2O_3 contents [20, 21]. The nitrogen activity, however, is greatly increased when the carbon potential is high, due to the formation of the CN^- ion rather than N^{3+}. The necessary carbon potential for this reaction to occur is much higher than that encountered in steel remelting, requiring effectively carbon saturation of the metal–slag system. The problem of nitrogen addition to the electrode or ESR process in quantities exceeding the 1 bar saturation solubility in the liquid remains to be defined, but ideally would be made using a low silicon, high nitrogen chromium or iron material with low oxygen content.

CONCLUSIONS

We may conclude from the above study that two phase or peritectic solidification in ESR ingots is under conditions which are close to the thermodynamic equilibrium and may be determined by directional solidification experiments or by using existing thermochemical models of solidification. The peritectic, V- and N-containing tool steels studied have a optimum nitrogen content of approximately 0.1 wt.%, corresponding to a pressure of 1.4 bar for saturation of nitrogen in the liquid phase. Segregation then produces only a small amount of VN primary phase as small particles but leaves sufficient nitrogen in solution for the required hardening reactions. Changing the composition of the steel as indicated above shows promise for increasing the nitrogen-driven hardening characteristics without the need for excessive pressures in either the preparation of the electrode or in the ESR process itself.

Acknowledgements. The author is indebted to the provision of financial support from the Royal Technical University and the Uddeholm Tooling Corp. A substantial part of the experimental work was carried out by Dr. Fjellstedt and the technical staff of the KTH.

1. Humbert, J.C., Elliot, J.F. (1960) *Transact. AIME*, **218**, 1076–1088.
2. Pehike, R.D., Elliot, J.F. (1960) *Ibid*., 1088–1100.
3. Fisk, K. (1990) *PhD Thesis*. Stockholm: RIT.
4. Paton, B.E., Medovar, B.I., Saenko, V.Ya. et al. (1990) *Problemy Spets. Elektrometallurgii*, **3**, 4–13.
5. Rachev, Ts. (1995) *High nitrogen steels — metallurgy under pressure*. Sofia: Acad. Publ. House.
6. Medovar, B.I., Saenko, V.Ya., Grigorienko, G.M. et al. (1996) *Arc-slag remelting of steels and alloys*. Cambridge Int. Sci. Publ.
7. Kamardin, V.A., Antropov, O.F. (1973) *Izvestiya AN SSSR*. Metally, **6**, 49–56.
8. Grigorenko, G.M., Pomarin, Yu.M. (1989) *Hydrogen and nitrogen in metals in plasma melting*. Kiev: Naukova Dumka.
9. Feichtinger, H.K., Stein, G. (1999) *Materials science forum*. Vol. 320, 261–270.
10. (1999) *Materials science forum*. Ed. by H. Hanninen et al. Vol. 318–320). Trans. Tech. Publ.
11. Houghton, D.C. (1993) *Acta Metall. Mater.*, **41**, 2993–3006.
12. (1977) Guide to the solidification of steels. *Steel*, **302**, 58–59.
13. Arola, R., Wendt, J., Kinineva, E. (1999) *Materials science forum*. Vol. 318–320, 297–302.
14. Wendt, J. (1998) *COST 512: Modelling in materials science and processing*. Final report. Ed. by M. Rappaz et al. Brussels. 11–16.
15. Svyazhin, A.G., Skuza, Z., Hutny, A. (1999) *Materials science forum*. Vol. 318–320, 377–384.
16. Svennsson, I., Frederiksson, H. (1980) Solidification technology in the foundry and casthouse. *Metals Soc.*, 376–380.
17. Manolov, V., Yotova, A., Bijev, S. et al. (1999) *Materials science forum*. Vol. 320, 341–346.
18. Atwood, R.C., Lee, P.D. (2002) *Met. Transact.*, **33B**, 209–221.
19. Mitchell, A. (1972) *Ironmaking and Steelmaking J.*, **2**, 198–204.
20. Shimoo, T., Kimura, H., Kawai, M. (1971) *Nippon Kinzoku Gakkaishi*, **35**, 417–422.
21. Schwerdtfeger, K., Schubert, H.-G. (1977) *Met. Transact.*, **26**, 502–531.

Comments of Editorial Board. The present article is a shortened variant of the paper presented at the International Symposium on Special Electrometallurgy LMPC-2003 (Nancy, France, September 2003). By its publication the Editorial Board tried to attract attention of the readers to some aspects of production of steels with a super-equilibrium content of nitrogen. These steels find the more and more wide spreading in industry. It should be noted that, except 16 bar pressure of ESR industrial furnaces mentioned in the article, the ESR furnace of chamber pressure up to 40 bar is operated successfully over many years at the VSG Company in Germany. And not long ago a unique ESR chamber furnace with pressure up to 80 bar was put into operation at the Italian Research Center of Materials (this information will be published in the next issue of the journal). It is quite evident (and this is confirmed by the data of investigations) that different pressure is required for alloys of different types to produce dense ingots with a super-equilibrium content of nitrogen. For the practical purposes, the pressure below 5 bar represents a special interest as the chamber furnace design in this case is much simpler than at pressure above 5 bar, where the requirements are valid applied to the high-pressure vessels. Generally, the key problem in the production of high-nitrogen steels is connected with methods of alloying by nitrogen. Statement of the authors about the expediency of use of the silicon nitride instead of a direct alloying from the gas phase contradicts the data of many-year investigations carried out at the E.O. Paton Electric Welding Institute. Nevertheless, the methodological approaches described in the present works, are very useful for the metallurgists working with high-nitrogen steels. The Editorial Board is looking forward to continue the publications on this actual subject.

APPLICATION OF ELECTROSLAG MELTING FOR PRODUCTION OF FERROALLOYS FROM MINERAL RAW MATERIAL

M.L. ZHADKEVICH, F.K. BIKTAGIROV, V.A. SHAPOVALOV, A.P. IGNATOV and **A.V. GNATUSHENKO**
E.O. Paton Electric Welding Institute, NASU, Kiev, Ukraine

It is shown that the electroslag melting with non-consumable electrodes has much in common with a multi-slag ore-thermal process. In either case the power is generated mainly in the condition of resistance, which is a molten slag. Therefore, the electroslag melting is rather suitable for the processing of mineral raw material with a selective recovery of metals in case of producing of a large amount of slag melt (slag ratio is 3–4 and more), that was confirmed, for example, in melting out of titanium slag from ilmenite concentrate.

Keywords: electroslag melting, ore-thermal furnaces, mineral raw material, ilmenite concentrate, ferrotitanium, vanadium-containing master alloy

Most metals are available in nature in the form of compounds with other elements, for example, different ores and minerals, in which the metals are located mainly in the form of oxides. Except the natural compounds, various waste materials in the form of slags, slime, ash and others, containing compounds of metals, are accumulated in use of different production processes and can be used as a raw material for metal extraction.

Electroslag melting (ESM) with application of non-consumable electrodes for conductance of the electroslag process is well-known and used widely for heating or melting of metal, contacting with a molten slag, earlier produced in any other melting unit, and also for recycling of different metallic and metal-containing waste materials. Numerous examples of this application are given in works [1–3].

At the same time the ESM can be used also in the production (melting) of metal products directly from initial mineral raw material (ores, concentrates, slags, different non-metallic waste) similar to the processes realized in other metallurgical units, in particular in ore-thermal furnaces, designed for producing ferroalloys, master alloys and alloying elements.

Similarity of ESM with ore-thermal melting is noted in work [4]. Unlike the pure arc melting, where the power is generated in a column of arc, burning between the current-carrying electrode and an object heated, the power in the most widely spread types of ore-thermal melting is generated both in arc and also in resistance which may serve a current-conducting charge and a formed slag melt. Depending on the raw material being processed, type and content of fluxing and reducing components, and also some other factors, the relation between these kinds of power can be different.

In ESM with non-consumable electrodes a part of energy can generate in arc condition due to the presence of an electrode contact resistance at the electrode–slag interface and formation of microarcs here, especially in the period of melting of slag-forming elements (of charge). Therefore, according to work [5], both the ore-thermal and also electroslag installations refer to the group of electric arc furnaces of resistance, moreover, the electroslag installations refer to the furnaces with an under-developed arc discharge where the share of power, generated in arc, is less than 10–20 % of the total power.

Theory and practice of ore-thermal melting of ferroalloys is well-studied and developed [6, 7]. Due to use of various raw materials and producing different products (from most widely spread ferromanganese and ferrosilicon and up to such products as alloys of iron with rare-earth-metals), the ferroalloy production is characterized by a variety of used technologies and equipment. By the mode of melting conductance the ore-thermal processes, in which the power is generated in slag mass and operation is performed using closed arcs (electrodes immersed into slag) and a hot top, are most close to the electroslag process. These are so-called multi-slag processes when the charge melting is accompanied by the formation of a large amount of slag, and a slag ratio, i.e. ratio between the mass of the forming slag and metal, reaches 2.5–3.5 and more. And with account for the difference in a specific mass of a molten slag and metal the volume of the former exceeds the volume of the latter.

It is rational for the multi-slag processes from the power point of view to use melting by conversion of electrical power into heat power at the expense of the slag resistance. In this case the power is generated inside the slag pool in the entire its volume, the powerful convective flows are formed, providing the uniform heating of slag and intensification of the supplied charge melting.

In arc condition of melting the heat is spread only to slag layers adjacent to the arc discharge, while the rest its mass is heated owing to heat transfer in a slag pool. The effective coefficient of slag heat conductivity, especially in arc burning over the slag, occurred to be lower than in conductance of melting in the

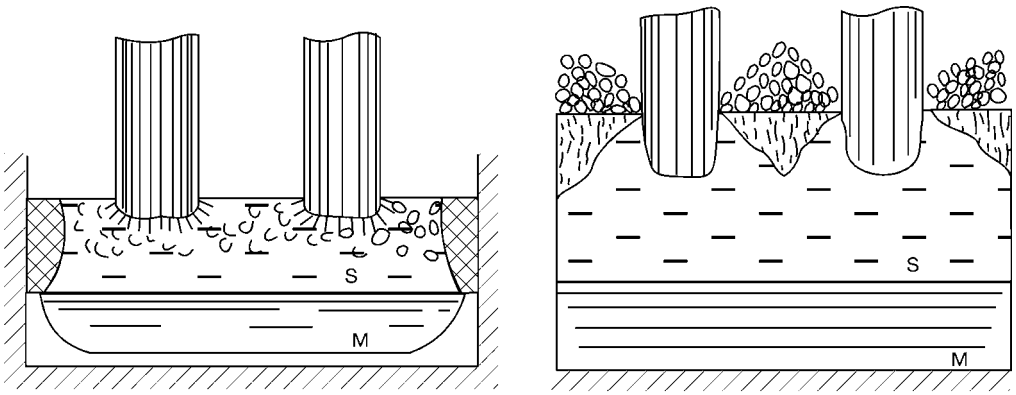

Figure 1. Scheme of arrangement of materials in a pool of multi-slag ore-thermal furnace in melting of ferrotungsten (*a*) and Cu–Ni matte (*b*): S — slag; M — metal

resistance condition due to a weaker thermogravitational and electromagnetic stirring of the molten metal in this case. Besides, the absence of arc and local slag overheating decreases the loss of easily-oxidizing components, and also those having a comparatively low temperature of melting and high vapor pressure.

Figure 1 shows the typical scheme of a melting pool of an ore-thermal furnace in melting of ferrotungsten and Cu–Ni matte [6]. In the first variant the charge is immersed into a layer of the molten slag due to a high specific weight of the tungsten concentrate, and melting is proceeding mainly with an open mirror of the slag pool. The lighter charge can cover completely or partially the slag surface (Figure 1, *b*). But in any case the electrodes are immersed into molten slag, the power, generated at the expense of resistance of this slag, exceeds significantly the power, generated in arc transition, i.e. the ESM is realized in principle. Therefore, many statements and relationships, determined for the similar ore-thermal melting, are suitable also for ESM. However, they concern mainly mass production in large-tonnage ore-thermal furnaces allowing melting tens and hundreds of tons of products per day. And in case of ESM it is necessary to take into consideration that it is designed mainly for small-serial production in furnaces of capacity from hundreds of kilograms up to several tons. In addition, the electroslag installations have their peculiarities connected both with used power sources and also with a condition of their service.

Due to small dimensions of ESM furnaces, operating with a hot top, their efficiency factor is lower than that of the ore-thermal furnaces. By this parameter, the electroslag furnaces operating with an open mirror of the slag pool are close to the arc furnaces where, due to the presence of open arc, the heat losses are also relatively high by radiation and with exhausting gases [4]. Electrical efficiency factor of electroslag furnaces is very high due to operation in the condition of resistance and is 0.85–0.95. Due to this, the overall power factor of ESM furnaces is at the level of values of this characteristic for arc furnaces.

The ESM furnaces, being inferior to ore-thermal furnaces by power consumption, have also a number of advantages. The ore-thermal furnaces are designed more often for production of definite ferroalloy from the raw material of a definite deposit. Coming from this, the power source, design of furnace and conditions of its operation are selected. In case of changing the composition of charge materials, for example, in transition for raw material from another deposit, the significant expenses are often required for the furnace modification and optimization of the melting technology.

The electroslag furnaces are more flexible and can be used without great changes for melting of various raw materials, including that having comparatively small resources. In addition, they are simpler in maintenance, they require smaller capital investments in putting into operation, they can be arranged near stocks or accumulation of the material to be recycled.

One more rather important advantage of the comparatively small furnaces owing to the feasibility of a flexible varying of the technological process is the increase in a degree of extraction of the required component from the initial material into the metal being produced, i.e. decrease in losses of important and expensive elements.

Thus, the ESM of the mineral raw materials to produce ferroalloys and master alloys is suitable, as a rule, in those cases when a large amount of slag melt is formed in charge processing, whose heating can be realized mainly in the resistance condition. The high slag ratio is attained in use of raw material with a low content of the main element or when a large amount of fluxing components is added to the charge to attain the necessary melting properties (melting temperature, electric conductivity, viscosity) by a slag melt.

One more branch of application of ESM of mineral raw material are the processes, the final product of which is the slag enriched by a required component due to a selective recovery into a metallic phase and removal of other elements from it. The classic example of this process is the melting of titanium slag.

The present titanium production is based on a multi-stage processing of the so-called titanium slag produced by the ore-thermal melting of a Ti-containing concentrate, in particular, ilmenite. The latter represents mainly (by 90–93 %) the compound of iron oxides with titanium oxides of $FeO{\cdot}TiO_2$ with a low content of impurities SiO_2, Al_2O_3, MnO and others. The titanium content in ilmenite in recalculation for TiO_2 is usually 50–55 %.

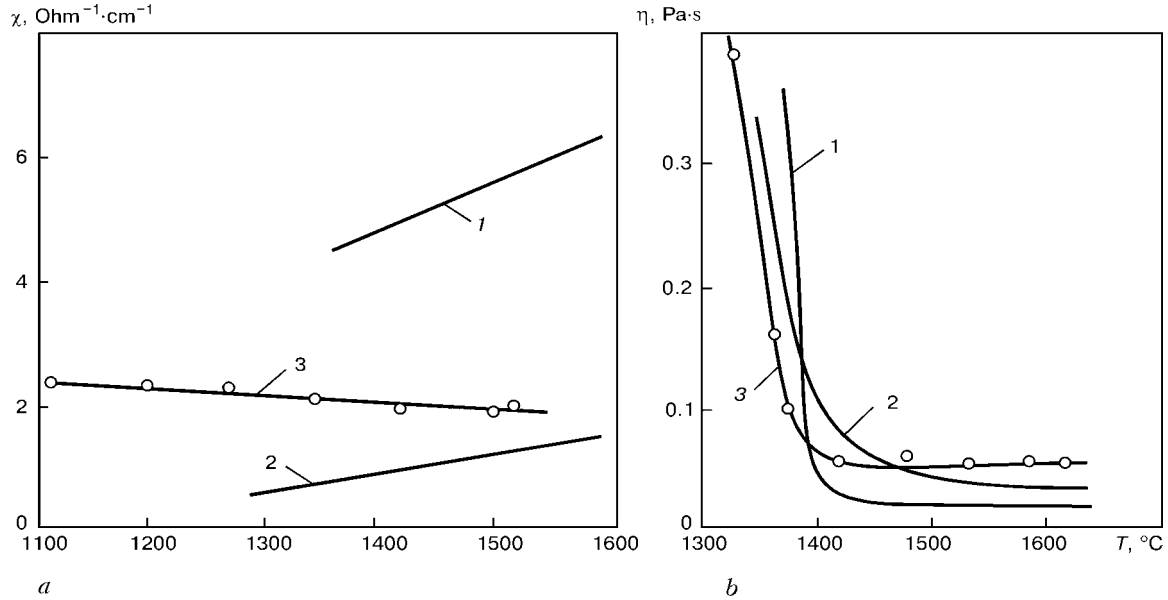

Figure 2. Physical properties of ilmenite concentrate and some slags of ESM: *a* — electric conductivity χ; *b* — viscosity η; *1* — ANF-1P; *2* — ANF-6; *3* — ilmenite

To produce the titanium sponge, it is necessary to produce slag containing not less than 80 % of titanium oxide, not more than 5 % of iron oxides, and also minimum of other oxides. The increase of TiO_2 concentration in slag is attained by a selective recovery of iron oxides from ilmenite. For this purpose, the carbon, containing a reducing agent, more often a crushed coke, is added into the charge. The iron oxides under the conditions of this melting are the thermodynamically less resistant than the titanium oxides and recovered in the first turn. As a result, the produced slag melt is enriched gradually by titanium oxides.

Owing to the formation of a large amount of slag in ilmenite melting (slag ratio is usually 5–6), the process is carried out by electrodes, immersed into slag, using mainly the resistance conditions, which is promoted by a high electric conductivity of the initial ilmenite. For FeO–TiO_2 system at 45–50 % titanium oxide content the electric conductivity of the molten metal under the conditions of 1300–1500 °C is at the level of 30 $Ohm^{-1}\cdot cm^{-1}$[8].

According to the carried out investigations, the electric conductivity of the ilmenite concentrate of Irshansk ore-dressing plant is 2.0–2.5 $Ohm^{-1}\cdot cm^{-1}$ (Figure 2, *a*), i.e. impurities, available in it, increase the resistance. By this characteristic it is close to slag of ANF-6 type. Moreover, the ilmenite has this conductivity even in a solid state at temperature about 1000 °C which is not almost changed in transition from solid into molten state.

The ilmenite melt is typical of a slight dependence of electric conductivity on temperature. Moreover, unlike other salt-oxide melts, the electric conductivity of ilmenite is decreased with increase in temperature. This proves that the Ti-containing slags are characterized not by ion conductivity, but by electron conductivity. Therefore, with increase of TiO_2 content in it the resistance of melt is abruptly decreased and highly-titanium slags approach by electric conductivity to metals [9].

Temperature of melting (1320–1350 °C) and viscosity (Figure 2, *b*) of initial ilmenite are also close to those of some slags used in electroslag technologies. Experiments, carried out in electroslag furnace of 260 kV·A capacity, showed that ilmenite melting using resistance condition at properly selected electrical parameters does not cause any difficulties.

Ilmenite concentrate, except its use in titanium sponge production, is the main raw material for producing ferrotitanium. The work [10] describes technology of melting of 25–35 % ferrotitanium from ilmenite using aluminothermic method. In this case the initial power necessary for slag formation and attaining of the required temperature, when the reduction of titanium oxides is proceeding actively, is generated owing to a heat of reactions of interaction of aluminium with oxidizers added to the charge.

To decrease the melting temperature of the forming slag, the fluxing components are also added. This promotes the additional use of aluminium, except that required for reduction of iron and titanium oxides. It is possible to decrease the aluminium consumption by melting ilmenite in electric thermal furnace, for example in electroslag furnace, and subsequent adding of reducing component into the prepared Fe–Ti slag. It is possible to increase the degree of titanium reduction into metal, and also to create the conditions for the better metal separation from the slag by attaining of required temperature parameters and application of different variants of aluminium adding. This technology of melting of a low-percent ferrotitanium is used successfully at some enterprises of Ukraine, having large resources of the ilmenite concentrate.

In electric melting of ilmenite concentrate the additional reserve for improving the profitability of ferrotitanium production is the use of the cheaper C-containing reducing component for transfer of iron from slag into metal instead of aluminium. For this purpose, similar to titanium production, the slag, enriched with titanium, is melted and then subjected not to the chlorination and Mg-thermic reduction to

produce the titanium sponge, but to aluminothermic reduction to produce the ferrotitanium. Here, to produce 70 % ferrotitanium there is no need in deep removal of iron oxides from ilmenite. With decrease in a share of iron oxides in $FeO–TiO_2$ system the physical properties of the melt are abruptly changed. Thus, at 5–7 % FeO content the melting temperature is increased up to 1600–1700 °C, and the electric conductivity is more than 100 $Ohm^{-1}·cm^{-1}$ [9]. Therefore, in melting of the highly-titanium slag the fluxing components (lime or soda) are added into charge, reducing the temperature of melting and electric conductivity of the melt. In electroslag melting of ilmenite to produce 70 % ferrotitanium in case of reduction of 80 % Ti, contained in concentrate, the residual content of FeO can amount to 15–18 %. This greatly facilitates the melting conductance, including the decrease in its time, because with decrease in FeO amount and minimizing of its activity the processes of reduction of iron oxides by carbon are delayed. Besides, the consumption of fluxing components is decreased, whose effect on subsequent process of reduction of titanium oxides by aluminium is not adequate.

The carried out complex of investigations showed that ESM allows producing 70 % ferrotitanium from ilmenite concentrate, corresponding by all the parameters to the technical conditions for the given product [11]. At present the works are carried out for correction and optimizing the given technology.

As one more example of ESM of mineral raw materials it is possible to mention the technology of recycling of ashes and slimes of heat electric stations operating on residual oil. The latter contain from 10 up to 30 % of vanadium compounds. Different processes of utilization of similar waste with extraction of vanadium are being developed [12, 13]. The pyrohydrochemical methods require the consumption of a large amount of expensive reagents and are not safe ecologically. The problem of the metallurgical processes is the presence of a significant amount of sulphur and carbon in ashes which contaminate the ferrovanadium produced in their melting.

Over the recent years the data have been appeared about the development of technologies of preliminary preparation of similar ashes allowing their granulation and decrease in content of undesirable impurities [14, 15]. In this case the metallurgical methods of processing, in particular those based on silicon or aluminothermic reduction of vanadium oxides from melt, become most effective, as the they allow maximum extraction of vanadium. Among them, the ESM is most suitable due to formation of a large amount of slag in melting of charge containing reducing and fluxing components for binding the reaction products. Laboratory and industrial meltings carried out with participation of the scientific staff of the E.O. Paton Electric Welding Institute, confirmed this fact. From the ashes of the heat electric station with use of 75 % FeSi, as a reducing component, the ferrovanadium was melted containing 35–37 % V suitable for steel alloying [16].

Not only the process of recycling of V-containing ashes, but also the melting of standard ferrovanadium from commercial pentaoxide of vanadium V_2O_5, moreover, the V-containing master alloys from V-containing converter slag, should proceed successfully in the electroslag condition.

According to data of works [17, 18], the developed technology of a single-stage recycling of converter slag, containing 16–20 % V_2O_5 and approximately the same amount of SiO_2, with producing of master alloy with 1–12 % V in ferroalloy furnaces, envisages the adding of lime, 75 %-ferrosilicon and fluorspar to the charge in such amounts that the forming metal and slag melts have the mass ratio of approximately 1:4, and volume ratio of not less than 1:12.

The composition of the produced slag consists of 80–85 % of compounds of oxides of calcium and silicon ($CaO·SiO_2$, $2CaO·SiO_2$), and as to the data of work [8] the electric conductivity, temperature of melting and viscosity of these melts, moreover at the presence up to 5 % CaF_2, favors the melting conductance in the resistance condition.

The carried out analysis and experimental investigations showed that the ESM as a method of processing of mineral raw material has its fields of application and can be successfully used for producing ferroalloys, master alloys and alloying components from appropriate non-metal charge.

1. Biktagirov, F.K. (2002) Application of electroslag process with non-consumable electrodes for melting, refining and treatment of metals. Report 1. *Advances in Electrometallurgy*, **4**, 9–14.
2. Biktagirov, F.K. (2003) Application of non-consumable electrode electroslag process for melting, refining and treatment of metals. Report 2. *Advances in Electrometallurgy*, **1**, 4–8.
3. Ryabtsev, I.A., Kuskov, Yu.A., Kuzmenko, O.G. (2003) Metal waste processing using the electroslag technologies. *Vest. Mashinostroeniya*, **11**, 76–80.
4. Lyuty, I.Yu., Latash, Yu.V. (1982) *Electroslag melting and refining of metals*. Kiev: Naukova Dumka.
5. Dantsis, Ya.B., Ershov, V.A., Zhilov, G.M. et al. (1984) *Electrothermal processes of chemical technology*. Leningrad: Khimiya.
6. Strunsky, B.M. (1972) *Ore-smelting furnaces*. Moscow: Metallurgiya.
7. Gasik, M.I., Lyakishev, N.P., Emlin, B.I. (1988) *Theory and technology of manufacturing of ferroalloys*. Moscow: Metallurgiya.
8. (1985) *Atlas of slags*. Ed. by I.S. Kulikov. Moscow: Metallurgiya.
9. Garmata, V.A., Gulyanitsky, B.S., Kramnik, V.Yu. et al. (1978) *Metallurgy of titanium*. Moscow: Metallurgiya.
10. Lyakishev, N.P., Pliner, Yu.L., Ignatenko, G.F. et al. (1978) *Aluminothermics*. Moscow: Metallurgiya.
11. Biktagirov, F.K., Shapovalov, V.A., Ignatov, A.P. et al. (2004) *Application of electroslag melting to produce the ferrotitanium from ilmenite concentrate*. Tbilisi.
12. Slotvinsky-Sidak, N.P., Zhukovsky, T.F. (1997) Recycling of vanadium-containing wastes of heat power plant. *Teploenergetika*, **2**, 55–58.
13. Kostyakov, V.N., Najdek, V.L., Poletaev, E.B. et al. (2004) Reduction of vanadium oxides in iron-carbon melt. *Protsessy Litia*, **2**, 3–5.
14. Chernousov, P.I., Ivanov, A.V., Pashkov, N.F. (2000) New technology of vanadium extraction from ash of heat power plants using the residual oil. *Izvestiya Vuzov, Chyorn. Metallurgiya*, **11**, 64.
15. Yusfin, Yu., Chernousov, P., Petelin, A. et al. (1998) Vanadium from ash. *Metally Evrazii*, **5**, 72–73.
16. Protsko, P.P., Prokhorenko, K.K., Lychko, I.I. et al. (1998) Wasteless processing of ashes and slimes of heat power plants operating on residual oil. In: *Proc. of Seminar on Environmental Protection*, Alushta, 1998. Kiev: Znanie.
17. Filippenkov, D.A., Deryabin, Yu.A., Smirnov, L.A. (2001) *Effective technologies of alloying of steel by vanadium*. Ekaterinburg.
18. Bajramov, B.I., Zajko, V.P. (1981) Melting of vanadium-containing master alloy. *Stal*, **7**, 37–39.

APPLICATION OF BIMETAL AND REFRACTORY MATERIALS IN ESR MOULD DESIGNS

K.A. TSYKULENKO, B.B. FEDOROVSKY and **A.K. TSYKULENKO**
E.O. Paton Electric Welding Institute, NASU, Kiev, Ukraine

Feasibility of increase in ESR mould service life is considered, factors influencing the fracture resistance of copper water-cooled mould walls and ways of its improvement are analyzed. New designs of current-carrying ESR moulds using bimetal and refractory materials, in selection of which the type of material being remelted should be taken into account, are described.

Keywords: ESR moulds, intensity of fracture of mould copper wall, process of electrocorrosion, process of electroerosion, repairability of mould, bimetals, refractory materials

It is known [1, 2] that during the process of electroslag remelting (ESR) in a copper water-cooled mould its wall is fractured due to passing of a part of current in electrode–slag–mould wall circuit. The fracture consists in appearance of pockets and cavities at the mould working surface which are increased with time both in sizes and amount, thus resulting in mould coming of order. The repairability of the copper mould is rather low. To repair the defects formed in hardfacing of the mould working surface, it is necessary to heat the copper sleeve as a whole.

Depending on the conditions of the electroslag process the intensity of the above-mentioned fractures can be different. Stationary moulds, in which the electroslag process is carried out at comparatively low coefficients of filling, are subjected to this type of fractures to the least extent. Walls of short movable moulds are fractured more intensively. This caused by the fact that a slag pool at a relative displacement of ingot and mould is constantly in contact with one and the same area of its wall. The fracture rate of the mould copper wall depends also on the composition of slag and mean density of current in the site of wall contact with the slag.

Authors of the work [2] came to the conclusion that the intensity of fracture of the mould copper wall structure depends on the density of current passing through it: for example, at current density above 3 A / cm^2 (in case of electroslag process using fluoride slags) it is increased jump-like. To protect the mould copper wall from fracture, it was suggested to decrease the value of current passing through the wall (for example, by using an additional adjustable resistance in the mould circuit) or to coat it with a layer of metal which is more resistant against the anodic fracture than copper. Here, the metals, which are more resistant against electrocorrosion in fluoride melts (as compared with copper), are molybdenum, tungsten, niobium, titanium, zirconium and iron, while nickel, cobalt, iron and aluminium (arranged in the order of resistance increase) are the more resistant against the electric spark fracture (electroerosion).

It seems, if the iron is the more resistant material against the electrocorrosion and electroerosion (as compared with copper), so steel should be used as a material for the water-cooled mould. It has the higher temperature of melting than copper, and at current density 40 A / cm^2 and holding in slag for 1.5–2.0 h it is not almost fractured [2]. In addition, the repair of a steel mould (repair of defects at its working surface) is much simpler than that of copper mould.

Everything is due to the heat conductivity of the material. It is known that copper, having a lower melting temperature, is characterized at the same time by the higher heat conductivity: it removes a large amount of heat from the mould working surface to the flow of water, cooling the mould. At similar thickness of mould wall and cooling parameters of a water channel (pressure and temperature of cooling water) the temperature of surface of steel mould water-cooled channel will be higher remarkably than that of copper mould. In service of steel mould a layer of scale, whose thickness is increased quickly, is formed at the water channel surface due to action of high temperature and possible local boiling of cooling water near its wall at the surface of the water channel. In this case the heat conductivity of this layer is negligible. Formation of the layer with a low heat conductivity at the surface of steel water-cooled channel leads to an abrupt reduction in gradient of temperatures in the steel mould wall and, consequently, to its burn-out. The possible water entering the slag and mirror of the metal pool causes the emergency situation. Therefore, in spite of earlier attempts to use steel moulds in the industry, almost all moulds for the standard ESR process are copper water-cooled designs at present.

The progress and improvement of electroslag technology have led to the separation of processes of melting and solidification of metal and to the creation of electroslag technologies of remelting and cladding using liquid metal. To realize these technologies the mould with a current-carrying section, fulfilling the function of a non-consumable electrode, is used.

The design of this mould (Figure 1) was suggested for the first time by G.V. Ksyondzyk and a group of scientists of the E.O. Paton Electric Welding Institute [3, 4].

In this mould the current density is much higher than the mentioned value (3 A / cm^2). Taking into account that the mould–ingot circuit is the main electric circuit of the electroslag process, the only method to prevent the fracture of the current-carrying section is the protection of its working section by the material which has a lower susceptibility to anode fracture than copper.

Molybdenum, tungsten and graphite were offered as this material. The practical realization of this problem was the creation of a composite design of the current-carrying section of the mould, i.e. a water-cooled copper water-jacket, protected by a changeable graphite ring. After the definite quantity of melts the worn-out graphite ring is replaced by the new one. The wear of the graphite ring is connected not so much with the anodic fracture, but with a high-temperature oxidation of graphite, occurring near the slag pool surface. The changeable rings of molybdenum or tungsten did not find the application due to a low resistance of these materials to oxidation at temperatures of the electroslag process (that leads to their quick coming out of order) and also due to their high cost.

The mould of the mentioned design (with a changeable graphite ring) is used in cladding of mill rolls of high-carbon materials. Transition of a small amount of carbon through slag into metal (with wear of graphite ring) is not a basic problem for the mentioned materials. However, the application of graphite as a material for the working surface of the current-carrying section is not admissible in remelting of steels and alloys with an ultra-low content of carbon. One more problem, occurring in use of the graphite ring for the protection of the water-cooled copper wall, is its dimensions. Thus, for melting large ingots (of 700 mm diameter and more) the mould and, consequently, graphite protective ring of appropriate sizes are necessary, whose manufacture represents a serious industrial problem.

To avoid the graphite enter into the metal pool and to increase the repairability of such mould, the current-carrying section was suggested to be manufactured of two parts, i.e. an inner sleeve, made from bimetal, and an external jacket. One of the possible types of bimetal is the copper–steel pair, representing a compromise solution between the copper and steel moulds. Layer of bimetal, contacting the external jacket, is made of copper, being the heat- and electrically-conductive material, providing a good heat removal from the second (steel) layer, contacting directly the slag pool and subjected negligibly to anode fracture. Components of steel (inner) layer at their entering the metal being remelted and clad (in any steel, including that with ultra-low content of carbon) do not change its properties.

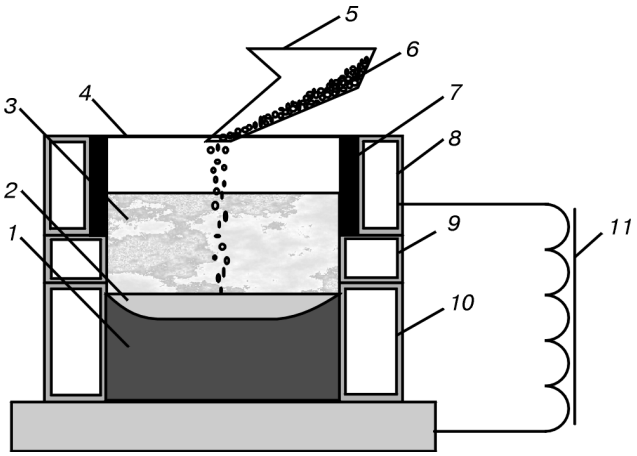

Figure 1. Scheme of ingot melting in current-carrying mould [3]: *1* — ingot; *2* — metal pool; *3* — slag pool; *4* — mould; *5* — mechanism of filler metal feeding; *6* — lumpy filler material; *7* — protective layer (molybdenum, tungsten and graphite); *8–10* — mould sections; *11* — transformer

Such type of the mould is repaired easily. At the same time the bimetal design of the inner sleeve at ratio of the first layer thickness to the thickness of the second layer (with a lower heat conductivity) from 1:1 up to 5:1 provides the reliable current supply through the inner sleeve to the slag pool and a sufficiently good heat removal from the crystallizing metal. At the ratio of thickness of the first layer to the thickness of the second layer of less than 1 the electric and heat conductivity of the inner sleeve is decreased so that the current supply to the slag pool and heat removal from the crystallizing metal are violated due to which the additional consumption of electric power and deterioration of the structure of solidifying metal are occurred. At the ratio of thickness of the first layer to the thickness of the second layer of more than 5:1 the repairability of the mould is deteriorated greatly that causes the hazard in burn-out of the layer being repaired and its contamination with the first metal layer. Moreover, there appears the hazard of contamination of metal being remelted or clad with metal of the first layer even in the process of remelting or cladding because of burn-out of the mould wall.

As a material of the inner sleeve, the copper–titanium, copper–nickel or copper–alloy deposited can also be used depending on the materials being remelted.

Moulds with the sleeve of a current-carrying section of copper–steel bimetal of up to 1500 mm diameter have passed the industrial tests and are used successfully for manufacture of mill rolls using the method of electroslag cladding with liquid metal at Novokramatorsk Machine Building Plant [5].

The drawbacks of design of moulds with a bimetal sleeve of a current-carrying section, as well as in usual copper sections, can refer to the fact that the heat effectiveness of the electroslag process in such moulds is lower than that in moulds with changeable graphite rings.

Attempts to increase the heat efficiency of the electroslag process were made also earlier by using

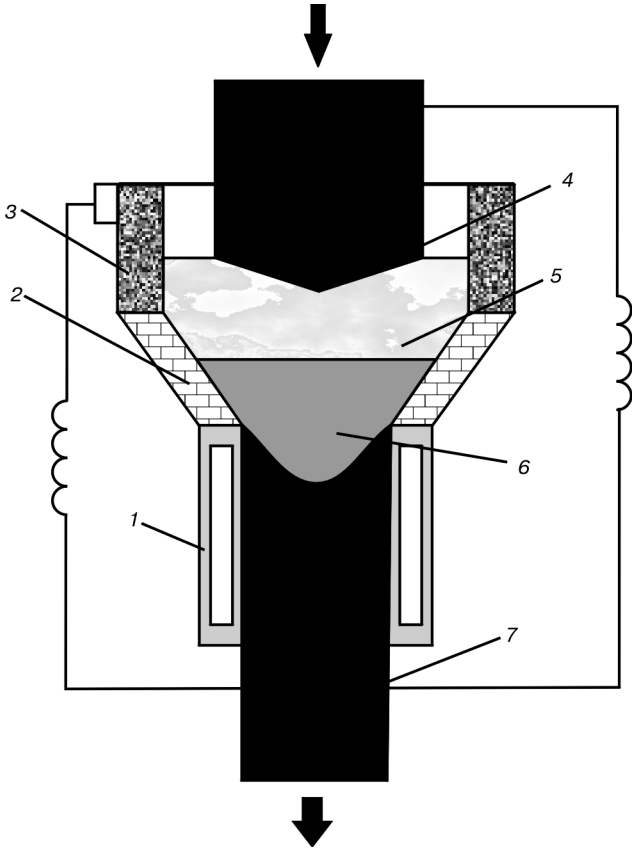

Figure 2. Scheme of ingot melting in three-section current-carrying mould: *1–3* — lower, middle and upper sections, respectively; *4* — consumable electrode; *5*, *6* — slag and metal pool, respectively; *7* — ingot

different types of slag hot tops, covers, gates, systems of differential cooling and others [6]. Except graphite, different slags, nitride ceramics, multi-layer materials were used as materials for lining of the mould upper part [6, 7]. The heat efficiency of the electroslag process in the mould with a lined upper part is approximately by 20 % higher than in conventional water-cooled copper mould [8].

At the present time the updating of the design of current-carrying mould, from the point of view of reduction in heat losses, may be thought of as follows. The upper current-carrying section of such three-section mould can be manufactured from the electroconductive material (Figure 2), resistant against the action of the molten slag, while the lower section can be manufactured from the material with a high heat conductivity, resistant to the action of the molten metal, and the intermediate section ---- from the non-electroconductive material of a low heat conductivity, resistant to the action of the molten slag and metal [9].

The need in use of non-electroconductive material with a low heat conductivity as a material for the intermediate section was caused by the desire to increase the heat efficiency of the process, from the one side, and to provide the reliable electric isolation of the upper current-carrying section from the lower forming section, from the other side. The same graphite can be used as a material for the intermediate section. Section, being under the slag layer, will be subjected to wear to much lower extent than the upper current-carrying section. However, taking into account that the intermediate section is also, as the upper section, not cooled, the insulating gaskets between the intermediate and other sections will operate under the conditions of high temperatures and burnout quickly, that will lead to the short circuiting.

Therefore, the following materials are offered for the sections of such mould: graphite ---- for the upper non-cooled section; copper ---- for lower water-cooled, and material on periclase base ---- for the intermediate section.

Coming from the above-said it can be concluded that the use of either type of current-carrying mould depends, first of all, on the type of material (steel, alloy) which is necessary to remelt. Composition of remelted (or clad) material influences the choice of material of the current-carrying section. It seems to us that bimetals can be widely used as such materials. If the main problem in remelting of metals is the heat efficiency of the process, then the current-carrying and intermediate sections should be non-cooled.

1. Dudko, V.A., Rublevsky, I.N. (1962) On problem of valve action nature in electroslag process. *Avtomatich. Svarka*, **3**, 40--48.
2. Artamonov, V.L., Medovar, B.I., Martyn, V.M. et al. (1972) On problem of anode failure in slag during ESR of current-carrying metallic elements. In: *Special electrometallurgy*. Issue 17.
3. *Sectional mold*. Pat. 4185682 USA. Int. Cl. B 22 B 27 / 02. Publ. 29.01.80.
4. Medovar, B.I., Medovar, L.B., Fedorovsky, B.B. et al. *Current-carrying mould*. Pat. 25605F UA. Int. Cl. B 22 D 19 / 00. Publ. 30.10.98.
5. (2002) Promotional material of NKMZ. *Problemy Spets. Elektrometallurgii*, **2**.
6. Paton, B.E., Medovar, B.I., Tsykulenko, K.A. et al. (1989) Electroslag melting in lined capacity. In: *Special electrometallurgy*. Issue 68.
7. Medovar, B.I., Tsykulenko, K.A., Bogachenko, A.G. et al. *Mould for electroslag remelting*. USSR author's cert. 1563252. Int. Cl. B 22 D 19 / 00. Publ. 05.04.88.
8. Medovar, B.I., Fedorovsky, B.B., Tsykulenko, K.A. et al. (1989) Decrease of heat losses from slag pool in ESR. *Problemy Spets. Elektrometallurgii*, **4**, 22–24.
9. Medovar, B.I., Medovar, L.B., Tsykulenko, A.K. et al. *Sectional mould of electroslag installations.* Pat. 49053 UA. Int. Cl. B 22 D 19 / 00. Publ. 16.09.02.

MODELING OF PROCESSES OF EVAPORATION OF ALLOYING ELEMENTS IN EBSM OF CYLINDRICAL INGOTS PRODUCED FROM Ti-BASE ALLOYS

S.V. AKHONIN, A.S. MILENIN and **A.N. PIKULIN**
E.O. Paton Electric Welding Institute, NASU, Kiev, Ukraine

Mathematical model of evaporation of alloying elements in electron beam surface melting (EBSM) of ingots produced from titanium-base alloys has been developed. In the scope of the offered model the dependencies of chemical composition of the ingot melted zone on power of electron beam guns and angular rate of ingot rotation were obtained. Adequacy of the model was confirmed by experimental data obtained in surface melting of cylindrical ingots produced from alloy Ti–6Al–4V.

Keywords: electron beam surface melting, cylindrical ingot, zone being surface melted, chemical composition, evaporation

To remove different defects in surface of ingots produced by methods of special electrometallurgy, the technology of electron beam surface melting (EBSM) of ingots has been developed at the E.O. Paton Electric Welding Institute [1]. The offered technology allows complete elimination of surface defects [2], that is confirmed both by examinations of quality of ingots using the methods of non-destructive testing, and also by direct studies of macrostructure of templets of surface melted ingots (Figure 1).

The distinguishing feature of EBSM technology is the fact that surface melting is performed in a high vacuum, as a result of which the alloying elements of the alloy, having a high vapor pressure, are evaporated very intensively that can lead to the change in chemical composition of the surface melted layer. Therefore, the important task of optimization of EBSM process is the assurance of conformity of chemical composition of alloy in surface melted zone to the requirements of standards.

The task of optimization of the EBSM process was solved by the methods of mathematical modeling on the example of surface melting of cylindrical ingots of titanium alloy Ti–6Al–4V. The main alloying element of this alloy is aluminium, which is the element with a high pressure of vapor. Therefore, the offered model is dealing with processes of aluminium evaporation from titanium alloy.

Technology of EBSM. The offered EBSM technology is based on heating and melting of a surface layer of the ingot by electron beams along its generatrix simultaneously along the entire length. The focal spot of electron beams takes a shape of an elongated ellipse, the large axis of which is directed along the generatrix. In this case, the ingot is rotated around the longitudinal axis.

Technological scheme of surface melting of ingots was realized on the base of a specialized electron beam installation UE-185, three electron beam guns are used for ingot heating [3].

Modeling of process of evaporation of alloying elements of alloy and determination of chemical composition of metal in the zone of surface melting. To determine the aluminium concentration in the zone being surface melted, it is necessary to derive the equation of material balance, i.e. ratios, reflecting the total mass exchange through the boundary of the area examined. In the given case the area of molten metal is considered in the surface zone of the ingot, i.e. molten pool.

In the reference system, associated with a molten pool, the following metal flows can be distinguished: metal of initial composition, flowing through the solid phase–liquid interface; evaporating metal, flowing through the liquid–gaseous phase interface; metal of final composition, flowing through the liquid–solid phase interface. Sum of these flows characterizes the change in metal mass with time in the region of molten metal. Besides, it was accepted that concentrations

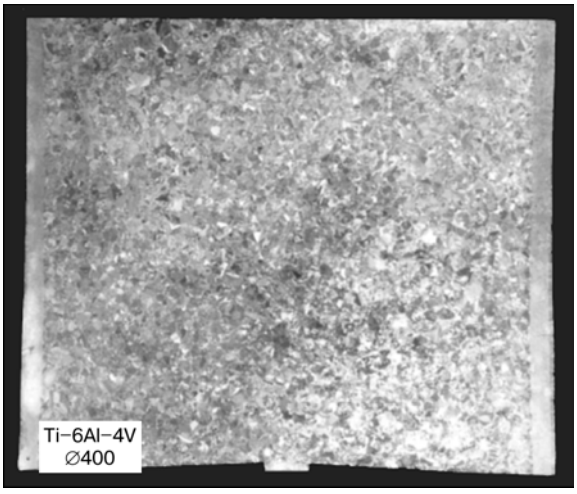

Figure 1. Longitudinal templet of titanium alloy ingot, the surface of which was melted using EBSM method

of elements directly in the molten pool are equal to final concentrations of appropriate elements in the ingot zone being surface melted. Therefore, the equations of the material balance will have the form

$$\begin{cases} \dfrac{d(\rho V[Al]_1)}{dt} = m\,[Al]_0 - S\pi_{Al} - m_1[Al]_1\,, \\ \dfrac{d(\rho V[Ti]_1)}{dt} = m\,[Ti]_0 - S\pi_{Ti} - m_1[Ti]_1\,, \end{cases} \quad (1)$$

where $[M]_0$, $[M]_1$ is the mass concentration of appropriate elements (aluminium and titanium) in the zone being surface melted before and after the beam passing; ρ is the alloy density, kg / m^3; S is the area of molten metal surface, m^2; V is the volume of molten metal pool, m^3; m is the mass of metal flowing through the solid phase–liquid interface per a time unity, kg / s; m_1 is the mass of metal flowing through liquid–solid phase interface per a time unity, kg / s; π_{Al}, π_{Ti} is the specific rate of evaporation of aluminium and titanium, respectively, from the surface of the molten pool, kg / (s·m^2).

Specific rate of evaporation from the surface of molten metal is determined by equations of Langmuir [4]:

$$\pi_i = k_i X_i, \quad (2)$$

where $k_i = \alpha_i \gamma_i P_i^0 \sqrt{\dfrac{M_i}{2\pi RT}}$ is the constant of evaporation rate; α_i is the coefficient of condensation; γ_i is the coefficient of activity; P_i^0 is the equilibrium pressure of element vapors, Pa; M_i is the molar mass of element, kg / mol; X_i is the molar share of element near surface of solution; R = 8.314 J / (mol·K) is the universal gas constant; T is the absolute temperature of melt, K.

For titanium and aluminium the dependencies of equilibrium pressure of vapors on temperature, respectively, have the following form [5]:

$$\log(P^0_{Ti}(T)) = -\frac{22946}{T} + 10.581 - 0.373\log(T);$$

$$\log(P^0_{Al}(T)) = -\frac{16379}{T} + 9.979 - 0.335\log(T).$$

Based on expression (2) for real alloys, in which the titanium concentration exceeds significantly the aluminium concentration, the specific rate of evaporation of elements from the surface of molten pool has the form [6]:

$$\begin{cases} \pi_{Ti} \cong k_{Ti}\left(1 - \dfrac{M_{Ti}}{M_{Al}}[Al]\right), \\ \pi_{Al} \cong \left(\dfrac{1}{\beta_{Al}\rho} + \dfrac{M_{Al}}{M_{Ti}k_{Al}}\right)^{-1}[Al], \end{cases}$$

where β_{Al} is the coefficient of mass transfer of aluminium in molten titanium, m / s.

The rate of metal entering the molten pool is calculated coming from geometric parameters as a ratio of mass of metal of surface melted zone to the time of one revolution, and determined by expression

$$m = Hl\left(R_{ing} - \frac{H}{2}\right)\rho\omega, \quad (3)$$

where H is the depth of penetration, m; l is the ingot length, m; L is the length of molten pool, m; R_{ing} is the radius of ingot, m; ω is the angular rate of ingot rotation, rad / s.

Taking into account that ingot diameter exceeds greatly the depth of penetration, the formula (3) acquires the form

$$m \cong HR_{ing}l\rho\omega.$$

The most part of time the process of surface melting is performed under the condition close to stationary, that can be defined by that the mass of metal in a molten pools is constant in time. From the mathematical point of view this means that time derivatives are equal to zero:

$$\frac{d(\rho V[Al]_1)}{dt} = \frac{d(\rho V[Ti]_1)}{dt} = 0.$$

With account for the above-mentioned, the system of equations of a material balance (1) takes the following form:

$$\begin{cases} m[Al]_0 - S\left(\dfrac{1}{\beta_{Al}\rho} + \dfrac{M_{Al}}{M_{Ti}k_{Al}}\right)^{-1}[Al]_1 - m_1[Al]_1 = 0, \\ m\,(1 - [Al]_0) - Sk_{Ti}\left(1 - \dfrac{M_{Ti}}{M_{Al}}[Al]_1\right) - m_1(1 - [Al]_1) = 0. \end{cases}$$

Solution of system with respect to unknown $[Al]_1$, has, thus, the form

$$[Al]_1 = \frac{S(\beta - k_{Ti}) + m}{2S\left(\beta - \dfrac{M_{Ti}}{M_{Al}}k_{Ti}\right)} - \quad (4)$$

$$- \frac{\sqrt{(S(\beta - k_{Ti}) + m)^2 - 4mS(\beta - (M_{Ti}/M_{Al})\,k_{Ti})[Al]_0}}{2S(\beta - M_{Ti}/M_{Al}k_{Ti})}.$$

where $\beta = \left(\dfrac{1}{\beta_{Al}\rho} + \dfrac{M_{Al}}{M_{Ti}k_{Al}}\right)^{-1}$ is the total coefficient of mass transfer of aluminium in molten titanium.

It is evident that the flow of metal through the liquid–solid phase interface exceeds much that of evaporating molten metal from the surface, i.e. $\dfrac{S\pi_i}{m[M]_0} << 1$. Taking this into account the expression (4) is greatly simplified:

$$[Al]_1 = \left(1 - \frac{1}{\omega R_{ing}}K\frac{L}{H}\right)[Al]_0, \quad (5)$$

where $K = \dfrac{1}{\rho}\left(\left(\dfrac{1}{\beta_{Al}\rho} + \dfrac{M_{Al}}{M_{Ti}k_{Al}}\right)^{-1} - k_{Ti}\right)$.

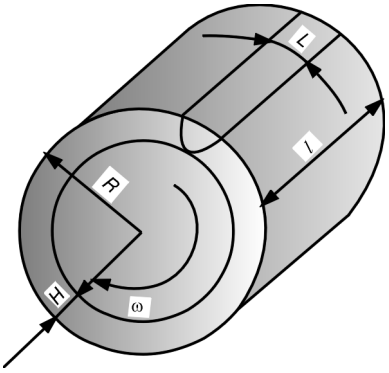

Figure 2. Geometric parameters of ingot

Substituting the length of molten metal pool L, penetration depth H into equation (5) allows obtaining the value of a final composition of ingot surface melted zone at appropriate parameters of the EBSM process.

Several revolutions of ingot can be required in a real production cycle to attain the required quality of the surface melted. Using formula (5) it is possible to obtain ratio for calculation of aluminium concentration in metal of surface melted zone at arbitrary number of ingot revolutions that makes it possible to account for a factor of a multiple passing of electron beams over the surface in optimization of the production cycle. Relationship of a mass concentration of aluminium in the zone being surface melted after n revolutions has the form

$$[\mathrm{Al}]_n = \left(1 - \frac{1}{\omega_1 R_{\mathrm{ing}}} K_1 \frac{L_1}{H_1}\right)\left(1 - \frac{1}{\omega_2 R_{\mathrm{ing}}} K_2 \frac{L_2}{H_2}\right) \times \times \left(1 - \frac{1}{\omega_n R_{\mathrm{ing}}} K_n \frac{L_n}{H_n}\right)[\mathrm{Al}]_0. \quad (6)$$

If to neglect small values of high orders, the expression (6) can be presented as follows:

$$[\mathrm{Al}]_n = (1 - \frac{1}{\omega_1 R_{\mathrm{ing}}} K_1 \frac{L_1}{H_1} - \frac{1}{\omega_2 R_{\mathrm{ing}}} K_2 \frac{L_2}{H_2} - - \frac{1}{\omega_n R_{\mathrm{ing}}} K_n \frac{L_n}{H_n})\,[\mathrm{Al}]_0. \quad (7)$$

It should be noted that if the angular rate of ingot rotation and the total capacity of electron beam guns in the process of melting are remained constant and, besides, the process of heat saturation can be neglected (for example, in case of a small number of revolutions), then the formula (7) takes the form:

$$[\mathrm{Al}]_n = \left(1 - \frac{n}{\omega R_{\mathrm{ing}}} K \frac{L}{H}\right)[\mathrm{Al}]_0. \quad (8)$$

To obtain dependencies of molten pool length and depth of penetration (Figure 2) on technological and physical-chemical parameters of EMSM process, the theoretical-experimental method of N.N. Rykalin was used [7, 8]. For conformity of this method to offered EBSM process, the distribution of energy in a focal spot, overheating of molten pool metal, heat saturation of ingot in the EBSM process were additionally taken into account.

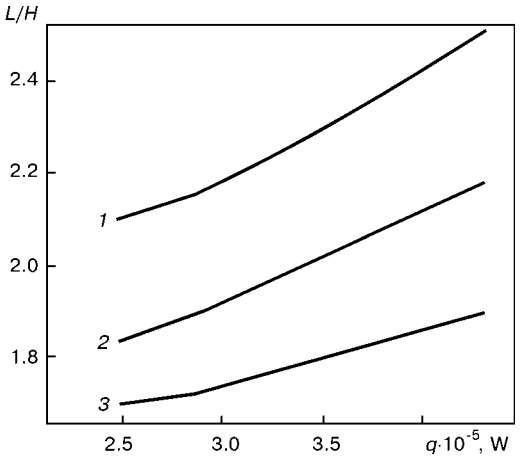

Figure 3. Dependence of ratio of molten pool length to the penetration depth on the total power of electron beam guns at different values of angular rate of ingot rotation, rad / s: *1* — 0.0060; *2* — 0.0045; *3* — 0.0030 (here and in Figures 4–6 R_{ing} = 0.2 m, l = = 2 m and n = 3)

Analysis of heat processes makes it possible to evaluate the dependence of ratio of molten pool length to its depth, given in relationships (5)–(8), on different technological parameters. Thus, for example, dependence of L/H on power (Figure 3) has a clear non-linearity in the area of small values of powers, while in the area of high powers this dependence is approximated at a high degree of accuracy with a linear function. Dependence of L/H on angular rate of ingot rotation (Figure 4) has an essentially nonlinear nature that is stipulated by specifics of heat spreading from the moving source.

The coefficient of activity of aluminium γ_{Al} in a general case is the function of temperature of the molten pool metal. Within the scope of model of Redlikh–Kister the dependence of γ_{Al} on temperature is expressed as follows [9]:

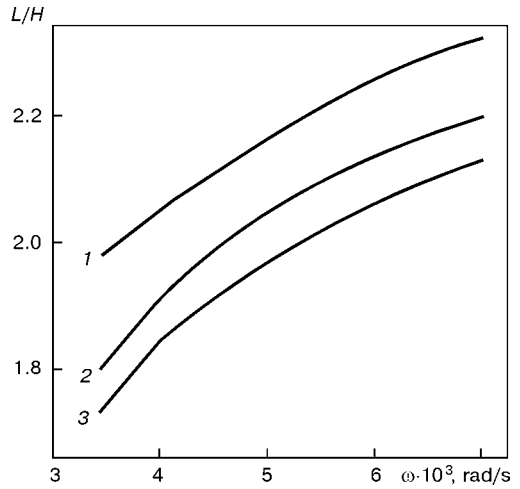

Figure 4. Dependence of ratio of molten pool length to the penetration depth on the angular rate of rotation at different values of total power of electron beam guns, W: *1* — 330,770; *2* — 297,000; *3* — 276,700

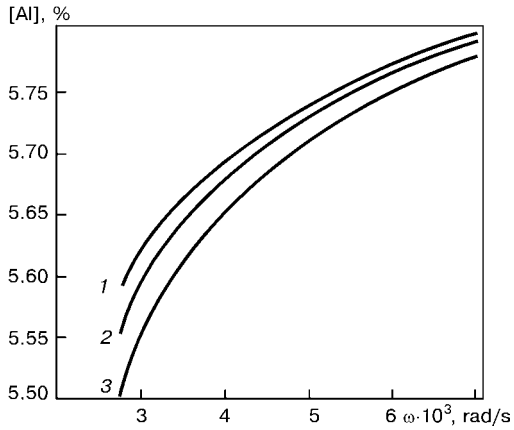

Figure 5. Dependence of mass concentration of aluminium in the zone being surface melted on the angular rate of ingot rotation at different values of total power of electron beam guns, W: *1* — 250,000; *2* — 297,000; *3* — 350,000 (here and in Figures 6 and 7 the initial concentration of aluminium in ingot is 6 %)

$$\gamma_{Al} = \exp\left(\Delta \bar{\bar{G}}^{ex}_{Al} / R\,T\right),$$

where $\Delta \bar{\bar{G}}^{ex}_{Al}$ is the partial excessive free energy having in this case the form:

$$\Delta \bar{\bar{G}}^{ex}_{Al} = X_{Ti}(1 - X_{Al}) \sum_{j=0}^{2} L^{(j)}_{Al,\,Ti} (X_{Al} - X_{Ti})^j + \\ + 2X_{Al}\, X^2_{Ti}\, [L^{(1)}_{Al,\,Ti} + L^{(2)}_{Al,\,Ti} (X_{Al} - X_{Ti})]. \quad (9)$$

Model parameters of liquid phases $L^{(j)}_{Al,\,Ti}$ for Al–Ti system, given in expression (9), are as follows:

$$\begin{cases} L^{(0)}_{Al,\,Ti} = -108250 + 38T, \\ L^{(1)}_{Al,\,Ti} = -6000 + 5T, \\ L^{(2)}_{Al,\,Ti} = 15000. \end{cases}$$

Thus, using the relationship (7) it is possible to evaluate the mass concentration of aluminium in the zone being melted at different technological parameters of EBSM. Thus, the dependence of aluminium concentration on the angular rate of rotation (Figure 5) is non-linear in principle with an asymptotic

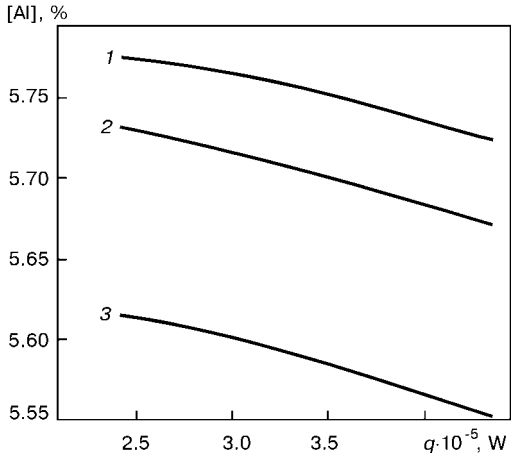

Figure 6. Dependence of mass concentration of aluminium in the zone being surface melted on the total power of electron beam guns at different values of angular rate of ingot rotation, rad / s: *1* — 0.0060; *2* — 0.0045; *3* — 0.0030

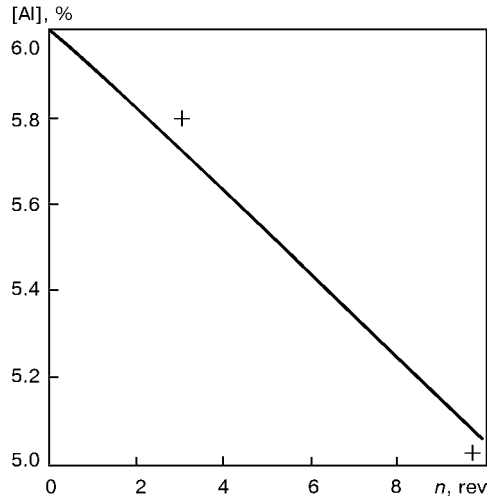

Figure 7. Dependence of mass concentration of aluminium in the zone being surface melted on the number of revolutions (plus denotes the experimental data; solid line — results of calculation according to mathematical model)

behavor in the region of high rates. The nature of dependence of aluminium concentration on effective capacity of heating (Figure 6) depends greatly on the angular rate of ingot rotation: at high rates of rotation this dependence is quasi-linear, but the significant non-linearity is manifested at low rates in the region of high heat capacities.

Check-out of model adequacy. The accuracy of the offered model was checked on the basis of experimental data obtained as a result of surface melting of a cylindrical ingot of alloy Ti–6Al–4V, performed in the following conditions:

Total power of source, W	297000
Ingot radius, m	0.2
Ingot length, m	2
Rate of rotation, rad / s	0.0045
Initial concentration of aluminium in ingot, %	6
Number of revolutions	3
Coefficient of mass transfer of aluminium in molten titanium, m / s	$1 \cdot 10^{-5}$

Chemical analysis of ingot produced at the given technological parameters showed that aluminium content in the melted zone is $[Al]_3 = 5.79$ %.

The suggested approach allows obtaining dependence of aluminium content in the zone being surface melted on the number of revolutions of ingot (Figure 7). Dependence is quasi-linear with a small non-linearity in the region of a large number of revolutions.

Mass concentration of aluminium in the zone examined $[Al]_3 = 5.72$ % corresponds to the number of revolutions $n = 3$.

To have an experimental confirmation of relationship (6) at a large number of revolutions, the surface melting of a cylindrical ingot at similar technological parameters was performed additionally, but at the number of revolutions $n = 10$.

According to relationship (6), the mass concentration of aluminium $[Al]_{10}$ in the zone melted was 5.6 %. Chemical analysis of composition of metal of the region examined showed that $[Al]_{10} = 5.02$ % in the given case.

Thus, the results in the scope of the described model correspond to experimental data with an error of 1.7 %.

CONCLUSIONS

1. Mathematical model allowing description of the processes of evaporation of alloying elements in surface melting of cylindrical ingots made from Ti-base alloys has been developed.

2. The suggested approach gives an opportunity to obtain the relationships associating the concentration of alloying elements in the ingot zone being melted with technological parameters of the EBSM process up to analytical solutions.

3. The given model reflects the appropriate physical-chemical processes with a sufficient degree of accuracy.

4. The allowable range of changing the technological parameters, at which the offered model is adequate to experimental data is sufficient for the description of the real EBSM process.

1. Paton, B.E., Trigub, N.P., Kozlitin, D.A. et al. *Electron beam melting*. Kiev: Naukova Dumka.
2. Pikulin, A.Y., Zhuk, G.V., Trigub, N.P. et al. (2003) Electron beam surface melting of titanium ingots. *Advances in Electrometallurgy*, **4**, 16–18.
3. Trigub, N.P., Zhuk, G.V., Pikulin, A.N. et al. (2003) Electron beam installation UE-185 for melting of surface layer of ingots. *Ibid.*, **3**, 10–12.
4. Zhukhovitsky, A.A., Shvartsman, L.A. (1976) *Physical chemistry*. Moscow: Metallurgiya.
5. Efimov, A.I., Belorukova, L.P., Vasilkova, I.V. et al. (1983) *Properties of inorganic compounds*. Refer. book. Leningrad: Khimiya.
6. Akhonin, S.V., Trigub, N.P., Zamkov, V.N. et al. (2003) Mathematical modeling of aluminium evaporation during electron-beam cold-hearth melting of Ti–6Al–4V ingots. *Metallurg. and Materials Transact.*, 34B(**8**), 447–454.
7. Rykalin, N.N. (1947) *Thermal principles of welding*. Part 1. Moscow: AN SSSR.
8. Rykalin, N.N. (1951) *Calculations of thermal processes in welding*. Moscow: Mashgiz.
9. Ivanchenko, N.V., Ustinov, A.I., Mokhort, V.A. (2003) Thermodynamic analysis of evaporation of titanium and nickel from Ti–Ni melt in vacuum. *Advances in Electrometallurgy*, **3**, 13–16.

INVESTIGATION OF TECHNOLOGICAL PARAMETERS OF PLASMA-ARC HEATING IN MELTING AND SPINNING OF MELT

M.L. ZHADKEVICH, V.A. SHAPOVALOV, G.F. TORKHOV, Yu.A. NIKITENKO and **V.R. BURNASHEV**
E.O. Paton Electric Welding Institute, NASU, Kiev, Ukraine

Effect of main technological parameters of plasma-arc skull melting on distribution of temperature in melt was studied. The change in temperature of a ceramic nozzle of OP-133 unit in the process of melt spinning was determined.

Keywords: plasma-arc heating, gradient of temperature, temperature equilibrium, spinning of melt, amorphous metals

Investigation of distribution of temperature in the molten metal pool, and also the capability to control the temperature gradient in technological processes of metal melting allows reaching their optimization and power saving. This is especially actual for installation where the powerful heat sources, such as plasma, electron beam and laser, are used.

In the present work the distribution of temperature in melt was investigated in experimental installation of the OP-133 type for manufacture of rapidly hardened metallic strips. Here, the DC plasmatron with up to 1200 A maximum operating current is used as a heat source.

As is known, the plasma arc is a sufficiently powerful and concentrated heat source. Temperature inside it can reach several tens of thousands of degrees [1]. Control of a powerful heat flow and monitoring of temperature distribution are the rather complex tasks, if to take into account that the mass of metal being treated is small, i.e. not more than 1 kg.

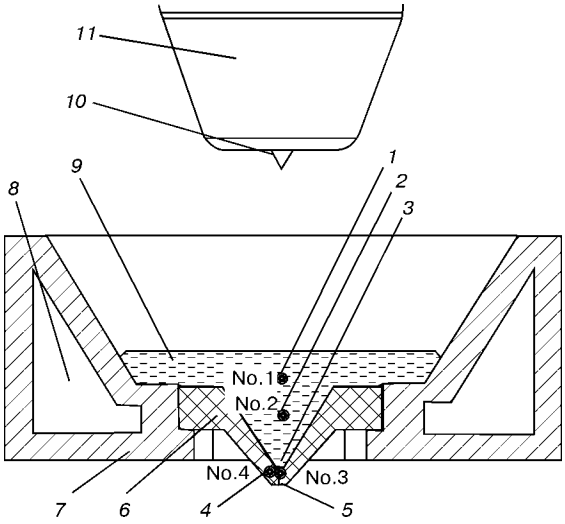

Figure 1. Scheme of melting unit of OP-133 installation: *1–4* — points in which the thermocouples are fastened; *5* — pouring nozzle slot; *6* — ceramic pouring nozzle; *7* — copper water-cooled crucible; *8* — channel for water-cooled crucible; *9* — molten metal pool; *10* — tungsten cathode; *11* — plasmatron nozzle

The producing of amorphous and quasi-amorphous metal strips is realized by the method of spinning. In this case the metal is melted under the action of plasma-arc heating in a copper water-cooled skull crucible. At a complete melting of metal and sufficient heating of a pouring nozzle, arranged in the center of a crucible bottom part (Figure 1), the excessive pressure of inert gas is created in the chamber. Under its action the molten metal is extruded through a pouring nozzle slot to a rotating drum-cooler. On its cold surface the metal is solidified quickly in the form of a strip having amorphous or microcrystalline structure, and then it is separated under the action of centrifugal forces.

In the present work the investigation of change in temperature was conducted in a ceramic nozzle and at different depth of molten metal directly under the plasmatron. Here, the effect of some technological parameters on temperature distribution was studied. The reference points of measurement of melt temperature were selected at different levels in the plasmatron axis.

The reference points are indicated in approximate model of melting unit, where the temperature measurement was made (see Figure 1).

The depth of fixation of thermocouple from the pool level was 9 mm for point No.1, 20 mm for point No.2; the point No.3 was located directly in the upper part of slot of a pouring nozzle and designed for temperature measurement at different conditions of melting; point No.4 was located in the hole from external side of the pouring nozzle slot at 3 mm distance from the melt. It was managed in this point to record the entire process of temperature change in spinning of melt on the rotating drum-cooler.

There are several methods of measurement of melt temperature in plasma-arc heating, some of them are characterized by a high labor consumption and require the complicated equipment [2, 3], but it is possible to measure the temperature only on the melt surface. However, to obtain the more complete pattern of temperature gradient in plasmatron axis it is necessary to make measurements inside the molten metal. The simplest and rather accurate measurements were made by a contact method [4] using standard tungsten thermocouples of VR 5 / 20 type (GOST 3044–77).

Thermocouple was placed into molten metal in a quartz tip from beneath through a pouring nozzle slot. Temperature measurements (Figure 2) were made in the series of melts with a constant mass of metal (500 g) at 9–10 l / min consumption of plasma-forming gas and 105 kPa pressure in the chamber. As a model alloy, the nickel-base alloy PRN-88 with a melting temperature, close to 1000 °C, was selected. In the process of experiments the arc current, voltage between the cathode and melt, arc length were measured. The change in thermal electromotive force was recorded by a self-recording potentiometer of RP-160 type which was calibrated by a reference power source.

Melt overheating in point No.1, located not much lower that the level of molten metal pool, is explained by physical processes proceeding in plasma-arc melting. In the process of melting the molten metal pool depression is observed under the action of a plasma-forming gas and electric arc. The arc pressure on the molten metal is defined almost completely by gas-dynamic effect of macroscopic flows of plasma (dynamic constituent) and compression of arc column (static constituent). The total action of electron and ion flows, and also of a reactive force of evaporating metal at arc heating is negligible [5]. For the selected alloy the depression may have a depth of about 5–7 mm. Hence, it follows that thermocouple was in contact with surface layers of the melt, overheated by the plasma arc. Temperature of plasma near the anode («molten metal») is much lower than that in a near-cathode region, but, nevertheless, it can reach several thousands of degrees [6].

The closer the melt to the surface, the more significant the temperature change, that is associated with some oscillations of arc at the melt surface. The arc instability is stipulated by several factors, which influence in different ways the site of arc contact with the melt. These factors refer to dynamic pulsation of the plasma-forming gas, cathode erosion and arc contact with different points, movement of large magnetic masses near the melting chamber, creating «magnetic blowing», and also slag movement over the surface of the molten metal pool.

The first factor is stipulated by the application of flexible hoses that leads to negligible changes in their discharge capacity and oscillations in the region of natural resonance frequencies or occurrence of local vortexes in a gas system. The cathode erosion at high currents was always a problem for metallurgical plasmatrons, as its burning round is occurred in the process of meltings (Figure 3, *a*). However, the burnt tungsten cathode can be replaced or restored partially by sharpening of its working part (Figure 3, *b*). The rotating massive drum-cooler and its working drive are referred to magnetic masses which are moved in the process of melting. The slag formation at the surface of the molten metal pool is possible as a result of interaction of alloy components with remnants of oxygen of inert atmosphere of melting chamber or other chemical reactions.

The carried out experiments showed that at the initial moment of melting (in plasma arc ignition) the metal melting and temperature distribution in melt can proceed in different ways depending on loading of charge materials. The loading plays an important role in protection of a ceramic pouring nozzle by a layer of molten metal from the direct action of the plasma arc. The following optimum form of loading can be defined: large granules of metal, filled up with granules of the finer fraction, are located directly under plasmatron. After the arc ignition the upper layer of the metal is melted, flowing and filling the crucible bottom, here it is solidified, forming a skull layer. In melting and upsetting of metal the arc length and, respectively, the voltage between cathode and anode are increased and, consequently, the plasmatron power transferred is changed. Curves of change in temperature depending on arc length were obtained (Table). It was determined that increase in arc leads to the increase in voltage, and, as a consequence, to the increase in the plasmatron power transferred. However, not all its power is transferred to the metal, as in this case the losses for heating the walls of chamber and crucible are increased, and this is compensated in metal by the skull layer thickness. The further increase in arc length can lead to the water boiling in channels of the crucible cooling or to the arc break. During the experiment with the change in arc length the current was maintained at the same level (700 A).

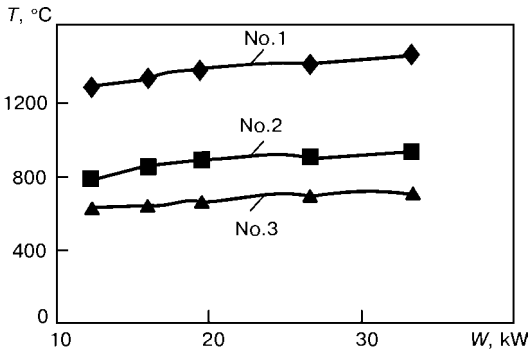

Figure 2. Change of temperature in melt depending on power *W* of plasmatron at 75 mm arc length (Nos. 1–3 — see Figure 1)

The change in nozzle temperature in the process of melt spinning is shown in Figure 4. Thermocouple was placed in point No.4 (see Figure 1). As is seen from Figure 4, the temperature equilibrium is commenced 5–6 min after the plasmatron ignition and coming to the optimum technological conditions. The further maintaining of this condition in the process of melting is not rational as the noticeable temperature changes are not already observed and the system reaches the temperature equilibrium. At coming to the preset stable condition the supply is realized to the pouring nozzle of the rotating drum-cooler with

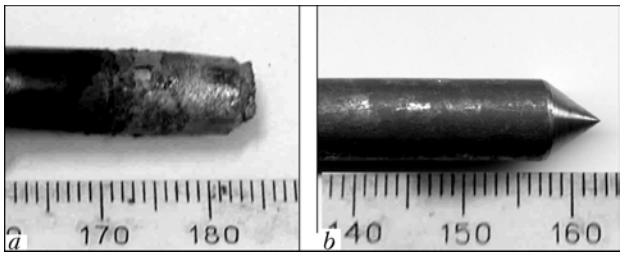

Figure 3. Apperance of cathode after melting (*a*) and restoration (*b*)

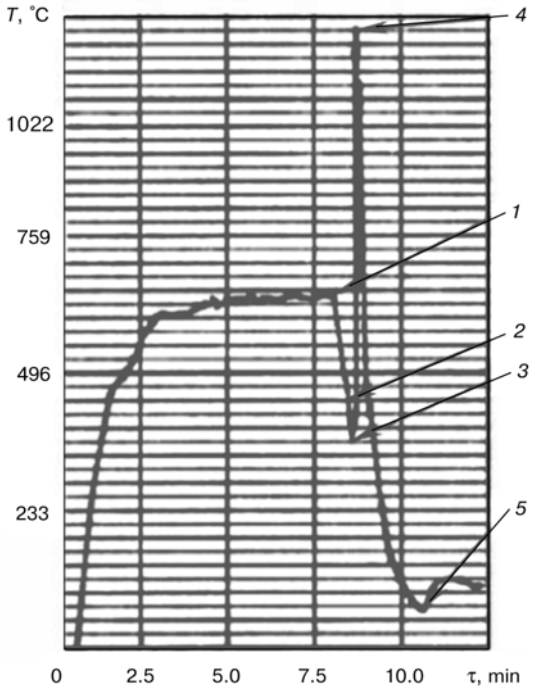

Figure 4. Change of nozzle temperature in the process of melt spinning: *1* — site of drum-cooler feeding; *2* — gap setting; *3* — beginning of melt pouring; *4* — finishing of pouring and plasmatron switching off; *5* — crucible switching off and cooling (τ — time of melting)

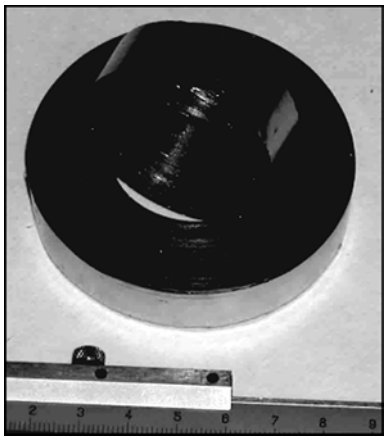

Figure 5. Metal strip produced by the method of molten metal spinning in plasma-arc skull melting

a preset gap between the nozzle and drum. At this moment the gas exhaustion from the melting chamber is cut off and the excessive pressure from the receiver is supplied. In a short period of time the cooling of a projected part of the nozzle is occurred, which is due to the fact that the gas masses of atmosphere are trapped by the surface of the rotating drum. During drum-cooler rotation at 1500–2000 rpm an intensive blowing of the nozzle is occurred, in particular by a gas surface layer of the drum-cooler. At the moment of spinning the gap between the nozzle cut and drum-cooler is 0.1–0.6 mm, that influences greatly the total temperature of the nozzle. In Figure 4 this abrupt temperature drop is approximately 300–350 °C. Owing to the high-speed of the process of molten metal pouring out and a low heat conductivity of the ceramics this has no time to influence greatly the melt temperature, thus creating the satisfactory conditions

Change of temperature (°C) of melt depending on arc length

Number of measurement point	Arc length, mm		
	56	66	76
1	1394	1404	1414
2	863	888	896

for proceeding the process of its spinning and promotes the producing of the quality strip (Figure 5).

It is seen from Figure 2 that the upper layers of the molten metal are overheated greatly as compared with lower layers. At its continuous flowing through the slot the pouring nozzle is heated greatly that corresponds to a temperature splash with about 900 °C drop. With the temperature change the density of melt, and also the rate of metal flowing are, respectively, changed. The decrease in molten metal viscosity leads to its better spreading that improves the melt contact with the drum-cooler surface. However, as the width of the strip is limited by a width of the pouring nozzle slot, then this is compensated by the increase in strip thickness, due to which it has different thickness in the entire length from 40 (at the beginning) to 60 μm (at the end). After flowing out of all the volume of metal the plasmatron is switched off. The further heat removal is realized very intensively, because the most part of the molten metal was already poured out.

CONCLUSIONS

1. When the operating conditions are used the temperature of metal near the anode spot is approximately 1400 °C, however, on the pool bottom near the pouring nozzle slot it exceeds negligibly the temperature of melting.

2. Temperature equilibrium is commenced 5–6 min after switching on of the plasmatron or changing the melting parameters: current and arc length.

3. For alloy PRN-88 of 500 g mass the optimum capacity of the plasmatron is 25–30 kW. The reduction in its capacity leads to the solidification of the molten metal near the nozzle slot, thus hindering its pouring. The exceed of the mentioned range of the plasmatron capacity leads to unjustified consumptions of electric power, and, as a consequence, to a strong overheating of metal and water boiling in the crucible cooling channels.

4. At low currents the arc is subjected to a significant effect of different factors and is instable. It is stabilized in case of a complete melting of all the mass of metal at current of more than 600 A.

1. Krasnov, A.N., Sharivker, S.Yu., Zilberberg, V.G. (1970) *Low-temperature plasma in metallurgy*. Moscow: Metallurgiya.
2. Laktionov, A.V., Stomakhin, A.Ya., Grigoryan, V.A. et al. (1980) Temperature of metal surface in plasma melting. In: *Problems of special electrometallurgy*. Issue 3.
3. Shapovalov, V.A., Grigorenko, G.M., Konstantinov, V.S. et al. (1983) Measuring of temperature on molten titanium surface in plasma-arc remelting. *Ibid*. Issue 19.
4. Grigorenko, G.M., Solovej, L.N., Lakomsky, V.I. (1978) Effect of tungsten and molybdenum on nitrogen absorption in plasma-arc melting. *Ibid*. Issue 9.
5. Latash, Yu.V., Torkhov, G.F., Kozakov, S.N. (1984) Investigation of gas-dynamic pressure of plasma arc on metal in rarefaction of environment. *Ibid*. Issue 21.
6. Klyuev, M.M. (1980) *Plasma-arc remelting*. Moscow: Metallurgiya.

TOWARDS THE PLASMA LIQUID-PHASE REDUCTION OF IRON FROM OXIDE RAW MATERIAL

V.A. SHAPOVALOV, G.A. MELNIK, D.M. ZHIROV, A.A. ZHDANOVSKY and **K.A. TSYKULENKO**
E.O. Paton Electric Welding Institute, NASU, Kiev, Ukraine

Scheme of plasma liquid-phase reduction of iron from its oxides has been offered. It is shown that the content of sulphur and phosphorus in the ready product is several times lower than the admissible content for pig iron.

Keywords: reduction, plasma heat source, iron-containing materials, ferriferous slag

At present many methods of iron reduction from molten oxides are existing [1–3]. The rise in temperature promotes the increase in the degree of its reduction and rate of reactions proceeding. It was established that the most effective required high temperatures can be attained in use of plasma heat sources [4, 5].

During the reduction process proceeding the activity of iron oxide in ore-slag melt is continuously minimized thus leading to the delay of the process, and in case of use of gas reducing agents it leads to the significant increase in their consumption. The high activity of FeO in melt can be maintained by a continuous feeding of iron-containing materials (ICM). Therefore, the investigation of feasibility of liquid-phase reduction of iron from its oxides using plasma heating, and also the study of specifics of the process with a high content of iron oxides in a slag melt represent an interest.

Pilot melts were performed in experimental stand (Figure). Argon or air were used as a plasma-forming gas, and oxidized pellets, fluxed agglomerate and oiled scale of delivery of OJSC «Krivoj Rog Mining-Metallurgical Works», and also metallized pellets of Oskol Electrometallurgical Works, were used as ICM. Content of sulphur, phosphorus and carbon was determined in oiled scale in making the chemical analysis. The main aim of the experiment using scale was to confirm the feasibility of processing the fine-dispersed raw material, containing of moisture and oil, using the offered method. Chemical composition of ICM is given in Table 1, and the melting conditions are given in Table 2.

In melts Nos. 2, 3 and 5 the reducing agent was added into charge composition in a stoichiometric amount, in melts Nos. 2 and 3 the coke fines with 0.026 % S and 0.045 % P were used, while in melt No.5 the powder-like graphite produced from electrode scrap was used. In melt No.4 the same graphite was added into melt together with a plasma-forming gas. It should be noted that melting was realized in a graphite crucible, that did not prevent the possibility of additional carburization of metal.

In melt No.4 the arc was ignited from the crucible bottom. And the charge materials were in a space between the heater and inner wall of the crucible. With charge melting the heater was lifted, but the arc remained closed until the complete melting of ICM. In all the rest melts the arc was first burning over the layer of charge materials, and then over the surface of the molten metal. It was noted that in melt No.4 the arc was burning more stably than in other melts, that can be explained by the absence of charge collapses in the zone of arc.

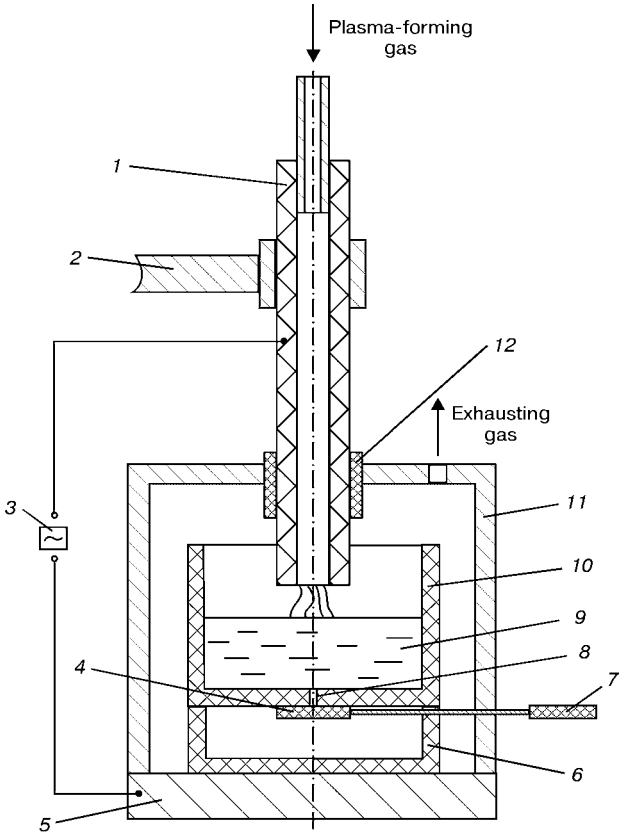

Scheme of experimental stand: *1* — plasma heater of direct action; *2* — mechanism of electrode displacement; *3* — AC source; *4* — stopper; *5* — platform; *6* — graphite mould; *7* — handle; *8* — outlet orifice; *9* — molten metal; *10* — graphite crucible; *11* — chamber; *12* — isolator

Table 1. Chemical composition of initial ICM

Type of ICM	Elements in ICM, wt.%							
	SiO_2	Al_2O_3	CaO	MgO	MnO	S	P	C
Metallized pellets	1.94	0.65	0.21	0.47	0.06	0.004	0.029	0.760
Oxidized pellets	9.18	0.32	0.87	0.37	0.12	0.039	0.007	0.062
Fluxed agglomerate	8.86	1.13	2.65	1.50	0.36	0.030	0.048	0.093
Oiled scale	–	–	–	–	–	0.029	0.014	1.000

Notes. 1. In ICM the compound Fe_xO_y is the base. 2. Oiled scale contains 35 % of moisture and oil.

Table 2. Conditions of melting

No. of melt	Type of ICM	Arc current, A	Arc voltage, V	Arc length, mm	Plasma-forming gas	Melting duration, min	Yield of iron, %	Mass of ICM, kg	Remarks
1	Metallized pellets	1200	60	55	Argon	27	79	6	
2	Oxidized pellets	1250	50	57	Same	30	74	3	Plus 750 g coke fines
3	Fluxed agglomerate	1250	57	60	»	20	69	3	Plus 600 g coke fines
4	Same	950	33	75	Air	40	76	5.13	With powdered graphite feeding through electrode
5	Oiled scale	300	30	22	Same	26	45	2.15	Charge contains 8 % powdered graphite and 14 % powdered CaO

The molten metal was poured through the bottom orifice into a heated graphite mould, when the equilibrium between slag and metal was not yet attained. In the ready products the phases had a clearly expressed boundary. Table 3 shows their chemical composition.

Coefficients of distribution of sulphur L_S and phosphorus L_P between slag and metal were determined:

$$L_S = \frac{(S)}{[S]}, \quad L_P = \frac{(P)}{[P]},$$

where (S), (P) is the content of appropriate elements in slag, and [S], [P] is their content in metal. Slag basicity was calculated by formula

$$B = \frac{(CaO) + 1.5(MgO)}{(SiO_2) + 0.6(Al_2O_3)} \qquad (1)$$

on the basis of expression

$$B = \frac{n_{CaO} + n_{MgO} + n_{MnO}}{n_{SiO_2} + 2n_{P_2O_5} + n_{Al_2O_3} + 0.5n_{Fe_2O_3}},$$

where (CaO), (MgO), (SiO_2) and (Al_2O_3) is the content of appropriate oxides in slag, wt.%; n is the amount of moles of oxides in 100 g of slag [6].

Formula (1) was obtained as working for our concrete cases, therefore, MnO and P_2O_5 are not indicated in it due to their small concentrations, as well as Fe_2O_3, as iron in slag was in the form of monoxide.

According to work [6], the maximum coefficient of activity of iron monoxide is attained at slag basicity 1.8–2.0, though with increase in FeO content at constant basicity the coefficient of activity is decreased.

In work [7] the effect of basicity of slags on the rate of iron reduction from ore-slag melts by solid carbon was investigated and shown that with increase in basicity from 0.6 to 1.4 the rate of iron reduction is continuously growing.

Table 3. Chemical composition of ready products

No. of melt	Elements, wt.%											B	L_S	L_P
	In metal			In slag										
	C	S	P	SiO_2	Al_2O_3	CaO	MgO	MnO	S	P	Fe			
1	4.1	0.010	0.034	52.17	16.0	6.7	9.0	1.10	0.010	0.011	12.7	0.33	1.0	0.32
2	3.1	0.050	0.024	2.44	1.27	2.1	1.0	0.19	0.025	0.026	77.5	1.12	0.5	1.08
3	3.2	0.120	0.026	36.0	6.52	16.0	6.54	1.55	0.078	0.041	28.0	0.65	0.65	1.58
4	3.8	0.035	0.022	0.68	1.56	2.36	1.48	0.34	0.022	0.036	77.5	2.83	0.63	1.64
5	6.3	0.007	0.020	–	–	–	–	–	–	–	–	–	–	–

At basicity of not less than 0.85 the slag is characterized by very low dephosphorizing ability [8]. Only at very high content of iron monoxide in it the noticeable dephosphorization of metal is possible. Increase in slag basicity up to 2.3 promotes increase in its dephosphorizing ability, and the further increase in basicity has already no great influence on this ability, however, the growth in content of iron monoxide increases greatly the metal dephosphorization by slag. Consequently, at slag basicity of about 2 both its sufficiently high dephosphorizing ability and also the highest rate of reduction should be recorded.

The carried out melts showed that at a high content of iron monoxide in slag the coefficient of phosphorus distribution exceeds 1 even at 0.65 basicity that is correlated with above-described. The results of melt No.2 are somewhat different, that was, probably, caused by too earlier pouring of metal.

As follows from Table 3, there was no desulphurization of metal by slag in the conducted melts. However, the sulphur content in the ready product is less than admissible content for pig iron, that is explained by its low content in initial raw material. But even at increased content of sulphur it can be easily removed [9].

Thus, it is necessary to define the optimum duration of metal in the molten state to have, from the one side, its effective dephosphorization, and, from the another side, to preserve the high efficiency of the aggregate.

CONCLUSIONS

1. It is shown that as a result of liquid-phase plasma reduction melting of ICM from the iron melt it is possible to produce metal with several times lower content of suphur and phosphorus than that admissible for pig iron. At $B = \frac{(CaO) + 1.5(MgO)}{(SiO_2) + 0.6(Al_2O_3)} \geq 0.65$ the percent content of phosphorus in metal is lower than in slag.

2. It was established that arc is burning most stably in the condition when it is «covered» with charge materials up to their complete melting.

3. The offered metal is suitable for processing of fine-dispersed raw material with a high content of moisture and oil, for example oiled scale.

4. High power consumption can be explained by the «cold start» and low capacity of crucible (6 kg).

1. Yusfin, Yu.S., Gimmelfarb, A.A., Pashkov, N.F. (1994) *New processes of metal production (metallurgy of iron)*: Manual for institutes of higher education. Moscow: Metallurgiya.
2. Bondarenko, B.I., Shapovalov, V.A., Garmash, N.I. (2003) *Theory and technology of coke-free metallurgy*. Ed. by B.I. Bondarenko. Kiev: Naukova Dumka.
3. Ivashchenko, V.P., Velichko, A.G., Tereshchenko, V.S. (2002) *Direct production of metal using the low-temperature plasma*. Dnepropetrovsk: Sist. Tekhn.
4. Dembovsky, V. (1981) *Plasma metallurgy*. Moscow: Metallurgiya.
5. Lakomsky, V.I. (1974) *Plasma-arc remelting*. Ed. by B.E. Paton. Kiev: Tekhnika.
6. Ajzatulov, R.S., Kharlashin, P.S., Protopopov, E.V. et al. (2002) *Theoretical principles of steelmaking processes*: Manual for institutes of higher education. Moscow: MISiS.
7. Kondakov, V.V., Ryzhonkov, D.I. (1963) Effect of basicity on rate of iron reduction from slag melts by solid carbon. *Izvestiya Vuzov. Chyorn. Metallurgiya*, **1**, 17–21.
8. Kramarov, A.D. (1964) *Steel production in electric furnaces*. Moscow: Metallurgiya.
9. Bornatsky, I.I., Machikin, V.I., Zhivchenko, V.S. et al. (1979) *Out-of-furnace refining of cast iron and steel*. Kiev: Tekhnika.

TECHNOLOGICAL PROCESS OF VACUUM-PLASMA TREATMENT OF METALLIC MELTS

V.L. NAJDEK and **A.V. NARIVSKY**
Physical-Technological Institute of Metals and Alloys, NASU, Kiev, Ukraine

Results of investigation of effect of vacuum-plasma treatment of molten metal on effectiveness of refining, structure and strength characteristics of aluminium alloys are presented.

Keywords: vacuum, plasma, jet, melt, refining, microstructure, intermetallics, oxides, blowing

Effective method of alloys refining from harmful and excessive impurities is the melt degassing. However, in vacuum treatment as a single operation the required level of purification from gases, non-metallic inclusions and harmful impurities has not been always attained. Moreover, the degassing of metallic melts requires the use of a complex equipment and here the difficulties arise connected with pressurization of vacuum chambers and separate sub-assemblies in installations operated at high temperatures. This can explain some reduction over the recent two decades in the interest to the use of processes of degassing of non-ferrous metals.

The method of treatment of molten metal [1] has been developed at the Physical-Technological Institute of Metals and Alloys of the NAS of Ukraine, in which the vacuum chamber pressurization is realized by the molten metal being refined. The new technology allows the vacuum-plasma treatment of non-ferrous alloys to be performed at portion and continuous conditions of metal pouring using simple devices (Figure 1). Operating plasmatron together with a chamber is immersed into the molten metal, and then a vacuum pump is switched on and compressed air is supplied to the ejector. Under the rarefaction action the metal is lifted for a definite height depending on the residual pressure in the chamber. Vacuum sealing of the chamber is provided by the molten metal into which it is deepened.

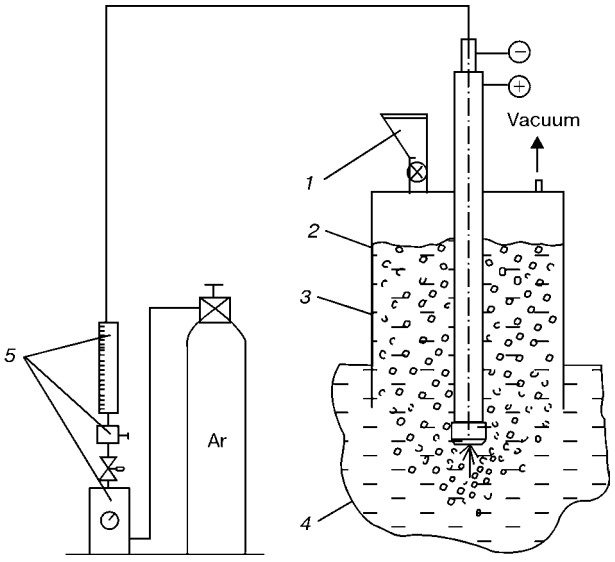

Figure 1. Scheme of process of vacuum-plasma treatment of molten metal: *1* — batcher of reagents; *2* — plasmatron; *3* — chamber; *4* — molten metal; *5* — system of gas supply

Diameter of the chamber and arrangement of the plasmatron nozzle are selected so that all the gas bubbles in metal blowing could enter the chamber. In this case the melt surface beyond the chamber is in a dead state; oxide film or flux induced at its surface prevents the hydrogen enter from atmosphere into melt during refining.

Reagents, necessary for the alloy treatment, are loaded preliminary into a batcher, and then are fed into a chamber in the process of metal refining. Reagents enter the upper layers of molten metal being degassed, where the highest intensity of mass exchange is attained in blowing by gas jets. As a result, the additions are mixed intensively and distributed uniformly in the metal.

Investigation of effectiveness of process of vacuum-plasma treatment of molten metal was performed using aluminium alloy AK7. Metal of 80 kg mass was melted and treated in the resistance furnace. To make comparison, the molten metal was refined by four methods during 10 min at similar argon consumption of 0.48–0.50 m^3 / h; blowing was made by cold or plasma jet at atmospheric pressure or in the conditions of a low vacuum. Effectiveness of the mentioned meth-

Dependence of content of hydrogen, oxide inclusions in alloy and its strength characteristics on method of treatment

Method of treatment	[H], cm^3 / 100 g	$[Al_2O_3]$, %	σ_t, MPa	δ, %
Without treatment	0.58	0.046	178	3.3
At atmospheric pressure	0.30 / 0.18	0.024 / 0.020	190 / 212	3.8 / 5.5
In vacuum with residual pressure 6 kPa	0.21 / 0.11	0.029 / 0.016	203 / 218	4.2 / 5.3

Note. In numerator the data are given in treatment by cold argon jet, in denominator the data are given in treatment by plasma jet.

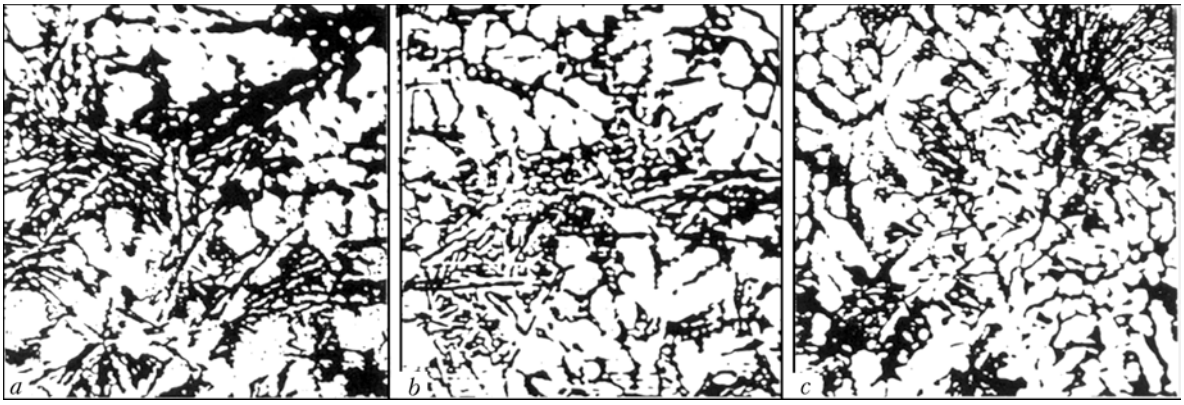

Figure 2. Microstructure of alloy AK12 + 80 % of chips in initial state (*a*) and after treatment for 10 (*b*) and 20 (*c*) min: *a* — σ_t = = 138 MPa, δ = 1.2 %; *b* — σ_t = 147 MPa, δ = 1.9 %; *c* — σ_t = 160 MPa, δ = 2.6 % (×100)

ods of melt refining and physical-mechanical properties can be judged from data given in the Table.

After molten metal blowing at atmospheric pressure by a cold argon jet the hydrogen content in the alloy is decreased to 0.30 cm^3 / 100 g, and in use of the plasma jet — to 0.18 cm^3 / 100 g. In creation of a low rarefaction (6 kPa residual pressure) the degree of alloy degassing in chamber over the melt in its treatment by gas jets is increased by 35–40 % as compared with metal refining under atmospheric conditions.

Contamination of the alloy with non-metallic inclusions during degassing is not changed in principle, while after treatment of metal by a cold jet of argon in vacuum it is increased as compared with a conventional blowing. This is stipulated by the fact that in release of residual vacuum pressure the oxide inclusions together with metal from the chamber enter again the pool. In case of a continuous refining of melt in the metal flow the above-mentioned drawback is eliminated. When the portion treatment of alloys is used (in ladle, melting unit, etc.) the flux is supplied to the chamber on the surface of molten metal, which prevents the oxides return to the melt.

Structure of alloys is fine-grained in the process of vacuum-plasma refining of metal. This is seen well on the example of alloy AK12, which is known as a hard-to-harden alloy by treatment. Microstructure of silumin, melted from a low-grade charge containing 80 % of chips, after molten metal treatment at different durations is shown in Figure 2. Owing to metal blowing by a plasma jet for 10 min the sizes of structural constituents in the alloy are decreased and its strength properties are increased. Here its microstructure is characterized by a negligible refinement. With increase in time of melt treatment up to 20 min the microstructure of alloy is refined to a larger extent, and the eutectic colonies are distributed more uniformly between α-solid solution. Here, the strength and elongation of metal are increased to the values specified by the State standard for this alloy.

Structural changes in the alloy are stipulated by the presence of a high-temperature volume of molten metal in the zone of the plasma jet outflow. In the overheated volume the alloy is subjected to a thermal-time treatment preventing the formation of intermetallic phases in it [2]. In addition, under the temperature action of plasma jet («thermal shock») the intermetallic and oxide inclusions can be destroyed in the melt. In local volumes of metal near the plasmatron nozzle the evaporation of alloy components with subsequent cooling of vapors («condensation») in removal from the zone of jet outflow is also possible. In case of cooling of vapors the particles of «condensate» and microvolumes are formed which, depending on sizes, promote the alloy crystallization and serve, like the oxide inclusions, the nuclei for hydrogen bubbles. The rest microvolumes can exist in the molten metal for a short time in the form of separate groups with a large amount of activated atoms [3], as a result of which the structure of molten metal and alloy structure in a cast state are changed [4]. With increase in time of alloy treatment the volume of metal, which is affected by high-temperature action of the plasma jet is increased, and the above-mentioned processes in the molten metal are proceeding more completely.

Results of investigations prove that the vacuum-plasma treatment of melt allows modifying alloys simultaneously with refining without use of special reagents and fluxes. Deep treatment of the molten metal by plasma contributes also to the decrease or elimination of a negative effect of inheritance of charge materials on the properties of non-ferrous metals. Application of this method of treatment is challenging in recycling technologies, and also in processes of continuous casting of metal, where the time of gas-reagent interaction in molten metal is limited.

1. Najdek, V.L., Narivsky, A.V., Ganzha, N.S. et al. *Method of molten metal processing*. Pat. 69091A Ukraine. Publ. 16.08.04.
2. Novokhatsky, I.A., Arkharov, V.I., Ladianov, V.I. (1982) On mechanism of structural transformations in molten metals. *Doklady AN SSSR*, 267(**2**), 367–369.
3. Ershov, G.S., Poznyak, L.A. (1985) *Microheterogeneity of metals and alloys*. Moscow: Metallurgiya.
4. Najdek, V.L., Narivsky, A.V. (2003) Effect of melt processing method on structure and properties of aluminium alloys. *Litejnoe Proizvodstvo*, **9**, 2–3.

EFFECT OF RHENIUM ON PROPERTIES OF HIGH-PURITY CHROMIUM AND ITS ALLOYS WITH LANTHANUM

A.P. RUDOJ, L.P. ZHUCHENKO, V.Kh. MELNIK and **A.P. PORTNOV**
I.N. Frantsevich Institute for Metals Science Problems, NASU, Kiev, Ukraine

Using induction and arc methods the ingots of chromium-lanthanum alloys with rhenium additions were melted in furnaces with copper crucibles and moulds. Hardness and transition temperature of these alloys were investigated. It is shown that hardness of chromium alloys with lanthanum at 0.10–0.13 wt.% of rhenium is decreased to 1140 MPa, while at 0.46 wt.% it is increased up to 1235 MPa. Transition temperature is increased from 20 to 180 °C with increase in rhenium concentration up to 4.0 wt.%.

Keywords: chromium, rhenium, lanthanum, hardness, transition temperature

The present work was conducted to check the feasibility of use of the alloy of Cr–Re–La ternary system as a material for deposition of heat-resistant and high-temperature-resistant coatings on the internal surfaces of artillery barrels and combustion chamber of liquid-propellant engines (LPE).

The base for creation of structural materials, characterized by the increased heat resistance and scale resistance, is inexpensive refractory metals with BCC-lattice, to which chromium can be referred first of all. However, chromium, as other transition metals of VIA group of the periodic system of elements (PSE), for example, molybdenum, tungsten, possesses insufficient low-temperature ductility, that is an important limitation in its application. It can be connected, first of all, with the high chemical affinity of chromium to impurities of interstitial elements, such as oxygen, nitrogen and carbon.

One of the most widely spread methods of chromium purification from these impurities is its refining with additions of highly-active elements, in particular rare-earth metals (REM), which are capable in their adding to chromium to form the hard-to-dissolve refractory compounds with oxygen and nitrogen, such as oxides and nitrides, distributed uniformly in the form of dispersed inclusions in the chromium grains.

Study of the REM effect on technological and low-temperature ductility of chromium allowed us to establish that the most suitable plasticizer for these purposes is lanthanum [1–3], whose optimum content in chromium should amount to 0.2–0.4 wt.% [4]. Moreover, the density and adhesion of Cr_2O_3 to chromium is increased, phase composition of surface oxidized layer is changed due to formation of chromites in it, abruptly increasing the material heat resistance. If to add more than 0.2–0.4 wt.% La into chromium, the fusible phases will be formed, which, arranging at the boundaries of grains, will lead to the deterioration of strength characteristics, as they become the nuclei for cracks at loading.

Adding of lanthanum into chromium not only increases its scale resistance but also makes it possible to decrease the temperature of cold brittleness T_{br} of cast chromium down to –10 °C [4]. This alloy is characterized by the increased deformability in a cast state that is manifested in the reduction of temperature of the deformation treatment and increase in the degree of reduction.

The positive effect of lanthanum on structure and properties of chrome is preserved also in a recrystallized state, that is manifested in a noticeable refining of grain structure and improvement of a low-temperature ductility.

As the alloys of Cr–La system are not characterized by a sufficient strength and are subjected to some extent to the recryatallization embrittlement, there seems no feasibility to use them as a material for the deposition of coatings without an additional alloying. Therefore, the need arose in the selection of such material, whose adding in small amounts into alloy Cr–La could improve its service properties.

Transition metal of VII group of PSE such as rhenium, is close at to its position in PSE to metals of a platinum group, in particular to osmium, known by its plasticizing effect on chromium, however, due to a high cost it is not acceptable for practical application in alloys designed for coating deposition on the internal surfaces of the above-mentioned products.

Rhenium, unlike the REM, cannot refine matrix of chromium from impurities of interstitial elements, as it has a comparatively low chemical affinity to nitrogen and oxygen, but is capable to influence the distribution of impurities in the alloy structure.

Alloying of chromium with a large amount of rhenium leads to so-called rhenium effect, i.e. to a significant increase in a low-temperature ductility at a

simultaneous improvement of strength characteristics, moreover, the highest effect was observed at content of rhenium in chromium close to the limit of solubility, because σ-phase is formed at further alloying and the ductility is deteriorated [5].

Thus, at approximately 800 °C temperature the rhenium of more than 30 wt.% is dissolved in chromium [6], at 1000 °C its limited solubility in chromium is already approximately 70 wt.%, and σ-phase is formed at 82–88 wt.% [7].

Brittleness threshold of the recrystallized alloy of chromium with 65 wt.% Re is, in accordance with data of testing of notched samples, 260 °C, and for recrystallized chromium iodine it is 380 °C [6]. It is evident that from the practical point of view this way of improving the impact strength of chromium is unacceptable due to high cost of rhenium, added to the alloy in large amounts.

However, there is also another method of improvement of properties of chromium ductility, consisting in alloying of the latter with small amounts of transition metals of other groups of PSE. As the solubility of elements of substitution, the same as of interstitial elements, is increased at defects of a crystalline ageing (grain boundaries, dislocations and so on), the segregation of alloying additions at defects of crystalline lattice hinders the formation of impurity atmospheres from interstitial elements on them.

In manuscript [8] the graphs, obtained by Allen et al., are given about the effect of some metals (iron, cobalt, osmium, iridium, ruthenium, rhenium) on chromium ductility, showing that there is a minimum on the curves of hardness at 1–2 wt.% content of alloying element. Rhenium is an exception, whose addition into chromium in the above-said limits leads to the increase in the level of hardness that was confirmed by the results of investigation of rhenium effect on the ductility of electrolytic refined chromium, subjected to the zonal remelting [9]. Here, the temperature of cold brittleness increased from 60 °C in pure chromium up to 250 °C in alloy containing 5 wt.% Re.

To check out these results using the method of induction melting in a «cold» crucible [10], a series of ingots of alloys of high-purity chromium with content of rhenium in them from 0 to 4.2 wt.% was produced. Melting was performed in additionally purified argon at pressure, somewhat exceeding the atmospheric pressure, to prevent the air in-leakage into the working space of the furnace in the process of producing ingots (Table).

Figure 1 gives the curve of T_{br} dependence on content of rhenium in chromium. As follows from the Figure, the additions of rhenium deteriorate significantly the ductility of chromium (T_{br} is changed from 18 °C in initial high-purity chromium to 190 °C in alloy Cr + 4 % Re).

Rhenium content in alloys determined by the method of X-ray diffraction analysis

Charge composition, wt.%	Mass share of rhenium in ingot, %
Cr	0
Cr + 0.5 Re	0.51
Cr + 1.0 Re	0.94
Cr + 1.5 Re	1.49
Cr + 2.0 Re	1.96
Cr + 2.5 Re	2.45
Cr + 3.0 Re	3.00
Cr + 3.5 Re	3.48
Cr + 4.0 Re	4.02

With alloying continuation the further deterioration of alloy ductility could occur, that is typical of almost all metals of a group of chromium alloyed with rhenium, when the temperature of cold brittleness passes through maximum (except system Mo–Re) with increase in amount of rhenium from 1–2 wt.% up to concentration close to the solubility limit and leading to «rhenium effect». Then, the value of T_{br} is abruptly decreased at a significant change in electron structure in the process of alloying [8], thus violating the optimum conditions of a resonance covalent bond and changing the filling of the energy zones. This leads to the increase in solubility of interstitial elements and feasibility of realization of additional mechanism of plastic deformation, i.e. twinning. The type of crystalline lattice is preserved here.

As is seen from Figure 1, the alloy of binary system Cr–Re at up to 4 wt.% Re has a low technological ductility and, therefore, cannot be used for manufacture of cathodes for deposition of coating on the internal surfaces of combustion chambers of LPE and tank barrels.

Having a positive result obtained in microalloying by copper deoxidized by lanthanum of high-purity chromium [11], the authors decided to check the behavior of cast alloy of ternary system Cr–La–Re, containing the tenth fractions of rhenium percent. For

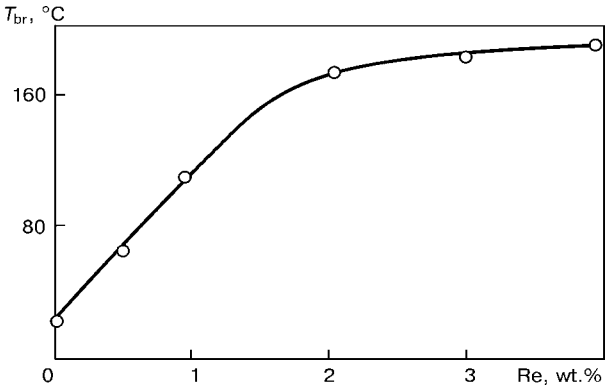

Figure 1. Effect of rhenium on temperature of cold brittleness of cast alloy Cr–La

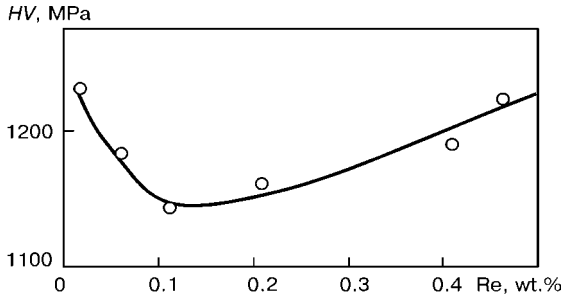

Figure 2. Effect of rhenium on hardness of cast alloy Cr–La

this purpose, a series of precision ingots of 34 mm diameter was produced in induction furnace with a copper water-cooled mould in high-purity conditions of melting. Chemical composition of alloys defined using X-ray diffraction analysis was as follows, wt.%: Cr + 0.11Re + 0.12La; Cr + 0.23Re + 0.12La; Cr + 0.11Re + 0.25La; Cr + 0.23Re + 0.26La; Cr + 0.10Re + 0.20La; Cr + 0.38Re + 0.20La: Cr + 0.19Re + 0.10La; Cr + 0.19Re + 0.55La; Cr + 0.45Re + 0.26La; Cr + 0.05Re + 0.26La; Cr + 0.18Re + 0.26La; Cr + 0.38Re + 0.25La.

To eliminate the effect of change in lanthanum concentration, those alloys, in which the lanthanum content varied within the 0.25–0.30 wt.% ranges and can be accepted constant, were selected from melted alloys. From results of measurement of hardness of these alloys, the curve of dependence of binary alloy Cr + 0.27 % La on content of rhenium in it was plotted (Figure 2), which shows that addition of 0.10–0.13 wt.% Re provides the maximum (though a little) reduction in hardness. With a further increase in rhenium concentration in alloy the hardness is increased that is, probable, connected with hardening of a solid solution, and some increase in ductility is explained by redistribution of interstitial elements.

1. Rakitsky, A.N., Rudoj, A.P. (1971) Effect of rare-earth metals on brittle transition temperature of chromium. In: *Metal physics*. Issue 36.
2. Mikadze, O.I., Tavadze, F.N., Rudoj, A.P. et al. (1973) Effect of rare-earth metals on evaporation of chromium. *Inform. 71 of AN of GSSR*, **2**, 409–411.
3. Gorbach, V.G., Rakitsky, A.N., Rudoj, A.P. et al. (1972) Effect of rare-earth metals on mechanical properties of chromium. *Problemy Prochnosti*, **2**, 78–82.
4. Rakitsky, A.N., Trefilov, V.I. (1986) Progress in development of chromium-base structural alloys. Possibilities and limitations. In: *Structural alloys of chromium*. Kiev: Naukova Dumka.
5. Gun, G.G., Gilbert, A., Jaffi, R.I. (1968) *Properties of refractory metals and alloys*. Moscow: Metallurgiya.
6. Salli, A., Brendz, E. (1971) *Chromium*. Moscow: Metallurgiya.
7. Savitsky, E.M., Tylkina, M.A., Povarova, K.B. (1965) *Rhenium alloys*. Moscow: Nauka.
8. Trefilov, V.I., Milman, Yu.V., Firstov, S.A. (1975) *Physical principles of strength of refractory metals*. Kiev: Naukova Dumka.
9. Butilenko, A.K., Gridnev, V.N. (1964) Study of plastic properties of chromium alloys with transient metals. *Voprosy Fiziki Metallov i Metalloved*., **19**, 54–68.
10. Epifanov, V.G., Lesnik, A.G. (1964) Zonal melting of metals in water-cooling crucibles. *Ibid*., **20**, 185–190.
11. Rudoj, A.P., Zhuchenko, L.P., Melnik, V.Kh. et al. (2004) Effect of copper on properties of high-purity chromium and its alloys containing lanthanum. *Advances in Electrometallurgy*, **1**, 24–26.

BRAZING OF DEFECTS OF AIRCRAFT AND SHIP TURBINE BLADES — CHALLENGING TECHNOLOGY OF EXTENSION OF THEIR LIFE (Retrospective analysis of status and prospects of development)

A.M. ZHADKEVICH
E.O. Paton Electric Welding Institute, NASU, Kiev, Ukraine

Retrospective analysis of status and prospects of development of brazing of parts of a gas turbine engine hot path is given. Problems of selection of heat-resistant alloys for turbine blades are shown. Methods of manufacture of cast blades are described. Volumes of possible repair works using brazing of blades are shown on the examples of three construction companies. History of brazing development is presented. Application of new brazing filler alloys is grounded. Methods of brazing of blades and parts of GTE are described and prospects of implementation of technologies in the sphere of repair manufacturing and their effectiveness are described.

Keywords: brazing, repair, extension of service life, repair technologies, heat-resistant alloys, turbine blades, structure, hardening phase, casting, defects of blades, engine construction companies, history of engineering, brazing filler alloys, problems of implementation

In spite of many-century experience of application, the brazing as a method of metals joining, was an object of handicraft until the last century for making ornaments and household goods [1, 2]. In the 1930s and, in particular in the 1950–1960s, the brazing became a main technological process in the period of a rapid scientific-technical progress in many branches of industry for manufacture of separate parts, sub-assemblies and structures [3].

The idea of creation of gas turbines could not be realized many years because of the absence of materials possessing a sufficient heat resistance. The investigations of cast heat-resistant nickel alloys used instead of wrought ones, carried out in VIAM, allowed exceeding the level of heat resistance of the foreign alloy Nimonic 75, the best alloy at that time, by 200 °C [4]. The higher level of strength and heat resistance of cast nickel alloys was obtained by an intermetallic strengthening in the presence of γ'-phase (Ni_3Al) in the form of dispersed precipitations, carbides and high structural stability of alloys. Results of investigations made it possible to use widely the cast heat-resistant nickel alloys for manufacture of blades of gas turbines, whose capabilities were recognized by the general designers, engine manufacturers, N.D. Kuznetsov and A.M. Lyulka at the beginning of the 1960s. Only after some years their experience became to be used in the USA and other countries [4, 5].

At present, the cast heat-resistant nickel alloys with a different crystalline structure: equiaxial, directional (columnar) and single-crystal [4–9] are used for manufacture of blades for GTE (Figure 1). Alloys with an equiaxial structure have grains, whose boundaries are approximately at an equal distance from a center (Figure 1, *a*). In this case there is no directed heat removal during crystallization. The level of strength and heat resistance depends on perfectness of grain boundaries and can be controlled by the conditions of crystallization [7].

The more promising are the alloys with a directional columnar structure, consisting of grains, elongated along the action of main load on the blade. The working part of casting of the blade should have no

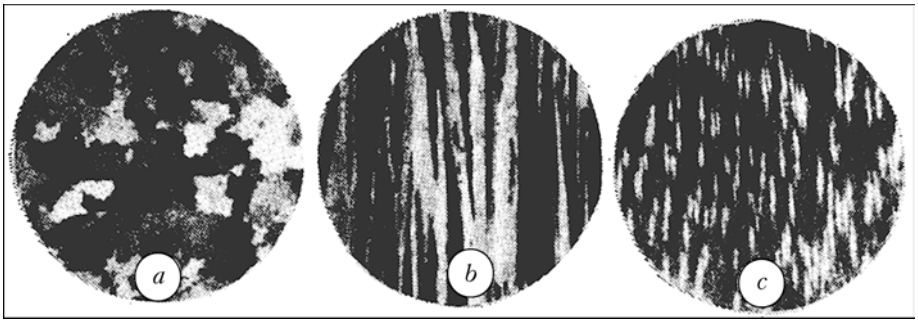

Figure 1. Macrostructure of heat-resistant alloys in GTE blades: *a* — equiaxial; *b* — directional columnar; *c* — single-crystal (×300)

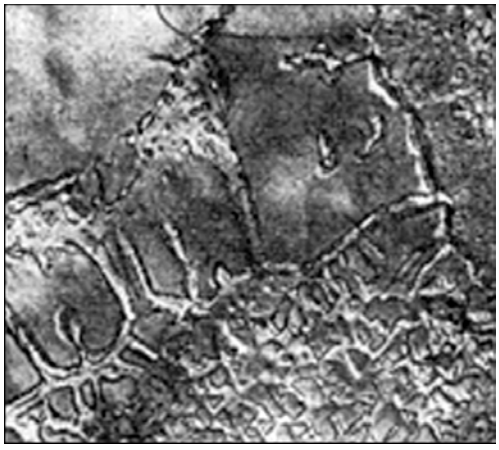

Figure 2. Microstructure of high-strength foundry heat-resistant alloy. Eutectics $\gamma + \gamma'$ (×8000)

boundaries located in the direction normal to the action of main stresses. Similar structure occurs at a directed heat dissipation [8, 9] (Figure 1, *b*).

Castings of blades with the directional crystallization, where the conditions of metal solidification from one center of crystallization are provided, represent a single crystal and named single-crystal. Structure of these castings is characterized by the most optimum combination of strength, ductile, fatigue and other characteristics. Having this structure, it is important to know the crystallographic orientation of phase constituents, as the nature and level of stresses, acting in blades, and also the mechanical properties depend greatly on them [10] (Figure 1, *c*).

In manufacture of blades of aircraft and ship turbines, other parts of hot path, operating under the conditions of high temperatures, at aggressive action of products of fuel combustion and high-temperature gas (sulphide-oxide) corrosion the wrought and cast heat-resistant alloys of complex alloying on nickel base (dispersion- and nondispersion-hardened) are widely used. Structure of the dispersion-hardened alloys consists of a matrix (γ-phase) representing a complex-alloyed solid solution on nickel base and γ'-phases on the base of intermetallic compound Ni_3Al [11] (Figure 2).

The most spread heat-resistant alloys for manufacture of hot path parts of the aircraft GTE are EP 102, EP 109, EP 220, EP 617, EP 718, EP 742, EP 748, EP 791, EI 437B, VZhL-12, VZhL-128, ZhS6, ZhS6K, ZhS6KP, ZhS6 FNK, ZhS6U, ZhS6U-VI, ZhS26-VI, ZhS30-VI, Nimonic 80A, Inconel 718 and others, and for ship power units they are: EP 99, EP 202, EP 367, ChS 70 VI, ChS 88 VI, ChS 102, EP 539, EP 648, EI 437A, EI 602, EI 617, VZh-36L, ZhS6K and others. These are complex in chemical composition nickel alloys, containing from 50 up to 80 % Ni, alloyed with aluminium, titanium, cobalt, chromium, molybdenum, tungsten, vanadium, niobium, tantalum in various combinations as to alloying elements and with a different mass share [4, 12, 13].

Blades from wrought heat-resistant alloys for aircraft and ship GTE are manufactured by the method of forging and stamping and subsequent mechanical treatment, while the blades from cast alloys with an equiaxial structure are manufactured using a shape memory casting [4, 6, 7]. If the higher temperature level of operation of blades is required, then the heat-resistant alloys with intermetallic strengthening, produced by a directional crystallization, are used [4, 5, 8, 9].

In 1963 VIAM produced blades for the first time from alloy ZhS6K with a directional structure using an induction vacuum melting. Electrocorundum was used as a material of a cast mould. These blades were tested in 1965 on engines of AI-20, AI-24 and NK-12 in airplanes TU-114 and AN-22 where they operated their double and trice service life without appearance of defects in the form of cracks [4].

At present a large experience has been gained in the development and implementation of technology of casting of monolithic and cooled blades using the method of a directional crystallization. Application of investment moulds of 5–8 mm thickness for blade casting using a simultaneous heating of the mould, melting metal in it and different methods of directed removal of heat of crystallization guarantees a columnar structure of metal at 15–20 mm / min rate of crystallization and efficiency of 20–30 blades per day [4, 8, 9].

At the first stage of development of industrial technology of directional crystallization the vacuum portion furnaces with lock chambers were created for loading and unloading moulds, then two-chamber furnaces were created with a high-frequency heating of the mould, and, finally, the continuously-operated furnaces with a vertical chamber of crystallization and horizontal lock chambers for loading and unloading of moulds were created [4]. Their daily efficiency reached 80 blades. Over the recent years the automatic multi-chamber units produce up to 60,000 blades per year.

Casting of blades with a single-crystalline structure can be considered as the further development of the process of directional crystallization using the modern methods of a special electrometallurgy. The more strict requirements for temperature and rate parameters of crystallization are specified to the processes of producing of these castings. Blades with a single-crystalline structure are manufactured using different methods, but in any case it is important to produce a single grain in a cast part. This can be attained, for example, by introducing a single-crystal primer with orientation [001] into the mould cavity, from which the crystallization of molten metal of all the casting is going on. Here, the growth of other crystals is blocked by using special starting devices and adjustment of heat field of metal crystallization.

To produce blades with a directional and single-crystalline structure, the continuous vacuum furnaces in which the metal is melted directly in the mould proper, heated up to 1500 °C, are used. In this case the investment mould with alloy billet, placed into a receiving cup, is mounted into a graphite flask and fastened by a support filler. Flask with a closed cover

is fed from a loading table automatically to the lock chamber. After passing the lock chamber, the flask is moved by a preset condition in the furnace through a melting zone into the zone of crystallization (thermal front in the furnace is located at 5–10° angle as regards to direction of the mould movement). After the complete solidification of metal and natural cooling to 350 °C the flask is unloaded to the unloading table through the lock chamber. All the operation in the furnace are programmed and realized automatically [4, 8, 9].

Blades for ship power units are manufactured monolithic, mainly with a solid section of an airfoil. The blades of aircraft GTE have inner channels in the airfoil body designed for their cooling in the process of the engine operation.

Application of cast heat-resistant alloys for GTE blades was promoted by the achievements in the development of ceramic materials, fixture and equipment allowing producing thin and intricate in shape castings of blades with channels for cooling, which cannot be almost produced by other methods.

To manufacture turbine blades, the multi-operation expensive technology is used. In a serial production of blades the high losses and rejection at each operation of the technological cycle are not admitted. In casting of blades the efficient metal as regards to simple single-flange blades is 95 %, while in casting with a directional crystallization it is 85 %. Rejection is increased in casting of blades of complex designs with cooling cavities where the output of efficient metal is only 60–65 %, and in casting of single-crystalline blades it does not exceed 50 %. The main kinds of rejection of blades in casting are cavities, bubbles and non-metallic inclusions at the blade surface.

In the process of forging, stamping, mechanical treatment of billets of blades, deposition of protective coatings, and also in service of turbines the different defects are occurred on the working surface of the blade airfoil, such as cavities, marks, dents, shape distortion, scratches, spallings, thinning of airfoil and so on. Service of these blades leads to the reduction in efficiency factor of turbine, and in some cases it is almost impossible.

It is not difficult to prevent the above-mentioned defects using welding of nondispersion-hardened alloys of EI 602 type, used in ship building. They are well welded by argon arc method using filler wire close by chemical composition. Mechanical properties of these welded joints are similar to the parent metal properties [13].

There are problems in welding of heat-resistant dispersion-hardened alloys, connected with the formation of hot cracks in metal in a HAZ, reduction in heat resistance and thermal strength of the joints (Figure 3). To prevent the hot crack occurrence in welding of these steels, there are many technological procedures, for example, the refining of structure of weld metal, alloying of weld metal by molybdenum, chromium, tungsten, boron in different combinations, adding of aluminium and titanium into weld metal, realizing of artificial removal of heat to change the directivity of metal crystallization along the weld axis, change in weld pool size, adjustment of heating rate in heat treatment, application of different methods of welding (laser, electron beam, diffusion) and so on [12, 13]. However, to obtain the high quality of welds on high-alloy heat-resistant nickel alloys is not possible in principle [13, 14].

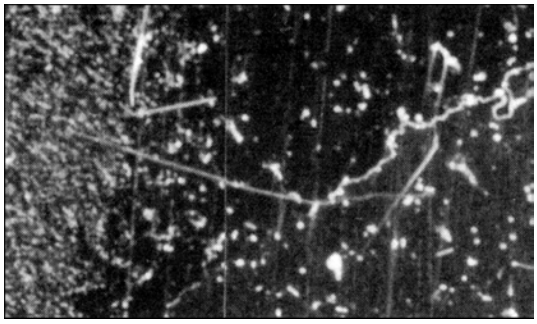

Figure 3. Microcracks in HAZ metal of welded joint made from Inconel 738 (×100)

The application of high-temperature brazing for experimental repair of blades of nozzle block and fire tube of combustion chamber of GTE after their service was made in the USA in 1971 by Pratt&Whitney Company of United Technology Corporation [15]. Frederik Renchler, the founder of the company, manufactured with a group of engineers the first piston engine for airplanes named Wasp at the end of 1925. From this event the history of P&W commenced, becoming the world's leader in the manufacture of aircraft engines.

Since the end of the 1940s P&W started the manufacture of jet engines, reliable and simple in service, of JT8D type (next model JT9D), the most widely used model for Boeing 727. In 1991 these engines were used in 42 % of airplanes of civil aviation in 350 aircraft companies, i.e. 14,000 engines and 450 million flying hours worked. The volume of realization of P&W (35,000 staff) at the world's market was $US 7.6 bln in 2002.

In 2003 above 600 aircraft companies from 150 countries of the world used GTE of P&W. The production activity of P&W is widening each year owing to the manufacture of new engines PW-2000, PW-4000, PW-6000, creation of new repair enterprises, and also owing to the joint ventures in other countries, including Russia and Ukraine, in which more than $US 400 mln were invested. In 1991 P&W and S.V. Ilyushin AC started the joint manufacture of engine PS-90A2. The US engine PW-2337 was installed in airplane IL-96M (Figure 4) [16].

Having a large industrial and scientific-technical experience, the company P&W has grounded and showed on example of production activity the technical and economic expediency and also the prospects in application of brazing in vacuum in repair of GTE blades and hot path parts of engine instead of argon arc welding [15, 16].

In Russia the repair of nozzle blades of GTE using brazing was performed in 1972 at MMZ «Saturn»

Figure 4. Engine PW-2337 during technical maintenance

(now OJSC «A. Lyulka-Saturn»), being more than 50 years the traditional developer and manufacturer of engines for the military and civil aviation. The high-temperature brazing on GTE blades was performed in a gas medium, consisting of argon with products of decomposition of potassium fluoro-borate without removal of an aluminized layer. This process preserved this aluminized layer and further heat resistance of the surface of blades.

The year of birth of one of the most advanced enterprises of engine construction of Russia, Experimental Design Bureau «A. Lyulka», can be considered 1946, when experimental base and pilot plant were given to A.M. Lyulka, as a chief designer, for construction of a flying model of turbo-jet engine (TJE). A.M. Lyulka, after studying the theoretical investigations of B.S. Stechkin in the field of air-jet engine, suggested the project in 1937 with a team of engineers from KhAI for feasibilities study of TJE, which was not accepted by the Kharkov specialists. The project was sent to Moscow and highly evaluated by Prof. V.V. Uvarov, the well-known specialist on new load-carrying units for aviation.

In April, 1941 A.M. Lyulka patented his by-pass TJE [17], which became the prototype of existing now designs of engines. By the summer of 1941 the engine was ready by 70 % in metal. The war interrupted its further manufacture.

In 1943 in TsIAM, and then in NII-1, A.M. Lyulka headed the department on investigation and designing of TJE and created the new design of engine S-18 (test stand variant), the prototype of TR-1. In May

Figure 6. A.M. Lyulka (on the right) and A.N. Tupolev, 1958

1947 the experimental fighter SU-11 was launched for the first time with a jet engine TR-1 (Figure 5). The dream was realized to which A.M. Lyulka was preparing over 10 years.

In 1950s A.M. Lyulka created AL-5 type TJE with a 5000 kgf thrust, the most powerful at that time. The second generation of this engine, AL-7, was the best in the world. It was used in a flying boat Beriev M-10 and passenger airplane TU-110, and from that time the creative friendship between A.M. Lyulka and A.N. Tupolev was lasting until the end of their life (Figure 6).

Engine AL-7 and its modification were produced for fighter and civil aviation. The volume of their production reached 20,000 pieces. New capabilities of TJE were embodied in engines AL-21R and AL-21 F-3 for airplanes SU-17, SU-17M, SU-24, used from 1973 to 1993. In the middle of the 1980s A.M. Lyulka created the by-pass engine AL-31F with 12,500 kgf thrust. In 1979 this engine launched SU-27 into air. 30 world's records were set later with its use.

Airplane SU-37 with two engines AL-31FP with a rotated nozzle, which was under the design since 1988, became the «star» of Air Shows in Farnboro, Seoul, Le Burge [17, 18].

The great scientific, research, experimental and industrial potential of team of OJSC «A. Lyulka-Saturn» allowed their enterprise to be leading in implementation of new challenging technologies in the sphere of production and repair of GTE.

It cannot be but mention about the prospects of the national flagman of engine construction, the OJSC «Motor Sich», which will celebrate its 85 this year. It occupies the deserving place among the leading engine construction companies working for the needs of aviation. At present, several tens of thousands

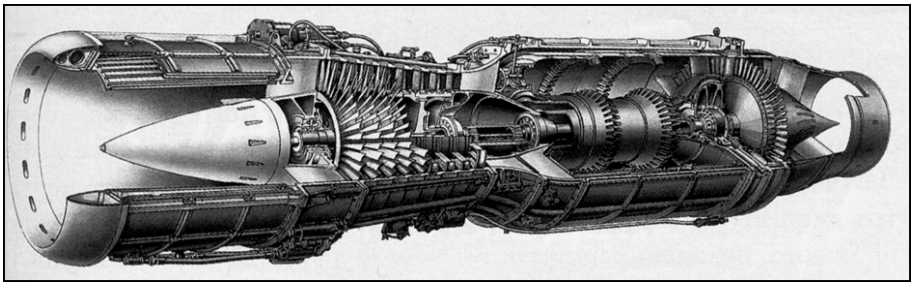

Figure 5. Gas turbine engine TR-1

of GTE of 55 designations, manufactured by «Motor Sich» are in service in 105 countries of the world.

In this enterprise the intensive preparation and mastering of new aircraft engines is going on, including the new generation of engines D-27, AI-450, D-436 (T1 and TP), TV3-117, VK-1500, AI-222-25, AI-22, designed for airplanes TU-334 and AN-74 (D-436), AN-38 and airplane-amphibious Be-32 (VK-150), AN-70 (D-27), YaK-130 (AI-222-25), AN-140 (TV3-117 and VK-2500) and helicopters (VK-1500V). In spite of separate difficulties the real prospects of development of one of the giants of national engine construction industry, «Motor Sich», gives all grounds to predict the fulfillment of a large volume of works using brazing in service and repair of many thousands of GTE [19].

The brief analysis of production of GTE only in three companies (P&W, «Motor Sich» and «A. Lyulka-Saturn», being truly the most advanced in the world), prove the great promises in use of repair works, including also brazing, for extension of service life of several tens of thousands of engines. Besides these manufacturers of GTE, the following companies are also successful at the market of aircraft and ship diesels: General Electric, Rolls Royce, Boeing, EADS, Mitsubishi, N.D. Kuznetsov SNTK, Ufa motor construction enterprise, Rybinsk motors, Salyut, Aviamotor, Zorya-Mashproekt, A.I. Ivchenko ZMKB Progress (Ivchenko-Progress), and many others. In total there are about 250 large companies, producing gas turbine engines. Most of these companies, firms and enterprises began to work successfully by a conversion program of creation of complexes with GTE for power engineering and oil-gas industry (Figures 7 and 8) [20–23].

The extension of service life of hundreds of thousands of operating GTE owing to repair and repeated use of the engine gives a great economic effect. Preservation and repeated use of hundreds of millions of expensive blades operating in turbines is one of the main tasks of the present repair manufacturing in engine construction in parallel with the design and manufacture of the new GTE.

Complex of research works, made over the recent 30 years by the engine construction organizations in collaboration with such scientific centers as VIAM, TsITM, NIAT, NIID, TsNII SM «Prometej», N.E. Bauman MGTU, MATI, E.O. Paton Electric Welding Institute, Admiral Makarov National University of Ship Construction and others, recommended brazing as a basic technological process for the repair of defects of blades after their casting and in-service formation [12, 13, 15, 24–30].

The brazing of GTE blades is a complex technological process in which the preparation of surface occupies 2 / 3 of the whole process as to the labor consumption. The wide implementation of brazing for repair of blades was limited by the absence of equipment for a guaranteed removal of oxides, deposits and heat-resistant coatings from its surface, and also

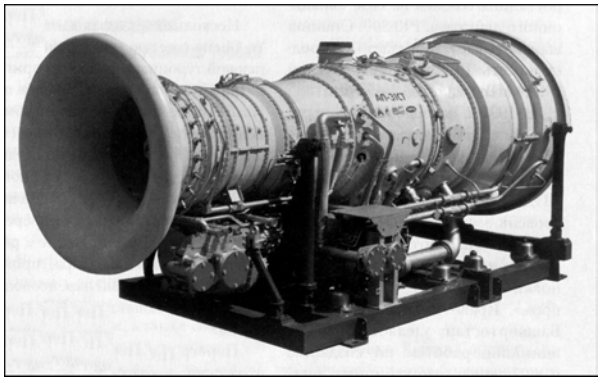

Figure 7. Aircraft gas turbine drive AL-31ST for gas pumping units of «A. Lyulka-Saturn» production

cracks from the inner surface that required the mechanical trepanning of the blade [15]. The existing methods of shot-blasting and abrasive-liquid treatment of the blade surface did not provide the careful and uniform treatment of the airfoil entire surface and led to the change in the product dimensions.

Composite brazing alloys developed in 1970 in NIAT and four years later in P&W, made it possible to implement brazing as a method of repair of blades, parts and sub-assemblies of GTE hot paths with a gap for brazing up to 0.15 mm after the mechanical treatment of defective areas. This was promoted also by the process, developed in 1980 by the Dayton Company (USA), for the fluoro-ion purification of the product surface being repaired from oxides, deposits and heat-resistant coatings.

The leading foreign companies P&W, General Electric, Rolls Royce, Mitsubishi, Interturbine started to use the high-temperature brazing actively and successfully in the first half of the 1980s for the repair of vanes of nozzle unit, flaps of an adjustable nozzle, honeycomb packings, holes in nozzle vanes for a pin and so on (Figure 9).

During the same years, the advanced Russian engine construction enterprises such as Saturn, Mashproekt, Trud, Salyut and others, in collaboration with NIAT, NIID, E.O. Paton Electric Welding Institute, Admiral Makarov NUSC, MGTU, MATI and others applied the thermovacuum annealing, shot-blasting and abrasive liquid purification of surface [24–26, 30] for brazing in repair of defective blades after their

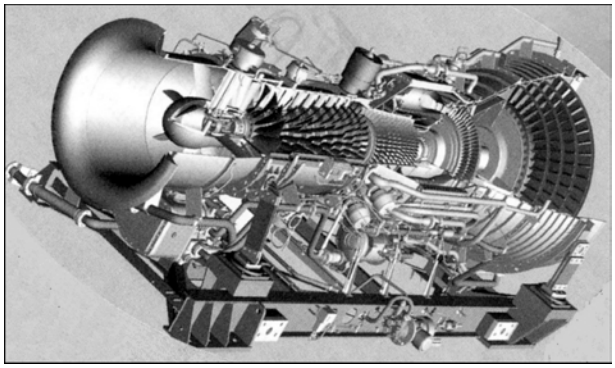

Figure 8. Gas turbine engine for drive of gas fillers, electric generators and ship engines of «Zorya-Mashproekt» production

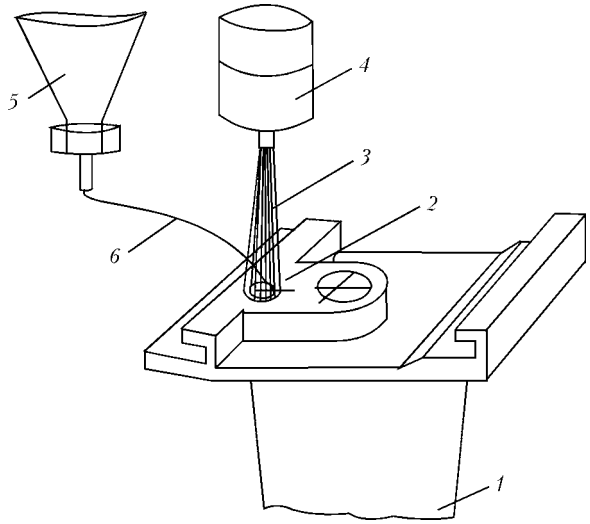

Figure 9. Scheme of process of arc brazing of a hole for pin of vane for nozzle unit GTD-30KU: *1* — vane; *2* — hole for pin; *3* — arc discharge; *4* — torch; *5* — feeder for powder brazing alloy; *6* — transporting pipe

service instead of equipment for the fluoro-ion purification.

Brazing of heat-resistant nickel alloys, alloyed by aluminium, titanium, chromium and other elements, is difficult first of all due to the need in removal of thermodynamically strong oxide films, and also due to guaranteed heat resistance of the brazed joints. The most effective and rational is the high-temperature brazing in vacuum ($1 \cdot 10^{-2}$–$1 \cdot 10^{-3}$ Pa) using nickel brazing alloys [31, 32].

In the world practice the alloys on the base of systems Ni–Cr–B, Ni–Cr–Si, Ni–Cr–Si–B (BNi-2, BNi-5, VPr24, VPr27, VPr42 and others) are used mainly for the repair by brazing of defective castings and worn-out surfaces of blades and parts of GTE. Analysis of brazing alloys of the mentioned systems showed that they have a number of drawbacks, and their application caused some insuperable difficulties. As regards to the B-containing alloys this is formation of brittle phases, containing borides of chromium and the intergranular chemical erosion of the metal being brazed, as regards to the Si-containing alloys this is the weak dissolution of metal being brazed, formation of silicides, development of a local and general chemical erosion with a noticeable increase of a grain at holdings above 15–30 min and temperature 1220 °C [12, 31, 33]. Nevertheless, these brazing alloys are widely used for the repair of blades [13, 24, 30] using different technological procedures and conditions of brazing.

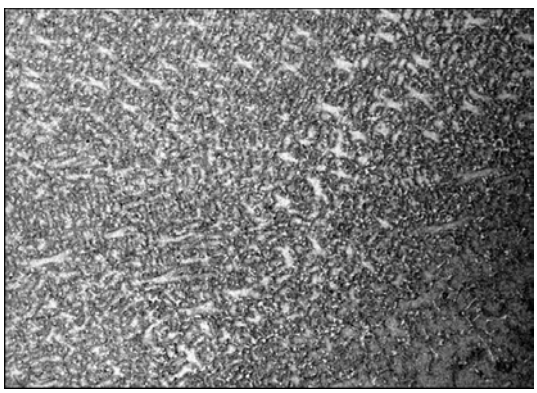

Figure 10. Microstructure of weld metal of alloy ZhS6U-VI produced by the method of brazing using composite powder brazing alloy (mixture of alloy Ni–Cr–Zr and heat-resistant alloy ZhS26U) (×200)

At the end of the 1980s the new direction in the creation of challenging and highly-effective brazing alloys on the base of alloyed eutectic alloys, in which the elements of IV and V groups of PSE (titanium, zirconium, hafnium, vanadium, niobium) were used as depressants, was developed at the E.O. Paton Electric Welding Institute in collaboration with G.V. Kurdyumov Institute of Metal Physics, Admiral Makarov NUSC and NPP «Mashproekt» (now «Zorya-Mashproekt»).

The Ni–Cr–Zr system is most comprehensively studied. The carried out complex of investigations made it possible to study the phase composition and structure of these brazing alloys, their spreading and wetting of surface, hardness and temperature of melting. It was established that the presence of intermetallics Ni_7Cr_2 with a low hardness in them gives an opportunity to control the hardness of brazed weld metal. The given brazing alloys are challenging, as they guarantee the high quality of products in manufacture using the brazing of honey-comb panels, composite blades of GTE, and also in repair of cast blades and GTE blades after service (Figure 10) [33–37].

At present the following methods of brazing are used for repair of blades and GTE hot path parts:

- high-temperature brazing with a brazing alloy in vacuum, in shielding argon atmosphere, in inert or reduction atmosphere [24, 28, 31, 32];
- brazing using arc heating with non-consumable electrode at argon shielding using brazing alloy as a filler material [24, 26, 34];
- pressure brazing in vacuum using brazing alloy and vacuum clamps at pressure 0.07–1.27 MPa [25, 30, 31].

To increase the level of mechanical properties the as-brazed products are subjected to the diffusion annealing. In pressure brazing the use of subsequent heat treatment using parent metal conditions is effective [31].

To restore the service properties of metal and characteristics of fatigue resistance the blades after long-term service are subjected to a reduction heat treatment and stabilizing tempering using specially-developed conditions [38, 39].

The repair technology of brazing of cast heat-resistant blades, and also blades, parts and sub-assemblies of a hot path of aircraft and ship GTE after their preset operation in service is promising and provides the guaranteed high quality of the products.

Implementation of recent research, technical and technological investigations in the field of brazing of heat-resistant alloys on nickel base into sphere of repair manufacturing allowed obtaining of a great economic effect by restoration and repeated use of ex-

pensive blades and other parts of GTE hot path both in construction of the new turbines and also in their service [39]. However, the absence of State standards for the repair technologies using brazing, specialized manufacturers of technological equipment and materials for brazing limits the wide-scale application of this highly-effective technology [40].

CONCLUSIONS

1. It is shown that blades, parts and sub-assemblies of a hot path of aircraft and ship turbines are the expensive products and the most weighable part of production cost and service of engines as a whole.

2. To manufacture blades, parts and sub-assemblies of aircraft and ship GTE, the use of special heat-resistant nickel alloys of a complex alloying is required.

3. It was established that multi-operational technological process of manufacture of GTE blades and their service leads to the formation of various defects, incompatible with requirements for turbine service.

4. In the world practice of service of aircraft and ship GTE the multi-million amount of blades are used, which can be restored using brazing, thus extending their service life.

5. Integrated R&D works carried out by scientific centers of Ukraine and Russia in collaboration with engine construction companies make it possible to implement these developments with a high economic effect in the sphere of repair manufacturing and to guarantee the high quality of the ready product.

6. The wide implementation of the technology of brazing for the repair of blades and parts of GTE hot path is limited due to the absence of standards for repair, and also specialized manufacturers of equipment and materials for brazing.

1. Rybakov, B.A. (1948) *Handicraft of ancient Russia*. Moscow: AN SSSR.
2. Zhadkevich, A.M. (2004) History of origination, technological features and technical capabilities of the first methods of soldering and brazing. *The Paton Welding J.*, **11**, 39–44.
3. Lotsmanov, S.N., Ilievsky, I.I., Petrunin, I.E. et al. (1962) Current achievements and problems in brazing of metals and other materials. In: *Brazing of metals in production and prospects of its development*. Moscow: MDNTP.
4. Paton, B.E., Stroganov, G.B., Kishkin, S.T. et al. (1987) *High-temperature strength of nickel alloys and their protection from oxidation*. Kiev: Naukova Dumka.
5. Shalin, R.E., Bulygin, I.P., Golubovsky, E.R. (1981) *High-temperature strength of alloys of gas turbine engines*. Moscow: Metallurgiya.
6. Stepanov, V.M., Chubarov, V.G., Kononova, A.E. et al. (1978) Progress in precision casting as one of governing factors to increase the power, service life and reliability of gas turbine engines. In: *Structural and heat-resistant materials for new engineering*. Moscow: Nauka.
7. Logunov, A.V., Petrushin, N.V., Kuleshova, E.A. et al. (1981) Prediction of structural factor effect on properties of heat-resistant alloys. *Metalloved. i Term. Obrab. Metallov*, **6**, 16–20.
8. Chumakov, V.A., Stepanov, V.M., Ivanov, B.G. et al. (1978) Technology of casting of gas turbine engine blades by the directed crystallization method. *Litejnoe Proizvodstvo*, **1**, 23–24.
9. Kishkin, S.T., Stroganov, G.B., Logunov, A.V. et al. (1984) Directed crystallization of heat-resistant alloys. *Ibid.*, **4**, 17–19.
10. Lyuttsau, V.G., Kostyukova, E.P., Toloraia, V.N. et al. (1981) Analysis of long-term strength of monocrystals of heat-resistant nickel alloys. *Izvestiya AN SSSR. Metally*, **6**, 180–184.
11. Bokshtejn, S.Z., Brofin, M.B., Drugova, I.A. (1973) Properties of intermetallic phases in nickel-aluminium alloys. In: *Current methods of strengthening of machinery parts by heat treatment*. Tashkent: Nauka.
12. Kvasnitsky, V.F. (1986) *Welding and brazing of heat-resistant alloys in shipbuilding*. Leningrad: Sudostroenie.
13. Kvasnitsky, V.F. (1985) Welding and brazing of heat-resistant alloys in shipbuilding. *Avtomatich. Svarka*, **6**, 26–30.
14. Yushchenko, K.A., Savchenko, V.S., Chervyakov, N.O. et al. (2004) Character of formation of hot cracks in welding cast heat-resistant nickel alloys. *The Paton Welding J.*, **8**, 34–38.
15. Klyuchnikov, I.P., Gejkin, V.A. (2001) Repair of high-loaded parts and assembly units of gas turbine engine hot section by brazing method. In: *Brazing. Current technologies, materials, structures*. Coll. 2. Moscow: TsRDZ.
16. Glina, O., Tyuryakova-Matveeva, D. (2003) Pratt & Whitney where it is demanded. *Gazoturbin. Tekhnologii*, **2**, 38–40.
17. Zinchenko, G., Morgunov, E. (2003) Talent multiplied by daring, labour and perseverance. *Ibid.*, **2**, 30–32.
18. (1999) The present and the future of Russian turbine construction. Review. OAO «A. Lyulka-Saturn». *Ibid.*, **1**, 34.
19. Goncharov, S. (2001) Surge in pumping. *Telegraf*, Dec. 24–30, 12–13.
20. Komarova, T., Mikhajlov, A., Palatidi, S. et al. (2003) Development of family of GTU based on the 3rd series of engine D-30. *Gazoturbin. Tekhnologii*, **3**, 6–8.
21. Kuznetsov, A., Kuprik, V., Khoroshikh, A. (2004) Experience of production, optimization and service of control systems of standard gas turbine engines of AL-31 family. *Ibid.*, **1**, 8.
22. Muravchenko, A. (2004) Improvement of gas turbine engines «Ivchenko-Progress» for industrial power units. *Ibid.*, **2**, 52–54.
23. Boguslaev, V. (2003) Gas turbine units of «Motor Sich» for power engineering and oil and gas industry. *Ibid.*, **6**, 46–47.
24. Yampolsky, V.M., Nerovny, V.M. (1981) Strengthening and repair of gas turbine engine blades by brazing. In: *Transact. of MVTU*, **383**, 72–78.
25. Orlov, A.V., Bereznikov, Yu.I., Samsonova, T.S. (1984) Repair of gas turbine parts by arc brazing method. *Energomashinostroenie*, **2**, 33–34.
26. Khorunov, V.F., Kudashov, A.O. (1991) Pressure brazing of high-temperature steels and heat-resistant alloys. In: *Transact. on Materials and Technology of Brazing*. Kiev: PWI.
27. Vorobiov, V.M., Chernyaev, V.G., Nerovny, V.M. et al. (1991) Increase of life of aircraft engine turbine blades by arc brazing method. *Ibid*.
28. Gruzdev, B.L., Kozlov, V.V., Vangnits, I.S. et al. (1974) Special features of brazing technology of ZhS6K alloy by VPr11 filler metal. *Svarochn. Proizvodstvo*, **2**, 34–35.
29. Wrede, U., Bohrenkamper, G., Umluuft, R. (1999) Lebensdauerverlaengerungsmassnahmen an Gasturbinen. *Allianz Report*, **2**, 97–103.
30. Kvasnitsky, V.F., Korsun, A.I. (1986) Study of possibility to repair the surface defects of cast blades and producing of braze alloy sublayers before the coating deposition. In: *Shipbuilding*. Issue 35.
31. Kvasnitsky, V.F. (1984) *Special methods of welding and brazing in shipbuilding*. Leningrad: Sudostroenie.
32. Lashko, N.F., Lashko, S.V. (1988) *Brazing of metals*. Moscow: Mashinostroenie.
33. Khorunov, V.F., Maksymova, S.V., Zvolinsky, I.V. (2004) Examination of chemical inhomogeneity of brazed seams of heat-resistant nickel alloy joints. In: *Proc. of All-Union and Int. Particip. Sci.-Techn. Conf. on Welding and Control*, Perm, Oct. 2004. Perm: PGTU.
34. Khorunov, V.F., Maksymova, S.V., Samokhin, S.M. (2000) Brazing of current and prospective heat-resistant materials for gas turbine construction. In: *Problems of advanced materials science: Transact. of 4th Session of Sci. Council on New Materials MAAN*. Kiev-Gomel: IMMS ANB.
35. Khorunov, V.F., Maksymova, S.V., Ivanchenko, V.G. (2004) Development of filler metals for brazing heat-resistant nickel- and titanium-base alloys. *The Paton Welding J.*, **9**, 26–31.
36. Khorunov, V.F., Maksymova, S.V., Zvolinsky, I.V. (2003) Structure of brazed joints in high nickel alloys produced by using arc heating. *Ibid.*, **7**, 16–18.
37. Kvasnitsky, V.V., Khorunov, V.F. (1996) Study of state diagrams of nickel-base systems to develop new brazing alloys for heat-resistant materials. In: *Transact. on Technology of Shipbuilding and Welding Production*. Nikolaev: UGMTU.
38. Belov, A.F., Khayurov, S.S., Kleshchev, A.S. et al. (1984) Recovery of structure and properties of ZhS6U alloy blades after long-term service. *Aviats. Promyshlennost*, **2**, 54–56.
39. Ivanov, Yu., Kuzmenko, M., Mikhajlov, A. (2003) Heat treatment of heat-resistant nickel alloys. *Gasoturbin. Tekhnologii*, **2**, 10–12.
40. Khorunov, V.F. (1998) Brazing: Achievements and prospects. *Avtomatich. Svarka*, **11**, 51–53.

ANALYTICAL MODEL OF SPECIFIC RESISTANCE OF ELECTROCONDUCTIVE BULK MATERIAL

V.I. LAKOMSKY and **G.A. TSYBULKIN**
E.O. Paton Electric Welding Institute, NASU, Kiev, Ukraine

New analytical model of a functional dependence of electric resistance of bulk mixture on sizes of its particles has been offered. Results of experimental check-out of the produced model for the estimation of external specific resistance of a crushed thermoanthracite are given.

Keywords: bulk mixture, electric conductivity, specific electric resistance, mathematical model, thermoanthracite

The method of electric contact heating is widely used in the electrode industry throughout the world for annealing of a bulk anthracite and preparation of products of its recycling, i.e. thermoanthracite, in the process of manufacture of carbon electrodes. In this connection, the problem of calculation of specific electric resistance of bulk carbon material with a different fractional composition has been still remained difficult in spite of earlier attempts [1]. The difficulty in the solution of this problem, faced by investigators, consists in the development of a mathematical model of a dispersed system of the thermoanthracite, which could reflect as much as possible the electric conductivity of a real bulk mixture.

In mixtures of bulk carbon materials the electric current is passing both along the grains of the material and also in sites of their possible contact. Therefore, when developing the mathematical model it is necessary to imagine clearly the transfer of electric charges in mass of grains and to reproduce adequately the real transfer of charges through the interface of two solid bodies.

In a classic work of R. Holm [2] an approximated formula of calculation of specific resistance of metallic powder, compressed by a piston in a closed cylindrical space, is given:

$$\rho_{b.m} = c\left(\frac{a}{b} - \frac{1}{2r}\right), \qquad (1)$$

where c and b are the constants; a is the given value of radius of elementary contact spots (so-called a-spots by Holm); r is the mean radius of grains of the metallic powder. To use this formula it is necessary to know the numerical values of all these coefficients, that is acceptable, if to speak about the determination of specific electric resistance using known standardized instruments. However, this formula is not suitable for engineering calculations, if the bulk mixtures of different fractional composition are considered.

In work [1] a simpler and suitable for engineering calculations formula is offered

$$\rho_{b.m} = \rho_0 \frac{r}{a}, \qquad (2)$$

where ρ_0 is the specific electric resistance of material of grains. In materials science of dispersed systems this value is usually named as internal, and $\rho_{b.m}$ as external specific resistance of the bulk material. The equation (2), unlike the equation (1), is rather convenient for express-estimation of value $\rho_{b.m}$, but, as it will be shown below, in case of a fine-grain bulk mixture it gives the overestimated results. In this connection the attempt was made in the present work to find the new analytical expression, which will reflect properly the real pattern of electric conductivity of bulk mixture consisting of fine grains.

Electric resistance of separate grain of bulk mixture. Let us estimate first the resistance of one grain, included into electric circuit of direct current. For the simplicity of calculation (as it is made in modeling of dispersed systems [3]), the grain shape is taken spherical. Let us consider two plane contact areas of radius a on a spherical layer (Figure 1, *a*). Let us imagine these areas as contact surfaces of grain, through which the transfer of electric charges from the lower neighboring grain is realized into the grain considered, and from it into the upper grain.

It is seen in Figure 1, *a* that the distance $2h$ between areas in the grain is related to sphere radii r and a contact area a by an evident relationship

$$a^2 = r^2 - h^2. \qquad (3)$$

The spherical grain will be a conductor with a variable section for the electric current. It can be imagined that the lines of electric current at input of the latter through the contact area into a sphere volume will widen at first, and then, passing through a diametric section of the sphere, will compress to come to the next grain through a contact spot. To determine the grain resistance at such diagram of current passing, let us do the following. Let us divide the spherical layer imaginary into multiple elementary layers where each of them has thickness dx. Let us denote the radii of bases of layers as r_x (Figure 1, *b*). Resistance dR of one such elementary layer can be determined from

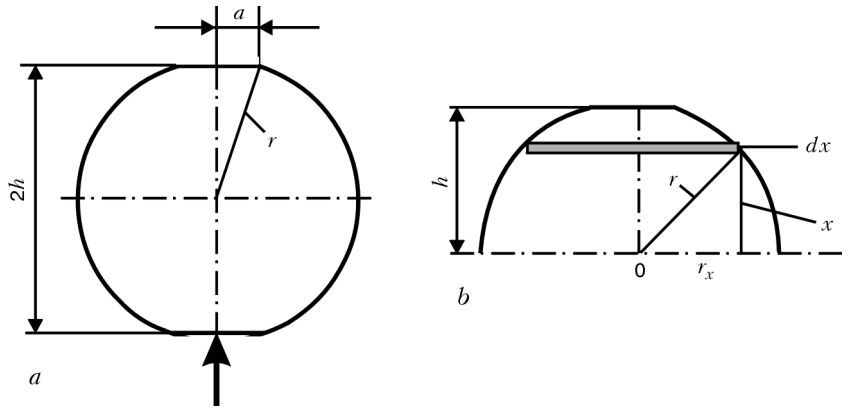

Figure 1. Scheme of spherical grain for calculation of its electric resistance: dark arrow is the direction of electric current, the rest designations see in the text

the generally-known formula for round-section conductor:

$$dR = \rho_0 \frac{dx}{\pi r_x^2}. \quad (4)$$

It is seen from Figure 1, *b* that $r_x^2 = r^2 - x^2$. Taking this into account, let us write the equation (4) in a convenient following form for the next integrating:

$$dR = \frac{\rho_0}{\pi} \frac{dx}{r^2 - x^2}.$$

After integrating the last expression within the ranges from $x = 0$ up to $x = h$ and multiplying of the result obtained by 2, we shall have an equation, describing the resistance of the entire spherical layer of $2h$ thickness, being considered:

$$R_{\text{sph}} = \frac{2\rho_0}{\pi} \int_0^h \frac{dx}{r^2 - x^2} = \frac{\rho}{\pi r} \ln\left(\frac{r+h}{r-h}\right).$$

Using ratio $a^2 = r^2 - h^2$ and taking into account that $a << r$, we shall obtain finally:

$$R_{\text{sph}} = \frac{2\rho_0}{\pi r} \ln \frac{2r}{a}. \quad (5)$$

It is seen from this formula that with decrease in radius *r* of bulk mixture grain the electric resistance of sphere R_{sph} is increased according to a non-linear law. The radius of a contact area *a* influence also the grain resistance, but more slightly.

As compared with work [1], where the resistance of grain mass and intergrain contact resistance of contraction by Holm was considered separately, both these parameters are presented in one equation (5) for the first time. It can be seen that in this equation, as compared with (1), the accents are shifted as regards to resistance of grain mass and contact resistance.

Specific electric resistance of dispersed material. Before describing the external specific resistance of the crushed material, let us dwell on the conception of a contact resistance. In the theory of contacts it is considered as a sum of two resistances, independent of each other, such as constriction and film resistances. The first resistance was described above and, as is seen from (5), it was taken into account by us. The second resistance represents the resistance occurred by current in its passing through the thin various films formed at the contact surface of solid body as a result of adsorption of different gases and, first of all, oxygen. At the surface of metallic contacts the adsorbed oxygen is transferred with time into oxide films possessing the high electric resistance. If the film thickness does not exceed 0.5 nm, then the current overcomes this barrier quite simply under the action of the tunnel effect. At small thickening of films their electric breakdown (fritting-effect) is also observed. If the thickness of film is highly increased, then the metallic contact can come out of order at all.

As regards to such material as thermoanthracite, then the effect of adsorbed oxygen on the formation of a film resistance has not been studied comprehensively. In this case the film resistance can be greatly affected by moisture, but it is not easy to prevent this by negligible heating of coal [4]. In this connection we shall not take into consideration the film resistance on grains of thermoanthracite in our further analysis. For the conditions of electric contact this assumption is quite acceptable.

So, to determine the external resistance of crushed material we shall find first the resistance of one layer of grains of similar size. For this purpose, let use pack grains tightly between two metal square plates of a good electric conductivity, as is shown in Figure 2. Length of sides *l* of both plates should be selected so that to arrange on it the sufficient amount of *n* grains, i.e. $l = 2nr$. As all grains of one layer are connected to electric circuit in parallel, then the resistance of all the layer will be $\overline{R} = R_{\text{sph}}/n^2$. Let us evaluate now the electric resistance R_* of grained material, tightly

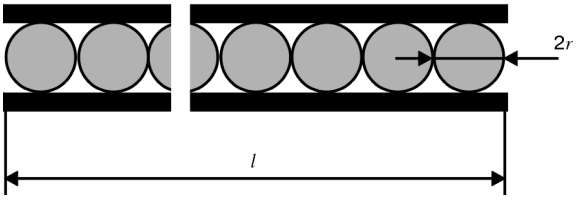

Figure 2. Scheme of packing of grains between current-conducting plane parallel plates

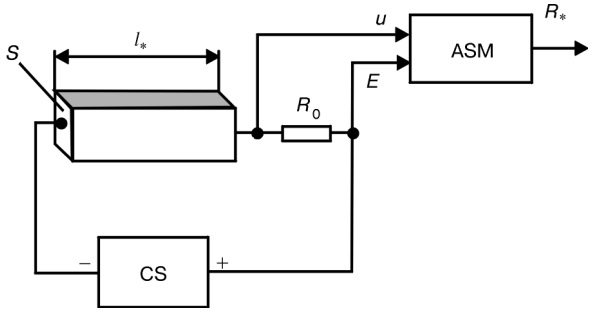

Figure 3. Simplified scheme of measurement of electric resistance of a powdered thermoanthracite

packed into container, having a shape of a cube with non-conductive lateral sides, whose edge length is also equal to l. Electric resistance R_*, represents a sum n of resistances $\overline{R}$ connected in-series. Consequently, it can be written $R_* = n\overline{R} = R_{sph}/n$. Hence, it is easily to come to the external specific resistance of bulk mixture $\rho_{b.m}$:

$$\rho_{b.m} = R_* l. \qquad (6)$$

Using (5) and (6) with account for $l = 2nr$, we shall receive below

$$\rho_{b.m} = \frac{4}{\pi}\rho_0 \ln\frac{2r}{a} \cong \rho_0 \ln\frac{2r}{a}. \qquad (7)$$

This relation can be considered as the new analytical solution of the problem put forward in the present work. As also in [1], the external specific resistance of bulk mixture is determined by a specific resistance, sizes of grain of the crushed material and contact area. However, the dependence of $\rho_{b.m}$ on r and a in this case is manifested very slightly.

Experimental check-out of the developed model. To check out the adequacy of the analytical model (7) of a real functional relation of $\rho_{b.m}$ to r, we have conducted three series of measurements of resistance of thermoanthracite grains of three fractions. Here, the sizes of grains in each fractional group were differed from each other (for example, r = 0.2–0.5 mm; r_2 = 0.5–0.8 mm; r_3 = 0.8–1.2 mm). If these grains have rather sufficient sizes, then it can be assumed that the radii of contact areas a on all the grains will be also almost similar.

Thermoanthracite for the given experiments was supplied from enterprise «Ukrgrafit», the degree of its annealing was not known. Measurements were conducted in a special installation, the scheme of which is presented in Figure 3. This scheme has the following designations: S and l_* are, respectively, the cross-section area of container for bulk material ($S = 8.75 \cdot 10^{-4}$ m^2) and its length (l_* = 0.118 m); R_0 is the reference resistance equal to 30 Ohm; CS is the current source; ASM is the automated system of measurements designed on base of microcomputer LSI-11 / 02.

Algorithm of calculation of resistances R_* using automatically measured values of voltage E and u was constructed by formula

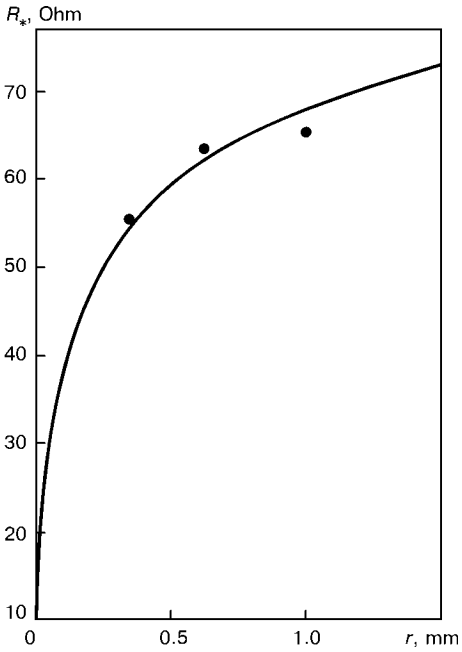

Figure 4. Dependence of electric resistance of crushed thermoanthracite on radius of grain

$$R_* = \frac{u}{E - u} R_0.$$

As a result of measurements the following pairs of averaged values (averaging was made from 100 measurements for each fraction) were obtained: r_1 = = 0.35 mm; R_{*1} = 56.3 Ohm; r_2 = 0.65 mm; R_{*2} = = 64.5 Ohm; r_3 = 1.0 mm; R_{*3} = 65.3 Ohm. Value a was calculated by formula:

$$a = \exp\left[\frac{R_{*2} \ln 2r_1 - R_{*1} \ln 2r_2}{R_{*2} - R_{*1}}\right].$$

It is equal to 0.001 mm. Results of measurements (●) are presented in Figure 4. Here, the curve $R_* = f(r)$ is plotted in accordance with (7) by formula

$$R_* = \rho_0 \frac{l_*}{S} \ln\frac{2r}{a}$$

at ρ_0 = 96 μOhm·m.

As is seen from Figure 4, there is a good correlation between the theoretical and experimental data.

Thus, the experimental check-out of the developed analytic model showed the sufficiently high degree of its adequacy to a real functional bond between external specific resistance of thermoanthracite bulk mixture and sizes of its particles.

1. Lakomsky, V.I. (2003) Mathematical model of calculation of specific electrical resistance of grained thermoanthracite depending on its fractional composition. *Advances in Electrometallurgy*, **3**, 44–47.
2. Holm, R. (1961) *Electric contacts*. Moscow: Inostr. Literatura.
3. Chudnovsky, A.F. (1954) *Heat exchange in dispersion medium*. Moscow: Gostekhteorizdat.
4. Lakomsky, V.I., Lebedev, V.A. (2004) Dependence of contact electric resistance of thermoanthracite on temperature and pressure. *Advances in Electrometallurgy*, **4**, 42–43.

THROTTLING OF COAL CHARGE FLOW IN ELECTRIC CALCINATOR

B.F. PETROV
OJSC «Ukrgrafit», Zaporozhie, Ukraine

Situation has been considered which was occurred in operation of electric calcinators IET-10-UkhLD-4 of PA «Sibelectroterm» at Dneprovsky electrode plant of OJSC «Ukrgrafit». Some results of joint work of the plant and E.O. Paton Electric Welding Institute of the NAS of Ukraine, which have led to the creation of almost new furnace having no drawbacks of the old design, are described briefly. The full movement of thermoanthracite in it is ensured and the second adjustable source of heating of all the coal charge is created.

Keywords: electric calcinator, anthracite, thermoanthracite, throttling, electric shaft furnace, coal charge, electric resistance, throttle

Production of thermoanthracite for the needs of electrode industry, satisfying the requirements of GOST 47-94–97 (specific electric resistance of thermoanthracite should be lower than 1000 μOhm·m), is concentrated now in shaft furnaces of the design similar to that produced by the Norwegian company ELKEM. In high-efficient calcination furnaces of a drum type, operating on gas fuel or residual oil it is not possible to produce thermoanthracite with a specific electric resistance lower than 1200 μOhm·m due to a comparatively low temperature of coal heating.

The advantage of shaft electric furnaces consists in the fact that the maximum temperature of heating in them can be obtained up to 2000 °C and higher without any difficulties, and the higher temperature of the anthracite calcination, the better quality of thermoanthracite and the lower its specific electric resistance [1]. However, the above-mentioned possibility of high-temperature heating concerns not all the coal loaded into furnace, but only to a small part of the coal charge located under the lower electrode of furnace in the axial zone of the furnace shaft.

In parallel with the mentioned advantage, the shaft electric furnaces are typical also of a number of serious drawbacks, the main of which is the significant heterogeneity of properties of the thermoanthracite, calcinated in it [2]. In particular, the specific electric resistance (main physical characteristic of the thermoanthracite used for manufacture of electrodes) is differed in parallel samples by more than twice, i.e. 520 and 1100 μOhm·m [3]. The cause of such high heterogeneity in properties of the thermoanthracite consists in non-homogeneity of temperature field of coal charge and specific configuration of the furnace.

If to consider the cross-section of the furnace shaft, then it is possible to reveal that the highest temperature is recorded in the center (at furnace axis), and near walls it hardly reaches 950 °C at the furnace output. In a vertical section of the furnace shaft the distribution of temperature in axis is as follows: the highest temperature of coal was recorded in the zone of heating under the upper electrode; the temperature in the direction to the lower electrode is decreased, but slightly.

It should be noted that the furnace design under the consideration does not allow automation of its operation.

The electric shaft furnaces of a similar type have been more than 25 years in operation in industry. Nevertheless, there is no a cardinal solution until now, allowing prevention of their drawbacks, besides palliative variants of solutions [4], suggested by the staff members of ELKEM, according to which a part of coal (and a significant part) should be selected from the common flow of calcinated coal and passed again through the furnace for additional heat treatment.

At the Dneprovsky electrode plant of «Ukrgrafit» company they came themselves to conclusion after putting into operation of shop of electric calcination of anthracite about the need in works by the scheme of a double coal calcination to produce the brand thermoanthracite. To decrease here the specific consumption of electric power, it was decided to operate not at 13–15 kA current, as was recommended by the plant-manufacturer of furnaces, but at a half power of furnaces i.e. 6–7 kA. Nevertheless, in this case also the double calcination of thermoanthracite will lead to extra-consumption of electric power. It is necessary to consume up to 1400 kW·h of electric power for the production of 1 t of electrode thermoanthracite. Here, the certificate efficiency of furnaces is decreased and the labor content per ton of production is increased.

To find the methods of fighting with these drawbacks of electric calcinators of design of PA «Sibelectroterm», Dneprovsky electrode plant and the E.O. Paton Electric Welding Institute organized a creative team several years ago and started the search for so-

lutions directed to the improvement of homogeneity of electrode thermoanthracite produced in electric calcinators.

Study of temperature field of the calcinator, made using thermocouple probes on three horizons of furnace shaft, showed that the highest temperature (independently of the furnace power) is created in the zone located in the furnace axis under the upper electrode. The increase in the furnace power influences mainly the sizes of the heating zone, and the coal temperature in the mentioned zone is growing very moderate. The mentioned zone of coal heating was revealed also by other investigators [3, 5, 6]. The difference of their results is only in the zone location in furnace height.

It was established that this zone (Figure 1) is the only source of intensive heating of coal in the furnace. In our opinion, the basic share of electric power supplied to the calcinator is dissipated in it. The evolved heat energy from the zone of high temperature is spread in all the mass of crushed coal owing to heat conductivity. Temperature of coal in a radial direction at the zone level is abruptly lowered from the zone of heating to the furnace walls. It is understandable that under these conditions the near-wall masses of coal will be much cooler than the central masses. Beside the heat flow directed to the periphery of shaft of crushed anthracite, the heat power from the zone of heating is spread into direction to the lower electrode of the furnace. However, this flow, as compared with a radial flow, is very small. This is explained by the fact that the central zone of the furnace at the entire path to the lower electrode is heated itself, though slightly, by electric current, passing between the upper and lower electrodes.

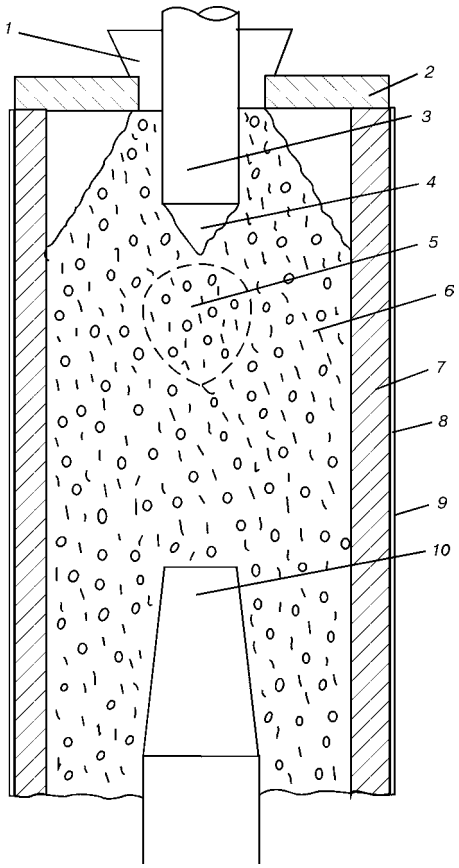

Figure 1. Scheme of location of the zone of intensive heating of coal charge in a shaft furnace of ELKEM design: *1* — loading device; *2* — plug from heat-resistant concrete; *3* — upper electrode; *4* — under-electrode space; *5* — zone of intensive heating of thermoanthracite; *6* — coal charge; *7* — refractory lining; *8* — mullite cotton; *9* — steel housing of furnace; *10* — lower electrode

The causes of arrangement of high-temperature zone in this place of the furnace shaft are as follows: firstly, the anthracite, entered the furnace by a loading device of the furnace, gains a sufficient electric conductivity as a result of heating by upward gases of a dry distillation of coal; secondly, coal grains undergo a slight pressure from above-laying layers of coal charge and, therefore, the contact electric resistance between coal grains is rather high and, consequently, the contact drop of voltage U_c will be high at the transition of electric current from grain to grain; thirdly, the high value U_c leads to a rather significant growth of a contact temperature, as the latter is in a quadratic dependence on U_c; fourthly, due to a very close vicinity to the upper electrode, the highest density of electric current by coal charge was recorded.

In our opinion, the formation of zone of high-temperature heating of coal is not occurred spontaneously, but it is developed with time. At the beginning, as is shown on a transparent model of calcinator [7, 8], the electric current finds its path in a randomly selected chain of thermoanthracite grains. By passing this path, the current heats the thermoanthracite chain grains. As the thermoanthracite is characterized by the negative temperature coefficient of electric resistance [9], then with increase in temperature its resistance is decreased and the current in the chain is increased. This is continued until the degree of coal grains heating in electric circuit reaches a white heat. Then, the radiation heat flow from the heated chain to the surrounding neighboring grains of thermoanthracite is increased abruptly, as the intensity of radiation of a heated body depends on its temperature in the fourth power. This results in heating of neighboring grains of thermoanthracite, and the electric current is spread in coal charge and passes now in several electric bridges, widening the section of its passing. This process is finished when the set current of the transformer will be reached.

As follows from experiments and practice of operation of calcinators, the electric current under these conditions cannot serve as on-line means of the furnace operation control. The control, according to recommendations of the furnace manufacturers, is performed as follows. A definite level of current is preset, which in the process of furnace operation is varied automatically between the set minimum and maxi-

mum values. In loading of a portion of «raw» anthracite into the furnace the current is spontaneously decreased to a set minimum, and then with a coal heating it is increased to a maximum level. The mentioned values of current indicate the changes of thermal situation only in the zone of maximum heating of coal and do not almost influence the temperature of all the mass of the coal charge. The temperature field in periphery regions of coal in the furnace charge remains here almost without changes.

Under these conditions the control of furnace operation is performed by a portion of coal which is loaded and unloaded from the furnace, and also by an interval between switching on of batchers, i.e. by changing the furnace efficiency.

To avoid the non-homogeneity of properties of the thermoanthracite, produced in electric calcinator, it is necessary to mix the crushed coal charge in the furnace, and for this purpose it is necessary to design a mixing device of a good performance, and, secondly, to select the material, from which the elements of this device could be manufactured. The high temperature and abruptly reducing conditions in the furnace hindered greatly the selection of the material capable to provide the sufficient service life of the mixing device.

The simplest solution could be installing of a throttle (washer) in the calcinator shaft between the upper and lower electrodes and feeding of all the mass of coal charge through this throttle. The throttle should have a conical surface in the upper part to impart the coal grains a horizontal constituent of movement, except vertical one. This device could, undoubtedly, provide the mixing of crushed coal in passing of all the bulk charge through the throttle. It should be noted that the mixing of the coal charge could occur without any power consumption from outside. The crushed coal could be poured from the over-throttle to under-throttle space under the action of the Earth gravitational field.

As the throttle is arranged in the electric field of the furnace, it should be manufactured from non-electroconductive material to avoid the electric current shunting along the mass of the crushed coal. Current should pass only along the coal charge because the active heating element of the furnace is electroconductive coal itself.

At the beginning, the proposal of throttle manufacture from refractory material was discussed. Most refractories preserve their electroinsulating properties even at high temperatures. However, under condition of operation of the calcinator, the refractories, manufactured from oxides, will react with carbon of the thermoanthracite and will be reduced up to carbides. In this connection their service life will be short.

The comprehensive study of nature of behavior of bulk materials at vertical their movement from one container into another through the orifice, smaller than the container diameter, helped to select the proper material for the throttle manufacture. In these conditions the dispersed material, which is a crushed anthracite, forms so-called cone of angle of repose at the orifice outlet.

At Dneprovsky electrode plant of «Ukrgrafit» company the charge of 6–25 mm fractional composition is used. The cone of angle of repose for this charge, as was found by us, is 60°. Consequently, the formation of cone of angle of repose of coal charge under 60° angle to horizontal will lead automatically to the creation of empty under-throttle space which will break the electric circuit in a column of electroconductive charge in a circular section equal to $\frac{\pi}{4}(D^2 - d^2)$, where D is the internal diameter of furnace; d is the diameter of cylindrical space of throttle (Figure 2).

Thus, the requirements to the non-electroconductivity of the throttle material are not reasonable, because the conditions of passing of all the current through the coal charge in the throttle orifice are created automatically. And, as all the coal charge is passed through the throttle orifice, then not only a part of charge will he heated by the current as in furnace of ELKEM company, but all the mass of the thermoanthracite.

Among all electroconductive and heat-resistant materials we have selected the material of carbon blast furnace blocks. Blocks of grade DBU are the standard product of our plant, containing more than 60 % of

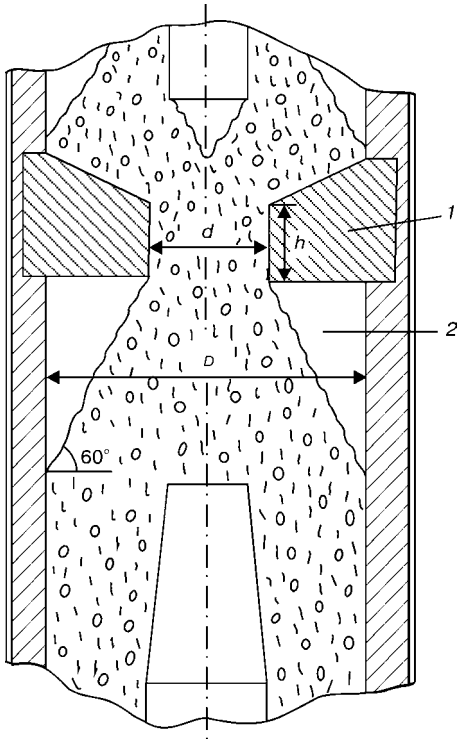

Figure 2. Scheme of formation of a cone of coal charge in under-throttle space of the furnace: *1* — throttle (washer); *2* — under-throttle empty space

low-quality thermoanthracite that is required for the throttle operation. The throttle material should be characterized by a specific electric resistance exceeding the corresponding characteristic for the bulk coal charge at 1500–2000 °C, should have a low coefficient of a linear expansion and high wear resistance. The thermoanthracite is characterized by a high hardness and, therefore, the throttle material should withstand well the abrasive action of the bulk coal mass sliding along the throttle surface.

To check out the working idea of the throttle design we have constructed a physical model of a calcinator in 1:4 scale (Figure 3). The model shaft was quickly and simply assembled from modular rings used at the plant for other purposes. Rings represented products from reinforced heat-resistant concrete with locks. The internal diameter of rings was 480 mm, the height of each ring was 80 mm. The total height of model in this case was easily varied by varying the number of rings. The level of mounting the throttle, manufactured specially for model from the electrode material, was changed by rearrangement of the rings. The throttle was arranged at the distance of 1 / 3, 1 / 2 and 2 / 3 of an interelectrode gap.

To determine the degree of coal mass mixing, the following experiments were made using the developed model. Anthracite of 4–6 mm fractional composition was divided into two equal portions, one of them was painted into white color. Equal amounts of black and white anthracite were loaded into over-throttle space of the model, dividing them by a tube. Then, the orifice in the washer was opened simultaneously and the tube was removed. Coal charge was poured from a space over throttle to a space under throttle. After charge passing through the throttle orifice the white and black anthracite was separated and amount of white and black grains were calculated. Experiments showed that ratio of white and black anthracite in the coal mixture after passing through the throttle was 50:50 and 40:60 independently of the throttle position in height of the model shaft. Condition of coal charge after passing through the orifice in the washer could be evaluated visually, there were no islands of white and black coal, that proved a good mixing of the coal charge.

Figure 3. General view of physical model of electric calcinator

Except of mixing the coal charge, the above-mentioned model was used to study the change in temperature of the coal in its passing through the cylindrical space of the throttle. Taking into account thermal properties of heat-resistant concrete the coal was heated by a low current insufficient for attaining temperatures comparable with a working condition of a full heating of thermoanthracite in the electric calcinator. Experiments were conducted not in a dynamic condition, but in a static condition. As was expected, the coal charge in the cylindrical space of the throttle is heated intensively. Thus, for example, shortly after electric power supply the temperature of the thermoanthracite in over-throttle space reached 400 °C, while at the throttle outlet it was already 620 °C. In extension of the time of heating the coal temperature in the cylindrical space was increased up to 840, 920 and 1020 °C. At the same time the coal temperature in over-throttle space was increased at much lower rates.

There is no doubts that with increase in duration of model heating by current or with increase in its value we could attain the higher temperature. However, the experiments were interrupted because of hazard of thermal fracture of ceramic rings, from which the model walls were composed.

The process of a contact electric heating of thermoanthracite in a cylindrical space of the throttle can be presented as follows.

As follows from Figure 2, the volume of cylindrical space of throttle is $\frac{\pi}{4} d^2 h$, and the mass of the coal charge, filling this space, is $\frac{\pi}{4} d^2 h\gamma$, where γ is the specific bulk weight of the coal charge of accepted fractional composition.

As the process of the thermoanthracite heating in the throttle is proceeding with time, let us determine the time τ, coming from efficiency P of the calcinator, during which the coal is subjected to heating in the throttle: $\tau = \frac{\pi}{4} \frac{d^2}{P} h\gamma$. Electric resistance of a round column of the coal charge of diameter d and height h will be $R = \frac{4h}{\pi d^2} \rho_{b.m}$, where $\rho_{b.m}$ is the specific electric resistance of thermoanthracite in the form of

bulk material at temperature of somewhat lower than 2000 °C.

Amount of heat generated in thermoanthracite during its heating in throttle by passing current I through coal for time τ will be $W = I^2R\tau$.

Let us derive equation of heat balance:

$$\frac{4\pi\rho_{b.m}h^2d^2\gamma}{4\pi d^2P}I^2 = \frac{\pi}{4}d^2hyC_PT, \qquad (1)$$

where C_p is the heat intensity of crushed thermoanthracite at constant pressure; T is the coal temperature.

After appropriate cancellations and rearrangements we shall obtain dependence of temperature of coal heating in a cylindrical space of the throttle on electric current passing between the furnace electrodes:

$$T = \frac{4}{\pi}\frac{h\rho_{b.m}}{d^2PC_P}I^2. \qquad (2)$$

It follows from equation (2) that the temperature of thermoanthracite heating in a cylindrical space of the throttle is in a direct dependence on squared current and determined by the diameter and height of the throttle cylindrical height, heat intensity and specific electric resistance of the coal bulk mass. This is very important conclusion because it indicates the use of furnace current as an efficient means of adjustment of the process of coal calcination.

Thus, in the furnace of existing design the current variation leads to the change in temperature not of all the mass of coal, but only that part which is located in the zone of intensive heating of thermoanthracite. If to install the throttle into the furnace through which all coal charge is fed, then the change in current will cause the change in temperature of the all the coal mass.

Consequently, the technology of coal calcination is changed radically in the modified electric calcinator. Now, the process of coal calcination is necessary to conduct by indications of ammeter on the furnace panel. An hour's efficiency of the furnace in these conditions plays a subordination role. By setting the value P, coming from the preset specific electric resistance of a final product, the furnace current value I is selected, which corresponds to the most economic condition of coal calcination.

Further, all terms of the equation (2) can be divided into design parameters of the throttle d and h, technological parameters furnace P and I, properties of thermoanthracite $\rho_{b.m}$ and C_p.

Current I and diameter of orifice in the throttle d influence most effectively the coal heating temperature, as both these terms of equation (2) are in the second power. The difference between them consists in the fact that diameter d can be changed only in replacement of the throttle, while the furnace current I is remained as an efficient parameter of control of the furnace operation in all the cases. By increasing the value of current I only by 5 % we shall rise the temperature of coal calcination from 1800 up to 2000 °C. At the same time to obtain the similar effect by changing the furnace efficiency it could be necessary to decrease this parameter by 11 %.

Variation of current I and diameter D promotes the change in specific density of current in the throttle cylindrical space. This explains the strong effect of these parameters on the calcination temperature. Such parameter of the throttle, as height of its cylindrical part h, influences the duration of heating process of each portion of coal locating in the throttle cylindrical space. This is a kinetic factor of the heating process. Time τ should be selected so that it was sufficient for calcination of largest grains of the thermoanthracite. If the selected time for anthracite processing is not sufficient, it is necessary to increase slightly the value h. By changing its value, it is necessary to remember that with increase in h the hazard of current path shunting is increased. Current should pass along the crushed mass of the coal, located in the throttle, but not along the walls of its cylindrical space. To widen the opportunities of the technologist, it is necessary to use material for the throttle with as low as possible electric conductivity.

In calculation of a heat balance, we did not take into account the heat losses from that part of coal which is located in the throttle cylindrical part. It should be supposed that at the beginning of the heating process the losses will be noticeable, and, then, at the throttle heat saturation they will greatly decrease. The estimation of heat losses into the throttle body shows that their value does not exceed 10 % of total heat evolution in the throttle under the conditions of a steady heating condition.

Figure 4 presents the results of calculation of temperature of coal heating in the throttle at different

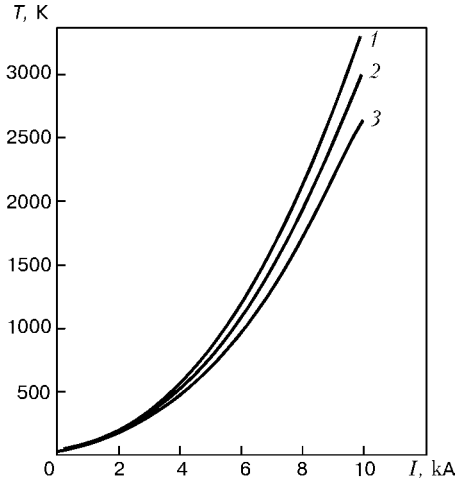

Figure 4. Dependence of thermoanthracite temperature on furnace current in the process of its heating in the throttle: *1* — perfect case (without heat losses); *2*, *3* — respectively, 10 and 20 % of heat losses into the throttle body

heat losses of this process. It was accepted that P = = 800 kg / h, while C_p at high temperatures is 0.47 (W·h) / (kg·deg) [10]. The Figure shows a parabolic dependence of thermoanthracite heat temperature in the throttle on current. Two times increase in the furnace current value leads to the four-fold increase in the coal heating temperature. After throttle installing in the furnace, there is no need to operate at 13–15 kA currents as the plant-manufacturer recommends. It is sufficient 9–10 kA only to heat all the coal loaded into furnace up to temperatures exceeding 2000 °C. This condition of the furnace control is the key to saving the specific consumption of the electric power.

The first tests of the modified electric calcinator showed that it is possible to produce thermoanthracite with a specific electric resistance of 680 μOhm·m at 763.6 kW·h / t consumption.

1. Fialkov, A.S. (1997) *Carbon, interlayer bonds and composites on their base*. Moscow: AspektPress.
2. Soldatov, A.I., Bekasov, V.N., Menshikova, S.D. et al. (1990) Inhomogeneity of electric thermoanthracite and its evaluation. *Tsvet. Metally*, **2**, 53–55.
3. Tatishchev, A.S., Mukhitdinov, A.M., Nikolaev, V.N. et al. (1985) Distribution of temperature fields in electric calcinator shaft and their effect on thermoanthracite quality production. In: *Transact. of GosNIIEP on Improvement of Technology and Quality of Electrode Products*. Chelyabinsk: Yuzhno-Uralskoe Izd.
4. Johansen, J.A., Vattlann, A. *Method and furnace for electric calcination of carbon-containing material*. Pat. RU 2167377 C1 Norway. Publ. 22.10.98.
5. Soldatov, A.I. (1991) *Electrocalcinated anthracite. Specifics of its production and application*. Syn. of Thesis for Cand. of Techn. Sci. Degree. Kharkov.
6. Soldatov, A.I., Mochalov, V.V. (1989) Technological aspects of production of electrocalcinated anthracite with preset properties. In: *Transact. of NIIGrafit, GosNIIEP*. Moscow.
7. Lakomsky, V.I., Bykovets, V.V. (2004) About contact heating of thermoanthracite in electric calcinator. *Tsvet. Metally*, **1**, 52–54.
8. Lakomsky, V.I., Grigorenko, G.M. (2004) Specifics of thermoanthracite heating in AC electric field. *Advances in Electrometallurgy*, **3**, 48–50.
9. Bykovets, V.V., Lakomsky, V.I. (2003) Specific electric resistance of thermal anthracite. *Ibid.*, **4**, 46–48.
10. Grinshpunt, A.G. (1998) Investigation of complex characteristics of anthracites used in mass composition of self-calcinated electrodes for ore-smelting electric furnaces. *Teoriya i Praktika Metallurgii*, **3**, 33–34.